Die approbierte Originalversion dieser Diplom-/Masterarbeit ist in der Hauptbibliothek der Technischen Universität Wien aufgestellt und zugänglich.
http://www.ub.tuwien.ac.at

The approved original version of this diploma or master thesis is available at the main library of the Vienna University of Technology.
http://www.ub.tuwien.ac.at/eng

TECHNISCHE UNIVERSITÄT WIEN

DIPLOMARBEIT

Thermochemical Heat Storage for Motor Vehicles – System Optimization of Heat Storage Based on Salt Hydrate

ausgeführt zum Zwecke der Erlangung des akademischen Grades eines „Diplom-Ingenieurs“ unter der Leitung von

Associate Prof. Dr.techn. Peter Hofmann

und

Dipl.-Ing. Fabian Havlik

E315

Institut für Fahrzeugantriebe und Automobiltechnik

eingereicht an der Technischen Universität Wien

Fakultät für Maschinenwesen und Betriebswissenschaften

von

Jure Galović

e1328725

Otto Bauer Gasse 20/24

1060 Wien

Wien, am 12. Februar 2018 B18003

Aufgabenstellung für die Diplomarbeit

Conceptual formulation

Herrn Jure Galovic, Matr.Nr.: 1328725 wird folgende Aufgabe gestellt:

Thermochemical Heat Storage for Motor Vehicles – System Optimization of Heat Storage Based on Salt Hydrate

Es ist eine praktische Weiterentwicklung eines Systems zur Speicherung von Abwärme zu entwickeln.

Schwerpunkte:

- Literaturrecherche zum Stand der Technik
- Untersuchungen am Komponentenprüfstand
- Gegenüberstellung verschiedener Methoden zur Sorbatverteilung
- Prüfen der zyklischen Dauerhaltbarkeit des Systems
- Versuche bei verschiedenen Umgebungstemperaturen
- Auswertung der Ergebnisse und schriftliche Ausarbeitung

Dauer: Februar 2017– November 2017

Ein gedrucktes Exemplar und eine Version der Diplomarbeit auf Datenträger sind am Institut für Fahrzeugantriebe und Automobiltechnik der Technischen Universität Wien abzugeben.

Die Ergebnisse der Arbeit sind vertraulich zu behandeln und dürfen nur mit schriftlicher Genehmigung des Institutsvorstandes weitergegeben bzw. veröffentlicht werden.

Die Benutzung der Versuchseinrichtungen des Institutes hat in den Dienststunden und unter Anleitung des Betreuers zu erfolgen. Dabei dürfen alle Arbeiten nur unter besonderer Beachtung der geltenden Sicherheitsvorschriften durchgeführt werden.

Einverstanden	Betreuender Assistent
_____	_____
Jure Galovic	DI Fabian Havlik
Betreuender Professor	Institutsvorstand
_____	_____
Assoc. Prof. Dr. Peter Hofmann	Prof. Dr. Bernhard Geringer

Wien, am 12. Februar 2018 B18003

Eidesstattliche Erklärung

Ich habe zur Kenntnis genommen, dass ich zur Drucklegung meiner Arbeit unter der Bezeichnung

Thermochemical Heat Storage for Motor Vehicles – System Optimization of Heat Storage Based on Salt Hydrate

–

Chemische Wärmespeicherung für Kraftfahrzeuge – Systemoptimierung eines Wärmespeichers auf Basis von Salzhydraten

nur mit Bewilligung der Prüfungskommission berechtigt bin. Ich erkläre weiters an Eides statt, dass ich meine Diplomarbeit nach den anerkannten Grundsätzen für wissenschaftliche Arbeiten selbständig ausgeführt habe und alle verwendeten Hilfsmittel, insbesondere die zugrunde gelegte Literatur genannt habe.

Weiters erkläre ich, dass ich dieses Diplomarbeitsthema bisher weder im In- noch im Ausland (einer Beurteilerin/ einem Beurteiler zur Begutachtung) in irgendeiner Form als Prüfungsarbeit vorgelegt habe und dass diese Arbeit mit der vom Begutachter beurteilten Arbeit übereinstimmt.

Wien, am 12. Februar 2018 _____

Jure Galović, BSc

Sperrvermerk:

Ich weise darauf hin, dass die Diplomarbeit vertrauliche Informationen und unternehmensinterne Daten beinhaltet. Daher ist eine Veröffentlichung oder Weitergabe von Inhalten an Dritte ohne die vorherige Einverständniserklärung des Instituts für Fahrzeugantriebe und Automobiltechnik nicht gestattet.

Preface

The present master thesis was carried out within the project “Wärmespeicherung III”, funded by the Research Association for Combustion Engines (FVV) eV at the Institute for Powertrains and Automotive Technology (IFA) at the Vienna University of Technology.

I would like to express my sincere gratitude to my co-supervisor Projektass. Dipl.-Ing. Fabian Havlik, BSc. for involving me in this project. I am thankful for his guidance, encouragement and the scientific and technical advices he provided during this research.

I would like to acknowledge, in full gratitude, Associate Prof. Dipl.-Ing. Dr.techn. Peter Hofmann, primary supervisor of this master thesis and Head of Institute Prof. Dr. Bernhard Geringer, who provided my engagement on this research project. Particular gratitude to Univ.Prof. Dipl.-Ing. Dr.techn Markus Haider for co-examining this master thesis.

To my colleges from IFA, thank you for the pleasant working atmosphere and the nice memories, which will never be forgotten.

To my Austrian friends, many thanks for the nice memories and the support you have provided me in German, during my studies in Vienna.

Special thanks to my beloved Katarina for her optimism, patience and support during my work on this master thesis.

I dedicate this master thesis to my parents, my brother and my family. They had devotion in me and gave me unconditional love and support during my studies at the Vienna University of Technology.

Vienna, 12. February 2018 Jure Galović

Table of Content

Preface.....I

Abstract.....IV

Kurzfassung.....V

List of Abbreviations.....VI

1. Introduction.....1

1.1 Thermochemical Heat Storage in Motor Vehicles.....1

1.2 Modular Thermochemical Heat Storage System.....3

1.3 Goals and Aims.....4

2 Fundamentals of Thermal Energy Storage Systems.....5

2.1 Heat Storage Systems.....5

2.1.1 Sensible Heat Storage.....6

2.1.2 Latent Heat Storage.....7

2.1.3 Chemical Heat Storage.....8

2.2 Mechanism of Sorption Processes.....13

2.3 Heat and Mass Transfer.....14

2.4 Effect of Non-Condensable Gas on Condensation Process.....18

2.5 Previous Findings.....21

2.6 Conclusion of Fundamentals.....22

3 Materials and Methods.....23

3.1 Thermochemical Cartridge Design and Development.....27

3.2 Sorbate Distribution System.....29

3.3 Test Procedure.....31

3.4 Test Evaluation.....36

3.4.1 Released Energy, Power Release and Dry Air Calculation.....36

3.4.2 Sorbate Flow Analysis.....38

3.4.2.1 Evaporation Rate.....42

3.4.2.2 Major Losses.....46

3.4.2.3 Minor Losses.....48

3.5 Conclusion of Materials and Methods.....52

4 Results and Discussion.....53

4.1 Sorbate Distribution System Investigation.....53

4.1.1 Performance Analysis.....53

4.1.2 Sorbate Flow Analysis.....56

4.1.3 Summary of Sorbate Distribution System Investigation.....64

4.2 Effect of Ambient Temperature on Cartridge Performance……..…..…65
4.2.1 Summary of the Chapter……..69
4.3 Durability Tests……70
4.3.1 Released Energy Trend and Reactive Bed Mass Growth…..……70
4.3.2 Average Power Release Trend……..……....73
4.3.3 Deviation from the Energy Trend Due to the Presence of Dry Air..74
4.3.4 Effect of Non-Condensable Gases on Cartridge Performance…..76
4.3.5 Summary of Durability Tests……..…79
4.4 Reversibility Analysis……..……....79
4.4.1 Variation of Desorption Temperature……....80
4.4.2 Variation of Sorbate Temperature……..81
4.4.3 Summary of Reversibility Analysis……..……..…83

5 Error Analysis……...84
5.1 Systematic Errors……84
5.2 Operating and Evaluation Errors……..……84
5.3 Simplifications……..….85
5.4 Relevant Errors……....86

6 Summary and Outlook……86
6.1 Summary……..……..86
6.2 Improvements and Outlook……....88

7 Bibliography……..……....90

Abstract

Thermochemical heat storage (TCHS) system aims to improve the efficiency of vehicles powered by an internal combustion engine, therefore reducing exhaust gas emissions and fuel consumption. On one hand, the engine coolant at engine operating temperature represents heat source, on the other hand it represents heat sink during engine cold start. During engine warm up phase, the released heat from thermochemical heat storage system helps to reach engine operating temperature faster. Thereby high power release of thermochemical system is desirable.

In this master thesis, the existing thermochemical heat storage system based on solid gas sorption process, with working pair lithium bromide (LiBr) and methanol (CH_3OH), was optimised. A sorbate distribution system, which connects a cartridge (absorber) with a sorbate reservoir, was developed. Performance of the thermochemical heat storage system was investigated according to different pipe diameter and pipe length of the sorbate distribution system.

Further, performance of the thermochemical heat storage system was examined according to different ambient temperatures maintained in climate chamber at -10°C, 0°C, 10°C, 20°C and 30°C. The performance trend was clarified considering the phenomena occurring in the reactive bed, such as heat and mass transfer.

Cyclic durability of the developed cartridge was investigated in successively conducted charging-discharging phases. A performance change depending on time was determined. In addition to durability tests, the effect of non-condensable gases on the cartridge performance was clarified.

Finally, the reversibility of heat storage process under possible engine conditions was examined. Charging-discharging phases were conducted and charging completeness depending on charging temperatures was investigated.

Kurzfassung

Der Einsatz chemischer Wärmespeicher im Kraftfahrzeug kann zur Reduktion des Kraftstoffverbrauchs, sowie der Emissionen während dem Kaltstart beitragen. Das Motorkühlmittel stellt bei Motorbetriebstemperatur eine Wärmequelle für Wärmespeicherung dar und bei Motorkaltstart wird dem Kühlmittel Wärme aus dem Wärmespeicher zugefügt. Die freigesetzte Wärme aus dem Wärmespeichersystem hilft, die Betriebstemperatur des Motors schneller zu erreichen. Eine hohe Leistung des thermochemischen Systems ist wünschenswert.

In dieser Masterarbeit wurde ein bestehendes thermochemisches Speichersystem, basierend auf auf einem Sorptionprozess mit den Reaktanden Lithiumbromid (LiBr) und Methanol (CH_3OH) weiterentwickelt. Ein Sorbatverteilungssystem, welches eine Speicherpatrone (Absorber) mit einem Sorbatbehälter verbindet, wurde erstellt. Die Leistung des Wärmespeichersystems wurde bezüglich der unterschiedlichen Sorbatverteilungssystemen, abhängig von Durchmesser und Länge der Sorbatleitungen, untersucht.

Ferner wurde die Leistung des Wärmespeichersystems gemäß verschiedenen Umgebungstemperaturen untersucht, die in der Klimakammer bei -10 °C, 0 °C, 10 °C, 20 °C und 30 °C gehalten wurden. Das Leistungsverhalten wurde unter Berücksichtigung der im reaktiven Bett auftretenden Phänomene wie Wärme- und Stoffübertragung geklärt.

Die zyklische Beständigkeit der entwickelten Speicherpatrone wurde in nacheinander durchgeführten Lade-Entlade-Phasen untersucht. Dabei ist eine zeitliche Veränderung der Entladeleistung der Speicherpatrone erkennbar. Zusätzlich wurde die nachteilige Wirkung von nicht kondensierbaren Gasen (Luft im System) auf die Speicherleistung geklärt.

Schließlich wurde die Reversibilität des Wärmespeicherprozesses unter Aufrechterhaltung der möglichen Motorbedingungen untersucht. Lade-Entlade-Phasen wurden durchgeführt und das Verhältnis der Vollständigkeit der Ladung abhängig von verschiedenen Ladetemperaturen wurde dargestellt.

List of abbreviations

BMEP	brake mean effective pressure
CH_3OH	methanol
CO_2	carbon dioxide
Cu	copper
D	diameter
EU	European Union
GHG	greenhouse gas
IUPAC	International Union of Pure and Applied Chemistry
LiBr	lithium bromide
NCG	non-condensable gas
NEDC	New European Driving Cycle
PCM	phase change material
TCHS	thermochemical heat storage

1 Introduction

1.1 Thermochemical Heat Storage in Motor Vehicles

Thermochemical heat storage in motor vehicles can lead to lower emissions in road transport. As shown in figure 1.1, road transport applications are responsible for 19% of the total greenhouse gas emissions (GHG) in the European Union (EU).

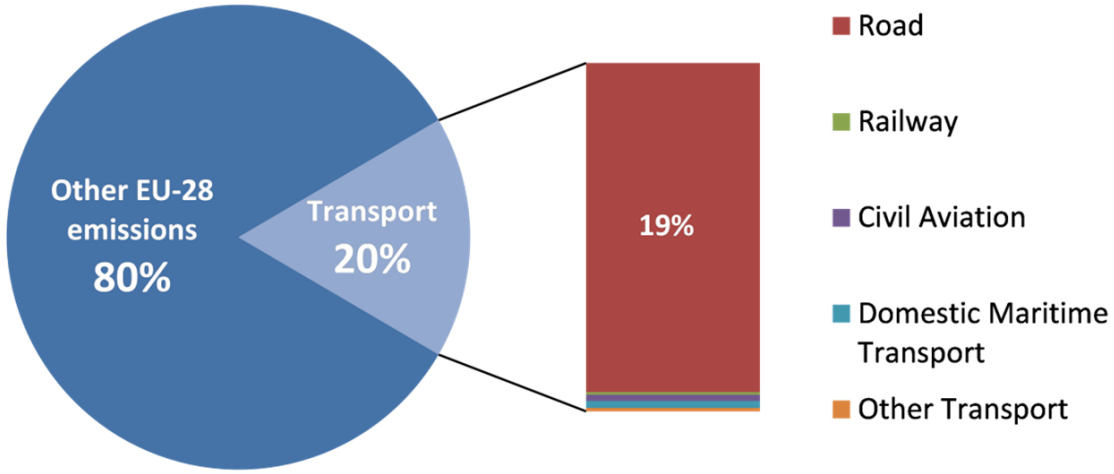

Figure 1.1: EU-28 GHG emissions (tons of CO_2 equivalent) by mode of transport in 2011 [1]

In order to reduce greenhouse gas emissions, the legislation has set mandatory emission reduction targets for new passenger cars. According to the European Environment Agency, average sales-weighted carbon dioxide (CO_2) emissions from new passenger cars in the EU were 118 g CO_2 /km in 2016 [2]. A decrease of 27% in average CO_2 emissions from new cars has been achieved from 2005 to 2016. With a similar pace of decrease, car manufacturers would meet the 2020/21 target[1] of 95 g CO_2 /km. As the reduction of CO_2 emissions and the fuel consumption are effectively proportional, an achievement of fewer fuel consumption and higher efficiency is the result. The gasoline fuel consumption has decreased from 6,9 l/100 km in 2005 to 5,1 l/100 km in 2016 [2]. The reduced fuel consumption contributes to the preservation of finite fossil fuels and the securing of energy supply as well. To reach these goals, thermal management plays an important role. Thermal management can reduce fuel consumption by 2% to 7,5 % over the next ten years [3]. Therefore, more than 60 thermal management technologies are currently in production or development. These technologies improve powertrain and passenger comfort system efficiencies.

[1] The 2020/21 target implies a decrease of 27% in average CO_2 emissions compared to the 2015 target, for each manufacturer group, as defined in [2].

During a cold start and a warm up phase, for example, the fuel consumption is higher than under optimal operating temperature because of a high oil viscosity and low combustion temperature. In order to reduce the fuel consumption during the cold start and the warm up phase, the engine operating temperature has to be reached in a possibly short period of time after starting the engine. One possibility to reach this goal is to store the waste heat during the operating temperature and to release it during the next cold start and warm up phase. In addition, this stored heat could be used for temperature regulation within the passenger cabin. As an optimal solution for the waste heat storage in automotive applications, a thermochemical heat storage system could be implemented, since it is able to store heat without losses for long term. In order to show how much energy is available to be stored in the thermochemical heat storage system integrated in automotive applications, exergy flow of an Otto engine at a typical load point with 2000 rpm and a 2 bar brake mean effective pressure (BMEP) during a new European driving cycle (NEDC)[2] is given in figure 1.2. The figure shows that, from the fuel converted exergy, 29% is effective power used to overcome driving forces, 32% is exhaust gas heat and 34% is coolant waste heat. The coolant waste heat represents the energy source for the thermochemical heat storage system.

Furthermore, the reuse of the coolant waste heat results in an increase of overall efficiency of the vehicle. An idealised thermochemical heat storage system implemented into a passenger car was simulated in research study [4]. The simulation showed reduced fuel consumption of up to 2% for a NEDC and over 7% for the starting temperature of -7°C.

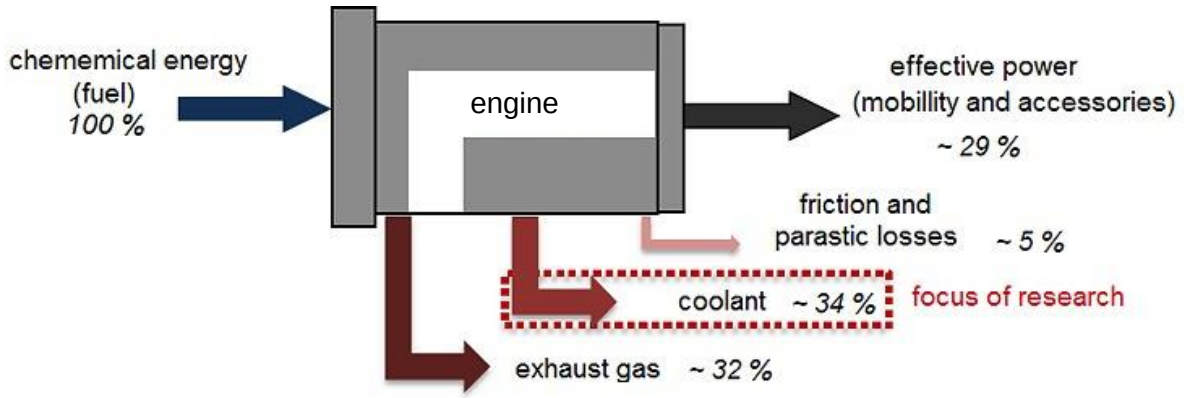

Figure 1.2: Fuel conversion efficiency for an Otto engine by 2000 rpm and 2 bar BMEP during a NEDC [5]

[2] NEDC considers the driving cycle as a combination between an urban cycle (800 s) and an extra urban cycle (400 s) with constant speeds, accelerations and decelerations.

1.2 Modular Thermochemical Heat Storage System

This master thesis is part of the research project “Wärmespeicherung III” funded by the Research Association for Combustion Engines (FVV) eV. The project is carried out by the Institute for Powertrains and Automotive Technology at the Vienna University of Technology, Austria. The aim of the project “Wärmespeicherung III” is to develop a modular thermochemical heat storage system for automotive applications and to examine its performance. Figure 1.3 gives a scheme of the modular thermochemical heat storage system for automotive applications. Since this is just a test system, the pump and valves v1 and v2 would not be necessary in a vehicle application. The working principle of the thermochemical sorption process is described in chapter 2.1.3 in more detail.

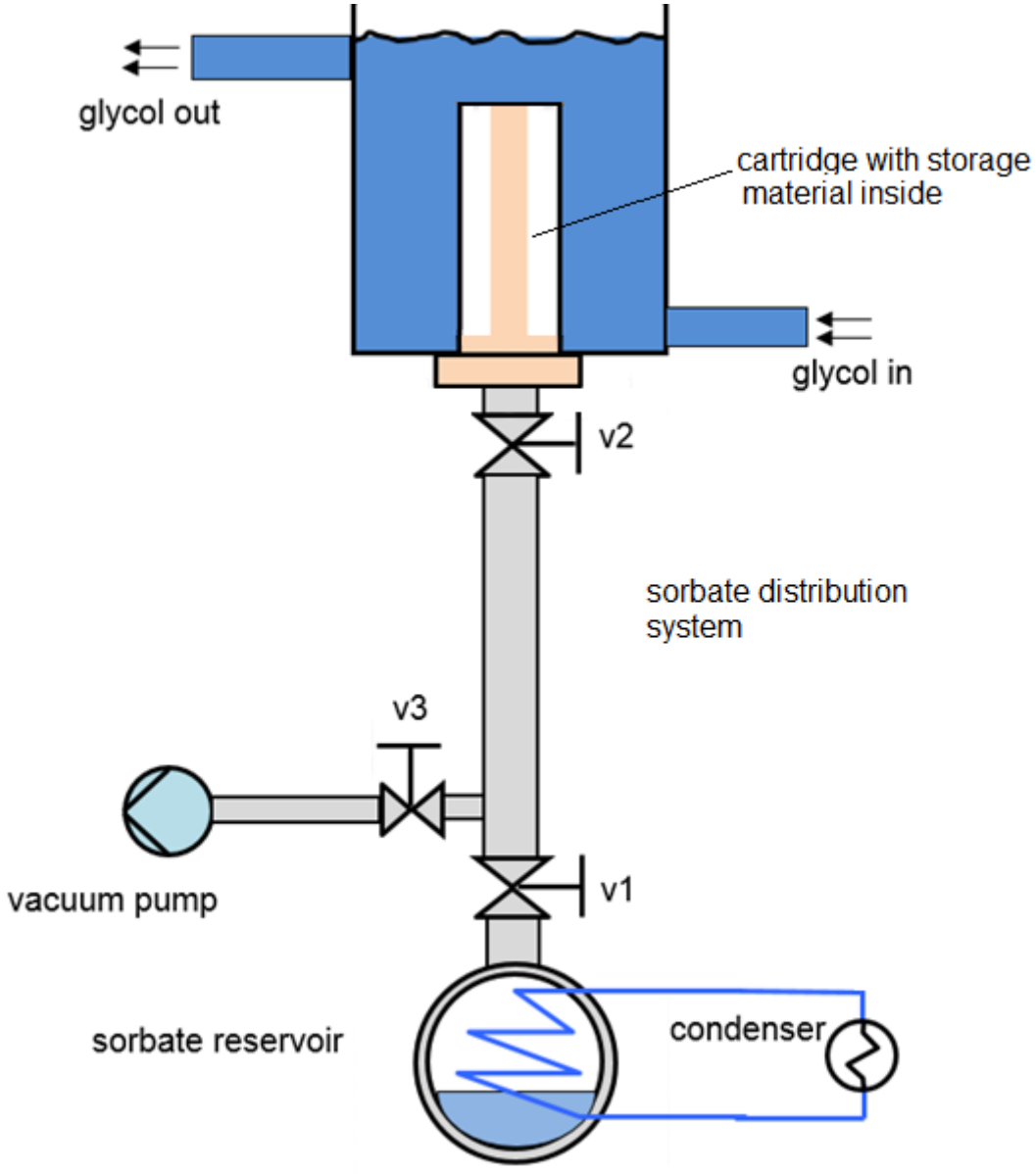

Figure 1.3: Test system of a modular thermochemical heat storage system [5]

The cartridge, where the thermochemical reaction takes place and the heat is released, is immersed in the engine coolant. The engine coolant represents a heat source or a heat sink, depending on the phase of thermal conversion. The sorbate distribution system is designed to connect the cartridge with the sorbate reservoir.

In the discharging phase, the sorbate in the reservoir evaporates. The evaporated sorbate streams through the pipes into the cartridge. The sorbate is then absorbed by the heat storage material and the heat is released. The released heat is transferred through the cartridge walls to the cold engine coolant which presents a heat sink at that moment. Once the engine operating temperature is reached, the coolant becomes the heat source and the phase of charging occurs.

In the phase of charging, the sorbate is decomposed from the heat storage material and the vapour condenses in the sorbate reservoir which has a lower temperature than the cartridge. After the phases of thermal conversion, discharging and charging, are finished, the reactants are separated by closing the valve. Thereby, the storage phase occurs.

Since the experimental prototype of the thermochemical heat storage system is often reassembled, the vacuum pump is added to eliminate the air from the system after the reassemble. An additional valve (v1) is added to keep the sorbate reservoir isolated from environment during the reassemble. The vacuum pump and the additional valve fall out in a thermochemical heat storage system which is to be implemented in automotive applications.

Considering the central design of a thermochemical heat storage system, the heat has to be transported through a heat transport system during the phases of thermal conversion. The main advantage of modular design of the thermochemical heat storage system is the lack of the heat transport system. Thereby complexity, weight and space requirements for the thermochemical heat storage system are reduced, compared to the central design. Furthermore, the modular thermochemical heat storage system can be integrated on different feasible locations due to the compact design [6].

1.3 Goals and Aims

In previous research work, developed cartridges were tested on a facility assembled without a sorbate distribution system. Since the cartridge will be integrated at variety feasible engine locations, the sorbate distribution system, which connects it with the sorbate reservoir, makes possible to situate the sorbate reservoir on different positions in passenger vehicle. In that way, space constraint of engine compartment could be overcome.

Nevertheless, the former prototypes have not shown constant performance during numerous tests and the reversibility of the cycle discharging – charging was not sufficient.

Therefore the goals as well as the aims of this master thesis are to optimise an existing thermochemical storage prototype in terms of modular design with an optimal sorbate distribution system and to investigate phenomena which might have adverse effect on the system performance.

A sorbate distribution system is developed and an effect of the sorbate distribution system on the cartridge performance is investigated. The research focuses on the flow losses in the sorbate distribution system, which might hinder delivery of one reactant to the other. Thus, the optimal sorbate distribution system which makes possible a modular integration of thermochemical heat storage system without adverse effect on the performance should be found.

Further, fluctuations of the cartridge performance with regard to different ambient temperatures as well as with regard to number of conducted tests are investigated. The research focuses on the phenomena referred in literature about the thermochemical heat storage systems. The research will clarify the limitation factors for high and constant cartridge performance as well as the capability of complete reversibility of phases of thermal conversion.

2 Fundamentals of Thermal Energy Storage Systems

Basic principles of thermal energy storage systems are briefly reviewed in this chapter. An attention is given to the chemical heat storage principle, whereby the solid-gas sorption process is discussed in more detail. The phenomena occurring during the sorption processes, which might have adverse effects on the thermochemical heat storage system, are referred from literature.

2.1 Heat Storage Systems

Desirable properties for any thermal energy storage system suitable to an application are high energy storage density, an adequate temperature level, high power capacity for charging and discharging, low thermal losses during the storage period, non-hazardousness to the environment and commercial availability, [7]. There are several types of categorization of thermal energy storage systems based on:

- Temperature level: low, medium and high temperature storage system
- Period of storage: short-, mid- and long-term storage
- Physical principle: sensible, latent and thermochemical heat storage
- Storage medium: e.g. water, salt, stone [8]

The division of thermal energy storage in sensible, latent and chemical heat storage is common for scientific purposes. The thermal energy storage materials used to realise the storage principles are represented in figure 2.1. An overview of the thermal energy storage principles is given in following chapters.

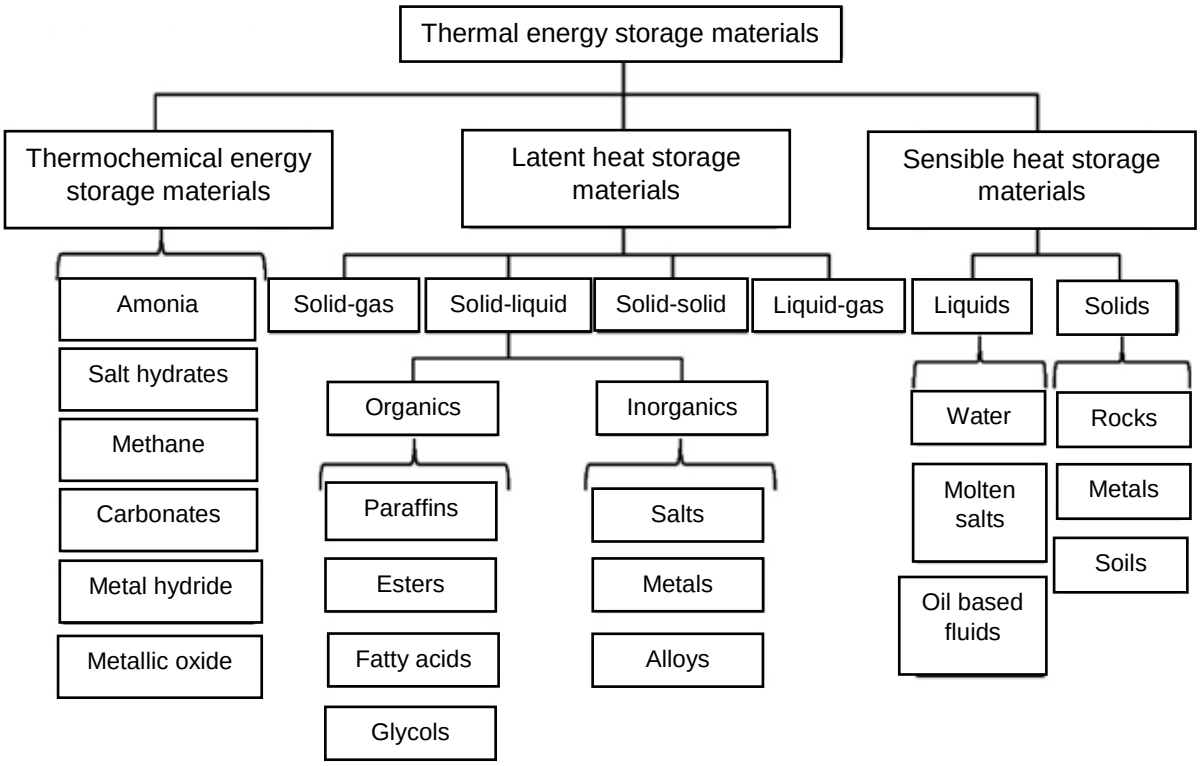

Figure 2.1: Thermal energy storage materials [9]

2.1.1 Sensible Heat Storage

The sensible heat storage is achieved through changing the temperature of a storage material. During charging and discharging, the temperature of the storage material increases and decreases, respectively. The amount of energy stored in the system is in correlation with the mass of storage material, a specific heat capacity of the storage material and the temperature change, as shown in the equation (1).

$$Q = m_{storage} \cdot cp_{storage} \cdot \Delta T \quad (1)$$

whereby

$m_{storage}$	mass of heat storage material [kg]
$cp_{storage}$	thermal capacity [J/kgK]
ΔT	temperature difference before and after charging [K]
Q	heat stored during charging [J]

Disadvantages of sensible heat storage systems are low volumetric and gravimetric storage density per temperature change and therefore the large temperature range needed for storing a significant amount of thermal energy. In order to minimize the heat losses during the storage, an insulation of the system is necessary [7], [10].

2.1.2 Latent Heat Storage

In an ideal situation of latent heat storage, no temperature change occurs during the phase change process as shown in figure 2.2. In theory, the temperature stays constant, while the amount of stored heat rises. While the heat is being added to the material, the phase transition of the material begins after the phase change temperature is reached. The phase change temperature stays constant until the phase transition finishes. The latent heat is stored through the phase transition of a material between solid, liquid and gas. The solid-liquid transition is called fusion and the liquid-vapour transition is called vaporisation. Molecules have lower freedom of movement in the solid phase than in the liquid phase and correspondingly, lower inner energy. Molecules in the liquid phase have still a lower degree of freedom than in the gas phase. In the gas phase, molecules are almost free of intermolecular attraction and possess a high inner energy. Therefore the heat of fusion is lower than the heat of vaporisation and correspondingly, more energy can be stored by liquid-vapour than by solid-liquid phase transition [11], [12].

The Ruths steam accumulator allows to charge heat of evaporation and condensation. This is the only industrially proven heat storage system with liquid – gas transformation. It uses sensible heat storage in pressurized saturated liquid water. By lowering the pressure of the saturated liquid during discharge, the water flashes to steam. During charging, either the saturated liquid water or superheated steam is injected into the accumulator. The superheated steam then condenses. The heat of condensation causes an increase of the temperature and the pressure with a small variation in mass [13], [14].

The amount of energy stored in the system is in correlation with the mass of heat storage material, the phase change enthalpy of storage material and sensible heat storage areas above and below the temperature of utilised phase change as shown in equation (2).

$$Q = m_{storage} \cdot \left[\int_{\vartheta_1}^{\vartheta_m} c_{ps} \cdot d\vartheta + \Delta h_m + \int_{\vartheta_m}^{\vartheta_2} c_{pl} \cdot d\vartheta \right] \quad (2)$$

whereby

$m_{storage}$ mass of heat storage material [kg]

Δh_m phase change enthalpy of storage material [J/kg]

$\vartheta_{m,1,2}$ melting-, initial-, final-temperature of the phase change material [°C]
c_{pl} thermal capacity of the phase change material in [J/kgK]
Q heat stored during charging [J]

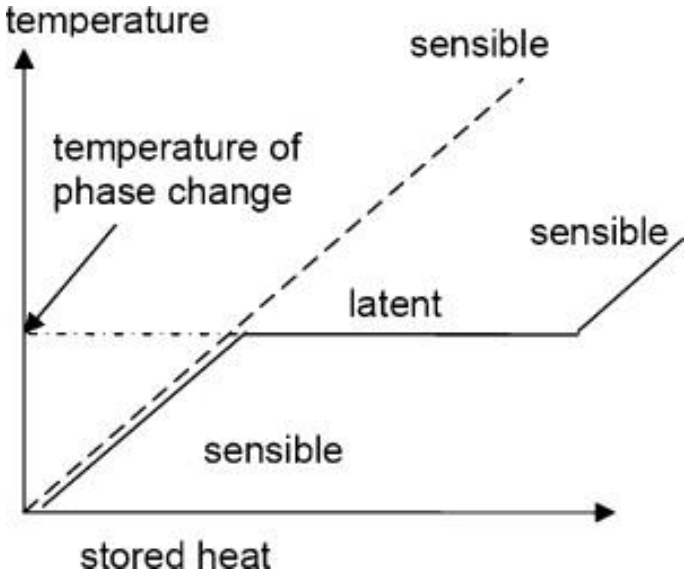

Figure 2.2: Temperature profile as a function of the amount of stored heat in the case of storage of sensible heat and latent heat [12]

Phase change materials (PCM) are divided into organic, inorganic and eutectics. Organic PCM are described as paraffin compounds and non-paraffin compounds, whereby the non-paraffin compounds are identified as esters, fatty acids and alcohols. Inorganic PCM are classified as salt hydrate and metallic. An eutectic is a composition of more components, for example Gallium–gallium antimony eutectic, Cerrolow eutectic, Cerrobend eutectic, etc. [15].

2.1.3 Chemical Heat Storage

In chemical heat storage systems, thermal energy is stored using stable chemical substances. Thereby, the thermal energy is converted into the chemical potential energy. The chemical substances undergo reversible chemical reactions to store or release the thermal energy. That kind of heat storage can be divided into chemical reaction heat storage and chemical sorption heat storage [16].

The heat storage and heat release process is described in (3) for **chemical reaction heat storage**.

$$A + heat \leftrightarrow B + C \tag{3}$$

Through an endothermic dissociation reaction, component A is split into B and C. The thermal energy is stored in produced substances B and C in form of chemical potential energy. During the storage period, B and C components are stored separately. When later the heat utilization is needed, A and B are brought together and the reversible reaction occurs. From the synthesis reaction between B and C, component A is regenerated and the stored thermal energy is retrieved.

Chemical reaction heat storage is realised using gas-gas reactions (reversible dissociation of ammonia $NH_3/N_2/H_2$ and sulphur trioxide $SO_3/O_2/SO_2$, decomposition of methanol $CH_3OH/H_2/CO$, etc), liquid-gas reactions (isopropanol/acetone/hydrogen, ammonium hydrogen sulfate, etc) and solid-gas reactions (thermal dissociation reaction of metal oxides, decarbonation reaction of carbonate, dehydration reaction of hydroxide, etc.) [16].

Similar to chemical reaction heat storage, during **sorption process heat storage**, the certain gas or vapour (sorbate) is captured or dissolved onto the surface of some solid or inner of liquid (sorbent) [16]. The storage of thermal energy is realized by breaking the binding force between the reactants in terms of chemical potential [17].

The sorption process heat storage is realised with different materials such as metallic halides ($CaCl_2$, $MnCl_2$, $CoCl_2$, $BaCl_2$, $NiCl_2$, NaBr, etc.) with gas reactant (NH_3, H_2O, H_2, CH_3OH, etc.). The working pairs are divided according to the reactants on ammoniated salts pairs, hydrate salts pairs, metal hydrides, concentrate dilutions, etc [16]. In addition, sorption processes based on salt hydrates are further divided in hydration reaction of salt hydrate with water and hydration reaction of salt hydrate with alcohol [17].

From the thermodynamical point of view, the thermochemical sorption processes are based on reversible reaction between sorbent and sorbate. For example, the thermochemical heat storage system based on salt hydrates uses a reversible chemical reaction represented in (4).

$$Salt \cdot xH_2O_{(s1)} + \Delta H_r \rightleftharpoons Salt \cdot (x-y)H_2O_{(s0)} + yH_2O_{(g)} \quad (4)$$

The system consists of three components ($Salt \cdot xH_2O_{(s1)}$, $Salt \cdot (x-y)H_2O_{(s0)}$ and $yH_2O_{(g)}$) in three phases (s_1-solid, s_0-less hydrate form and g-gas) and therefore, the thermodynamic equilibrium is monovariant. ΔH_r represents reaction enthalpy (J mol^{-1}) and x, y are stoichiometric coefficients. Theoretical thermodynamic equilibrium of the thermochemical sorption system (4) is given in Clausius-Clapeyron diagram, in figure 2.3. The solid-gas (S/G) and the liquid-gas (L/G) equilibrium lines are given by equation (5), [18].

$$ln\left(\frac{p_{eq}}{p^0}\right) = \frac{-\Delta H_r^0}{R \cdot T_{eq}} + \frac{\Delta S_r^0}{R} \quad (5)$$

Whereby is

p_{eq} equilibrium pressure (Pa)
ΔS_r^0 formation entropy of reaction (J $K^{-1}mol^{-1}$ of sorbent)
p^0 reference pressure (Pa)
R ideal gas constant (J $K^{-1}mol^{-1}$)
T_{eq} equilibrium temperature (K)
ΔH_r reaction enthalpy (J mol^{-1})

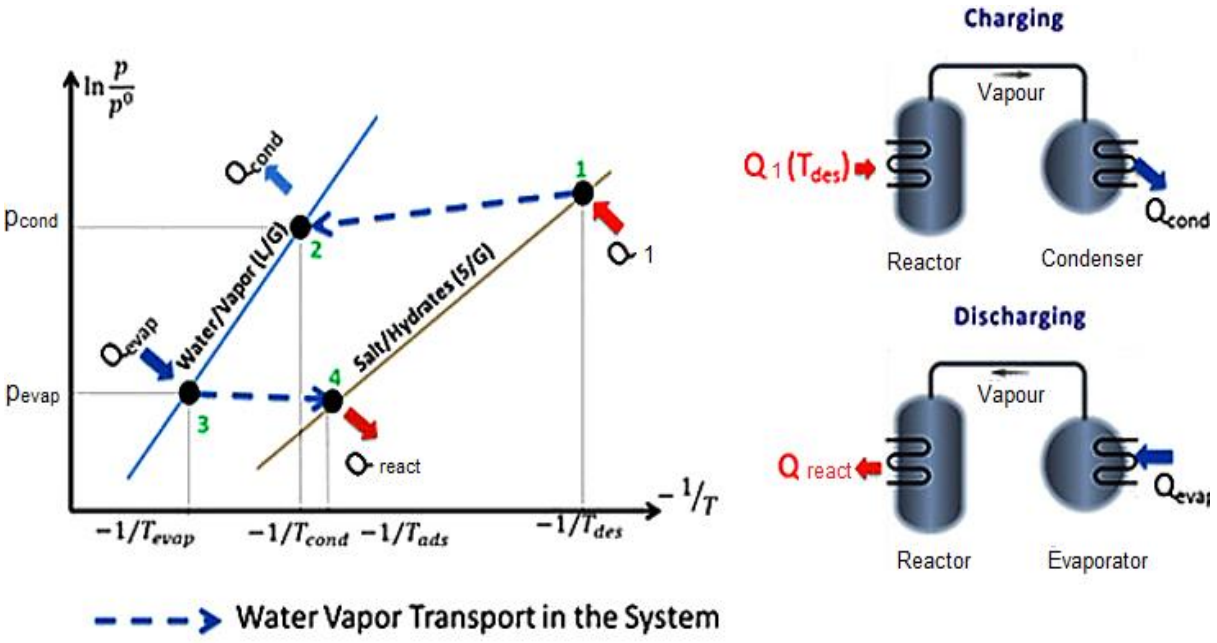

Figure 2.3: Theoretical thermodynamic equilibrium of a thermochemical system in the Clausius-Clapeyron diagram.1 decomposition; 2 condensation; 3 evaporation; 4 synthesis, [19]

Figure 2.3 right shows a simple thermochemical system which consist of a reactor and an evaporator/condenser. The system comprises four main processes: desorption, condensation, evaporation and adsorption/absorption. The system operates in two successive phases of thermal conversion with a time gap, called thermal energy storage, in between.

Figure 2.3 left shows theoretical thermodynamic equilibrium of the system in Clausius-Clapeyron diagram. The salt is in its desorbed solid less hydrate form (s_0) bellow the equilibrium line and in its solid hydrate form (s_1) above the equilibrium line of the solid gas reaction.

During the charging phase at high pressure (p_{cond}), the heat (Q_1) at high temperature (T_{des}) is supplied to the reactor and the solid state (s_1) decomposes. The released gas condenses at (T_{cond}) and (p_{cond}) by rejecting heat (Q_{cond}). During the discharging phase at low pressure (p_{evap}), the liquid evaporates by absorbing heat (Q_{evap}) at low temperature (T_{evap}) and the reaction heat (Q_{react}) is released at T_{sorp}.

Le Chatelier's principle[3] states that by increasing the temperature during thermal decomposition, the process shifts to vapour formation and an increase of pressure. The reaction can only take place if the reagent equilibrium is deviated to allow the reaction kinetic. The deviation is realized as a difference between temperature T_{des} imposed to the reactor and solid/gas equilibrium temperature $T_{eq}(p_{cond})$ at the reactor pressure, as represented in figure 2.4 right.

Similar to decomposition reaction, by decreasing the temperature during synthesis, the process shifts towards vapour absorption and decrease of vapour pressure. The deviation for synthesis is defined as the difference between temperature T_{ads} imposed to the reactor and solid/gas equilibrium temperature T_{eq} (p_{evap}) at the reactor pressure, (see figure 2.4 left) [17].

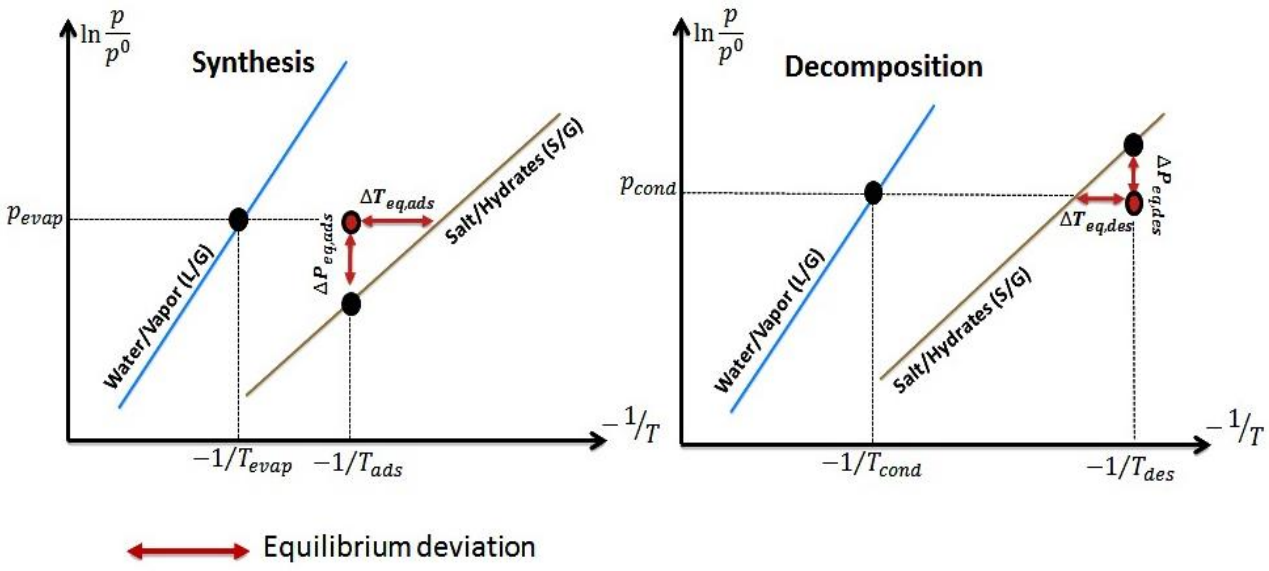

Figure 2.4: Deviation of thermodynamic equilibrium in synthesis (left) and decomposition (right) reaction [17]

[3] Le Chatelier's principle states that if temperature, pressure or concentration of a system in chemical or physical equilibrium are changed, then the system automatically alters itself so as to reduce the effects of the change. Le Chatelier, Henry Louis (1850 - 1936) was a French professor of chemistry, [64].

The stored thermal energy depends on the amount of storage material, the endothermic heat of reaction and the extent of conversion[4], as given in equation (6). [15]

$$Q = a_r m \Delta h_r \tag{6}$$

Whereby is:

Q heat stored during charging [J]
a_r extent of conversion
m mass of heat storage material [kg]
h_r reaction enthalpy [J/kg]

During the sorption process, molecules of sorbate are attracted by ions to form coordinate bonds. Since the molecular configuration of the compound is changed in a chemical reaction, there is no change in molecular configuration in the sorption process. Despite the difference between chemical reactions and sorption processes, they are all named chemical reactions, in order to homogenize the appellation [19].

Many research studies have been carried out on examining the various applications for thermal heat storage with sorption processes and material properties used in these systems [18], [19], [21], [22], [23] and [24]. In [19], the sorption process is described as fixation or capture of a gas or a vapour by a substance in condensed state, called sorbent. The sorption processes are further divided into adsorption and absorption.

During absorption process, the molecules of sorbate penetrate the surface layer and enter the structure of solid or liquid sorbent, causing the change of the composition of one or both bulk phases. Two different systems of absorption processes are described in the literature: absorption of a gas by a liquid [25], [26] and absorption of a gas by a solid [23], [27], [28].

On the other hand, during adsorption, the binding of a gas on a surface of a solid material occurs, whereby a physical adsorption and a chemical adsorption are possible. The physical adsorption involves the Van der Waals forces and the chemical adsorption is due to valence forces.

Further, the sorption processes are realised in open and closed systems. Open systems operate at atmospheric pressure, whereby the working fluid vapour is released to the environment. On the other hand, materials and working fluids are isolated from the environment and are under vacuum in the closed system. The vapour transport is improved due to lower resistance, in comparison with normal pressure, where additional gas molecules hinder vapour transport. The system pressure is

[4] Extent of reaction: ratio of the number of moles of a substance consumed or produced in a chemical reaction to its stoichiometric coefficient [64]

imposed by the pressure in the evaporator or condenser (sorbate reservoir) in a closed system, [19].

Advantages of chemically based thermal energy storage systems are their long-term storage possibility and high storage density. The specific storage density is defined by the reaction partners and respective reaction enthalpy. As the investigated system is based on the solid-gas salt hydrates reactions, the main important phenomena occurring in both desorption and absorption phase are described in more detail in following chapters.

2.2 Mechanism of Sorption Processes

The sorption processes are divided by the bonding mechanism of sorbate on sorbent to adsorption and absorption. Figure 2.5 represents a process of hydride formation, which corresponds to the mechanism of sorption processes of salts as listed in [27].

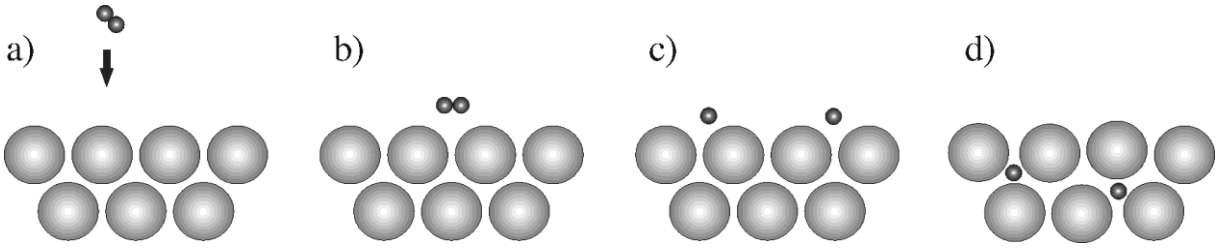

Figure 2.5: Dissociation and diffusion process of hydrogen in metal hydrides, steps a), b), c), d) [29]

The process of hydride formation, i.e. the absorption of hydrogen molecules into the metal lattice of the hydrides, occurs in four steps, as shown in the figure. The first step is called physisorption, represented in figure 2.5 a). Hydrogen molecules are attracted to the metal surface by Van Der Waals forces and no chemical bonds occur between the reactants [29]. For example, the physisorption occurs, under heat release, during enrichment of water vapour on surface of zeolites or silica gel [27]. In the next two steps, represented in figure 2.5 b) and c), the hydrogen gas molecule dissociates in two hydrogen atoms and the chemisorbed state is formed. The hydrogen atoms form new bonds on the metal surface. In the final step, represented in figure 2.5 d), the chemisorbed atoms can travel to subsurface layers and diffuse at the interstitial sites. This diffusion into the subsurface is called absorption. The diffused hydrogen atoms form a metal hydrogen solid solution called α-phase, which leads to the expansion of the metal lattice. α-phase is the solid solution phase, where the metal lattice expands proportional with the hydrogen concentration. With the diffusion progress and increase of hydrogen concentration, nucleation occurs and hydride β-phase is formed. α-phase, β-phase and (α − β) two phase region are represented in figure 2.6. It is evident that both the solid solution phase and the hydride phase coexist in two phase region [29].

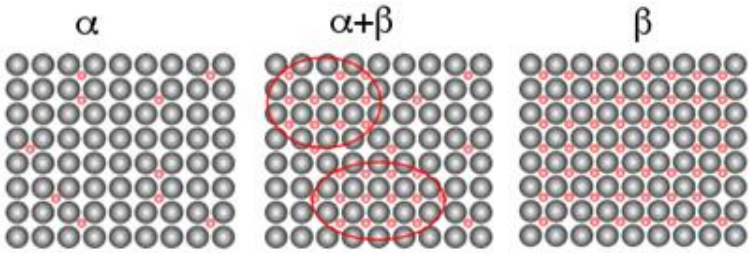

Figure 2.6: Formation of a hydride phase [29]

The term adsorption is understood as an enrichment of one or more components in the region between two bulk phases, i.e. the interfacial layer. In the system such as salt hydrates exposed to vapour, the adsorption is accompanied by a penetration of the adsorbate molecules into the interstices of the ionic lattice of the salt structure [19]. This penetration of adsorbate into the bulk of solid or liquid causes a change of composition of one or both phases. This process is called absorption.

The process of hydrate formation differs from the dissolution process [27]. The term absorption is sometimes referred to liquid/gas process, because it is widely applied in the refrigeration industry, [25] and [30]. The investigated thermochemical heat storage system consists of solid sorbent lithium bromide (LiBr) and gaseous sorbate methanol (CH_3OH). Therefore, the absorption is considered as absorption of gas by solid further in this thesis. The solid-gas sorption process is realised in a packed bed cartridge – designed vessels, in which the reaction takes place. According to the system configurations, the closed system has, besides advantages such as small and compact design and high reaction power, numerous disadvantages. They represent serious problem in the process operation. For example, the presence of non-condensable gases pose unneglectable problem, which will be discussed later on.

2.3 Heat and Mass Transfer

In order to analyse the performance behaviour of the thermochemical heat storage system at different conditions and an impact of different phenomena occurring during the sorption process, such as the effect of non-condensable gases on power release, it is necessary to discuss the heat and mass transfer in the reactive bed.

Taking into account the solid-gas thermochemical system, the solid phase is under porous media and it either receives or rejects the gas in order to fulfil the thermochemical reaction. To reach a high storage density, the density of the reactive bed needs to be high. High bed densities lead to reduced porosity[5] and permeability[6]

[5] Porosity – measure of the void spaces in material. Fraction of the volume of voids over the total volume [17]

[6] Permeability – measure of the ability of porous material to support the fluid flow through it [33]. Often related with porosity of a substance as it depends on the amount pore-space or porosity of the material [17].

of the reactive bed. Research study [31] showed that the permeability of the reactive bed varies during the reaction. The density of the reactive bed increases and the gas passage narrows during the absorption process due to a change in volume of salt hydrate grains. The gas passages become nearly blocked and result in a lower permeability at that position. Opposed to this, the reactive bed becomes more porous during desorption, leading to increased permeability. The reactive bed in solid – gas systems is sometimes built with composite materials, which consist of a host solid matrix and a reactive salt. They have random distributed pores in different sizes and shapes, whereby some of them are interconnected. The interconnected pores enable the heat and mass transfer through the reactive bed [32].

Heat transfer

The heat transfer occurs mainly by conduction in the case of solid-gas interaction and low temperature application in the packed reactive bed. The thermal conductivity of the reactive bed is a function of thermal conductivities of the sorbate, the sorbent, the host matrix, the porosity, the temperature and the diameter of the solid particles. The reaction rate between sorbent and sorbate is strongly linked to the thermal conductivity of the reactive bed during the composition reaction. With effective thermal conductivity of the reactive bed, the reaction rate increases [17]. Generally, low heat transfer in reactive beds occurs due to low conductivity of solid sorbent, sorbate gas and poor thermal contact between solid grains. The thermal contacts and the thermal resistances between the cartridge wall and the grain, between the grain and the gas and between the grains are clearly represented in figure 2.7. An additional thermal resistance due to voids filled with gas, which results from the lack of perfect contact between the wall and the thermochemical storage material, was observed in [33]. The host material, which could be integrated in reactive bed, improves the heat transfer because it has higher thermal conductivity than reactive salt.

Mass Transfer

The mass transfer of gas phase through the reactive bed occurs during desorption and absorption phases. It occurs from advection and from diffusion as referred in [17]. In advection, difference in pressure causes bulk motion of the gas, and diffusion describes relative motion of the gas. The pressure gradient along the porous bed is high, compared to diffusion coefficient in solid reactive beds.

According to [19], concentrations of the gas phase and of the solid phase change with time and with position in a fixed bed sorption. Figure 2.8 shows the concentration of the gas phase at positions in the reactive bed during absorption time.

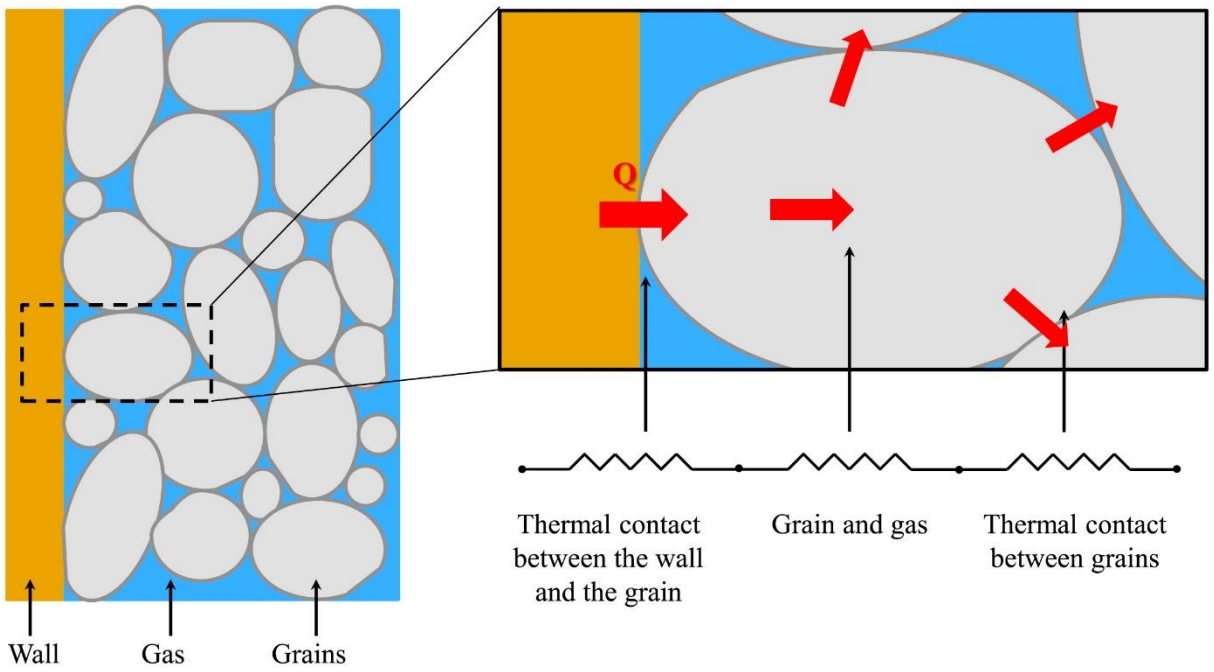

Figure 2.7: Thermal resistance along the heat transfer path in a porous bed [33]

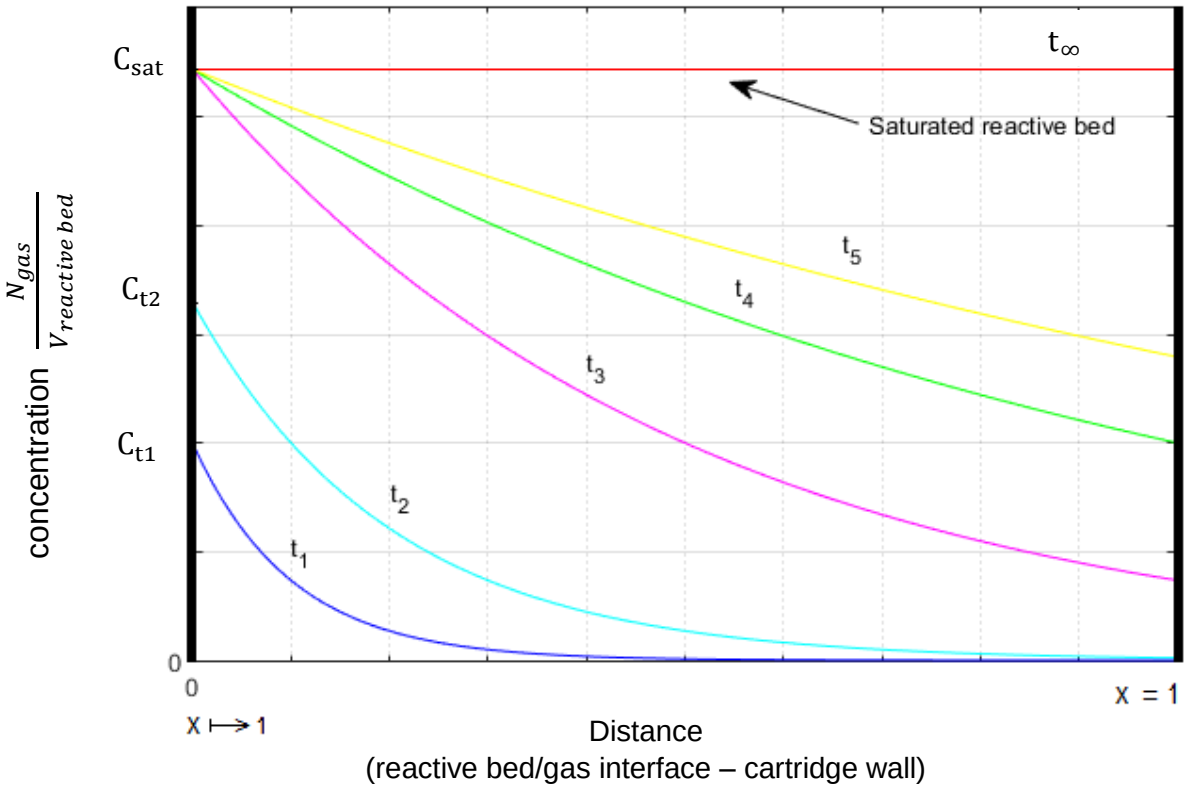

Figure 2.8: Concentration profile in the reactive bed

In figure 2.8, x-axis represents position in the reactive bed between inlet of the bed (reactive bed/gas interface, x=0) and cartridge wall (x=1) and y-axis represents concentration of gas in the reactive bed. The curves represent concentration of gas in the reactive bed in time step t_n ($t_0 < t_1 < t_2$ ...) from the beginning of the absorption phase, $t_0 = 0$.

The mass transfer takes place near the reactive bed/gas interface (x=0) most of the time. If the reactive bed is completely dehydrated to the anhydrous state at the beginning of the absorption phase, the concentration of the gas drops exponentially with distance essentially to zero before the end of the bed is reached [19]. That case can be clearly seen for time t_1 and t_2 in the figure. After some time, the reactive bed near the reactive bed/gas interface becomes slightly saturated. c_{sat} is reached at the interface and most of the mass transfer takes place further away from the reactive bed/gas interface. That case can be clearly seen in the figure for time points t_3, t_4, and t_5. In t_∞, the reactive bed becomes saturated and the gas concentration through the reactive bed profile is constant.

On the other hand, during desorption phase, the heat input causes an increase of temperature, which shifts the process towards vapour formation. Thereby, an increase of vapour pressure occurs [21]. The formed gas flows through the reactive bed to the low-pressure area and through the gas-solid interface to the sorbate reservoir. In order to ensure sufficient mass transfer, special consideration has to be given to the porosity of the reactive bed during the bed manufacturing process (see chapter 3.1). Furthermore, figure 2.9 shows the mass transfer mechanism in salt hydrates with porosity on the grain of salt level. The sorption mechanism depends on porosity levels of sorbent, whereby the higher porosity level results in the agglomeration of micro particles [33]. At first, extra-particular diffusion and diffusion through the grain surface into the macro-pores occurs. Vapour is transferred through macro-pores into the grain structure, in order to reach the micro grain of salt. A micro-porous transfer occurs on the micro grain level. The surface resistance layer and the thickness of the bed are limiting factors for the mass transfer.

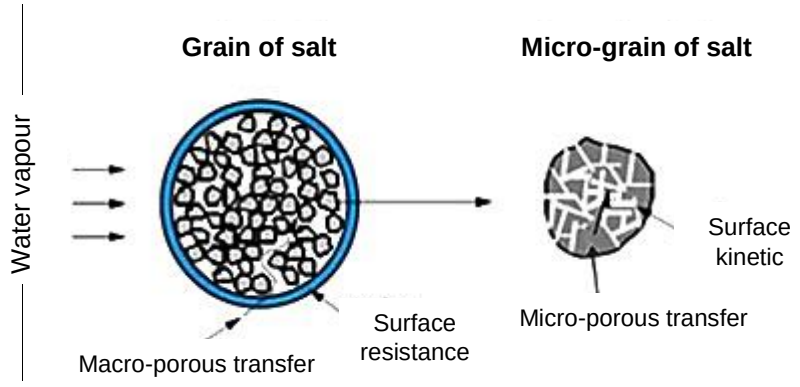

Figure 2.9: Mass transfer mechanism in salt hydrates with porosity [19]

During dehydration of salt hydrates, an additional phenomenon was reported in research study [33]. The sorbate is being transported through the crystal lattice, forming or breaking bonds, whereby the rearrangement of crystal lattice has been observed. The resulting resistance due to the rearrangement of the crystal lattice hinders the sorbate transport when the crystals are thick.

An adverse effect of low ambient temperature on sorption dynamic, which results with reduction of performances was reported in research study [27]. Reduction of pressure difference between the sorbate reservoir and the thermochemical reactor affected the sorbate evaporation quality.

In research studies [34] and [35], the effect of the non-condensable gases on the sorption processes in the solid-gas system was investigated. As referred in [35], a small amount of air or other non-condensable gases (0.3-0.9% of atmospheric pressure) in the system can drastically affect the performance of the heat storage system. In research study [34], it was observed that the mass and heat transfers are significantly hindered in the presence of air in closed systems during adsorption. The effect of non-condensable gases on absorption rates in aqueous LiBr was studied in [26]. The absorbed mass decreased by 50% in presence of 0,03%vol of air in the system.

Generally, the vapour adsorption and absorption on a grain of salt are controlled by surface and intraparticle heat and mass transfer resistance in the solid-gas system. As referred in [35], during the vapour adsorption, an extra heat and mass transfer resistance from the gas phase side is produced. If the non-condensable gas is present, it accumulates as a gas-rich layer at the solid surface and hinders the adsorption process. The vapour needs to diffuse through this non-condensable gas rich layer to reach the reactive salt or interface at which it condenses. This diffusion process is significantly slower than the absorption process and it results with reduced power release. The same phenomenon occurs during condensation process in presence of non-condensable gases.

2.4 Effect of Non-Condensable Gas on Condensation Process

In order to discuss the effect of non-condensable gas on condensation process, phenomena of evaporation and condensation are briefly discussed as referred in [36], [37] and [38]. The evaporation is a phenomenon of interfacial molecular transport, whereby a molecule is transported from liquid to vapour phase. The phenomenon is not well understood, since the temperature discontinuity at the liquid-vapour interface and, its direction and magnitude are controversial.

Considering the classical kinetic theory, on the molecular level, molecules are either escaping from a surface during evaporation, or they are being captured by a surface during condensation. The amount of molecules evaporated from the liquid is equal to those condensed from the vapour phase under equilibrium conditions. Under non-equilibrium conditions, a net mass flow occurs across the interface. The molecular flux leaving the liquid surface is greater than the flux coming from the gas phase during evaporation. On the other hand, condensation takes place when the molecular flux from the liquid surface is less than the flux coming from the gas phase. In general, there is a difference in temperature, pressure and chemical potential on either side of the liquid-vapour interface [37].

The evaporation or condensation process across the interfacial layer is largely driven by the difference between the bulk vapour pressure and the saturation pressure, corresponding to the liquid surface temperature [37]. The condensation occurs when the vapour comes into the contact with a surface, which has a lower temperature than the saturation temperature of vapour. The thermal energy of vapour is removed from the interface region. Thereby, the vapour loses its latent heat of vaporisation and condenses on the surface [38]. In presence of non-condensable gases, the condensation process is significantly hindered. Numerous research studies, [25], [39], [40] and [41], reported the influence of non-condensable gases on vapour condensation under different conditions. Theoretical investigations showed that the influence of non-condensable gases is important at lower pressure levels, since a non-condensable gas creates a significant mass and heat transfer resistance and therefore reduces the rate of condensation at the interface.

As reported in [35] and [42], in heterogeneous reactions accompanied by change in volume, a general flow of the reacting mixture occurs into the direction normal to the surface at which reaction is taking place. This flow, named Stephan flow, is added to the diffusion flux and changes the diffusion rate. The Stephan flow creates a layer of non-condensable gases on the interface during the condensation process. The condensation process is then governed by the diffusion of vapour (sorbate) through that layer, creating an extra mass and heat transfer resistance.

The phenomena occurring during film-wise condensation in presence of non-condensable gas are referred in [41]. A schematic of the condensation process with temperature and pressure distribution is given in figure 2.10. During the condensation process in presence of non-condensable gas, the non-condensable gas is carried with the vapour towards the interface and it will accumulate in the diffusion layer δ. Thereby, partial vapour pressure p_g drops and partial pressure of non-condensable gas p_a increases at the gas-liquid interface. In case of a higher partial pressure of the non-condensable gas at the gas-liquid interface than in the vapour gas mixture, $p_{ai} > p_{ao}$,

the driving force for gas diffusion is formed in reverse direction of the condensation. The motion of the non-condensable gas away from the surface is counterbalanced by the motion of the vapour-gas mixture towards the surface. The lower partial pressure of vapour at the interface than that in the bulk mixture, $p_{gi} < p_{go}$, provides driving force for vapour diffusion towards the interface. Temperature T_g corresponds to the saturation vapour pressure which is equivalent to the partial vapour pressure p_g.

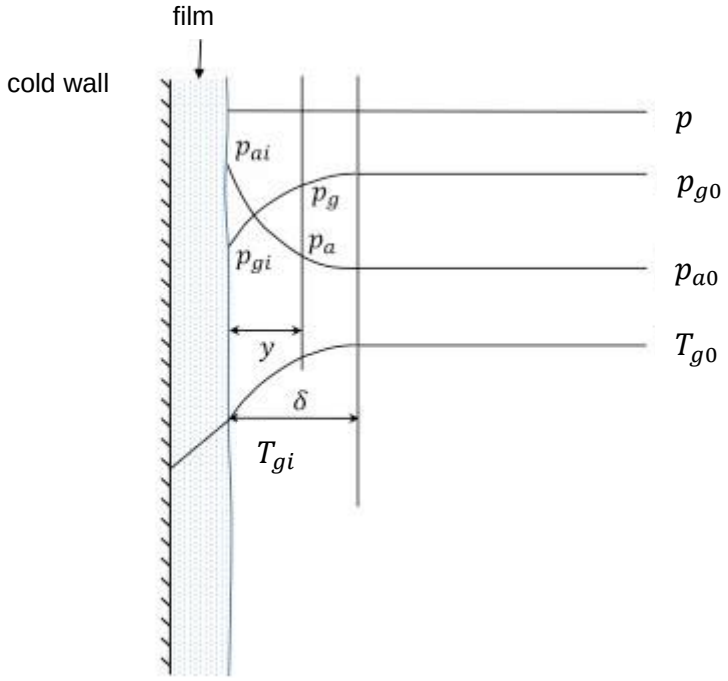

Figure 2.10: The influence of non-condensable gas on interfacial resistance [41]

In research study [39], the condensation heat transfer on horizontal tube was investigated. Although the bulk mixture of vapour- gas contained a small amount of non-condensable gas, a massive accumulation of the non-condensable gas was observed at the interface. On the other hand, desorption process was less affected by the non-condensable gas than the adsorption process in research study [34]. Thereby, the air-rich layer did not form during condensation.

2.5 Previous Findings

In the previous research work, various thermochemical storage materials were investigated for their suitability to be used in the thermochemical heat storage system for motor vehicles. Since the developed thermochemical heat storage system is based on the sorption processes of salt hydrates, LiBr, $MgSO_4$, $Al_2(SO_4)_3$, $CaCl_2$, $MgCl_2$ and $Mg(OH)_2$ were compared between each other. The characteristic power release, the heat storage capacity, the cycle stability, the environmental impact, the availability and the price of material were considered.

LiBr, $CaCl_2$ and $MgCl_2$ were further investigated with various carrier materials in order to form a suitable composite material, since they have shown the best performances. A carrier material is used in order to improve properties of reactive thermochemical storage material. Following advantages of a carrier material in composite are stated in [27]:

- improvement of mass transfer in reactive bed due to increased permeability
- improved material stability during cycling loads and reduction of adverse effects of volume change on cartridge
- fixation of reactive salt by the carrier material and hindering of active material leakage from the cartridge
- possible positive impact on thermal conductivity

Important criteria for selection of a suitable carrier material is chemical stability regarding the reactive salt and the sorbate. The carrier material has to be stable under operating conditions of the thermochemical heat storage system and has to ensure the heat and mass transfer through the reactive bed. Therefore, the chemically inert carrier materials glass wool, copper wool and ceramic foam have been tested in previous research works [6], [27] and [43].

The composite material composed of LiBr and glass wool showed the best properties regarding the tested characteristics referred above. Therefore, LiBr - glass wool composite was chosen as an optimal for this thermochemical heat storage system. Furthermore, as sorbate materials, methanol and water were examined in previous research works [6], [27] and [43]. The thermochemical heat storage system showed satisfactory sorption kinetics with both sorbates. Higher power release, higher total energy release as well as improved desorption kinetics were observed in the thermochemical heat storage system with methanol. The superior behaviour of methanol compared to water might be due to a higher vapour pressure of methanol, a lower heat of evaporation and a lower heat capacity compared to water. Better performance and lower desorption temperatures observed during the desorption of the thermochemical heat storage system with methanol than with water might be due to

lower binding forces between methanol and reactive salt. In addition, methanol posed safety concerns because of its flammability and toxic character and it is applicable at low operating temperatures under 0°C to which the thermochemical storage is exposed.

Furthermore, the cartridge is assembled of a thin copper sheet due to coppers high thermal conductivity. In order to enhance the heat transport from the storage material to the cartridge wall, copper fins are applied at the inside of the cartridge.

2.6 Conclusion of Fundamentals

The basic principles of thermal energy storage systems with main advantages and disadvantages are reviewed. The thermochemical heat storage system based on sorption process is discussed in more detail. Firstly, a distinction between thermochemical heat storage systems based on chemical reactions and sorption processes is clarified. Secondly, the principle of thermochemical heat storage system based on the sorption process of salt hydrates was described and different realizations are reviewed from the literature.

The main important phenomena such as the mechanism of sorption processes, the heat and mass transfers within the solid packed reactive beds are highlighted. Crucial for the cartridge performance are the reactive bed properties such as density, porosity and permeability. As referred in the literature, the heat transfer occurs mainly by conduction, whereas the mass transfer mechanism at a gas phase through the reactive bed occurs from advection, which is driven by a pressure gradient along the reactive bed and from diffusion. Finally, the phenomena which have had an adverse effect on the thermochemical heat storage systems such as the effect of non-condensable gases and the effect of low ambient temperatures on heat storage systems performance are referred from the literature in chapter 2.3.

3 Materials and Methods

The experimental facility used in previous research work was adapted with an additional sorbate distribution system to investigate the thermochemical heat storage system performance. A scheme of the experimental facility with heat and mass flows is given in figure 3.1. The facility comprises of the thermochemical heat storage system, a coolant system, a sorbate coolant system and a data acquisition system.

The thermochemical storage prototype system, based on heterogeneous evaporation[7], consists of the sorbate reservoir, the sorbate distribution system and the cartridge as described in chapter 1.2.

Further, the coolant system comprises of a coolant bath, a coolant reservoir, a coolant pump, an electric heater and coolant pipes. The coolant system represents the engine coolant system. The electric heater allows to simulate the engine operating temperature. The cartridge is immersed in the coolant bath and it exchanges heat with the coolant system.

An additional coolant system is connected to the thermochemical heat storage system in order to maintain temperatures in the sorbate reservoir. It comprises of a heat exchanger in the sorbate reservoir, a coolant pump, coolant pipes and a coolant reservoir. The sorbate coolant system can be connected to the public water supply system to maintain low sorbate temperatures during some experiments.

The data acquisition system comprises of temperature and pressure sensors. The sensors with their spatial arrangement and symbols are listed in table 3.1.

During the phases of thermal conversion, the heat and mass flows occur through the facility system. The heat and mass flow directions are marked with red and blue arrows for the absorption and the desorption phase respectively, see figure 3.1.

[7] Heterogeneous evaporation is a process based on the utilisation of heterogeneous reactions which take place simultaneously with a phase change from solid to gaseous state, whereby the evaporation is limited entirely to one of the reactants [27].

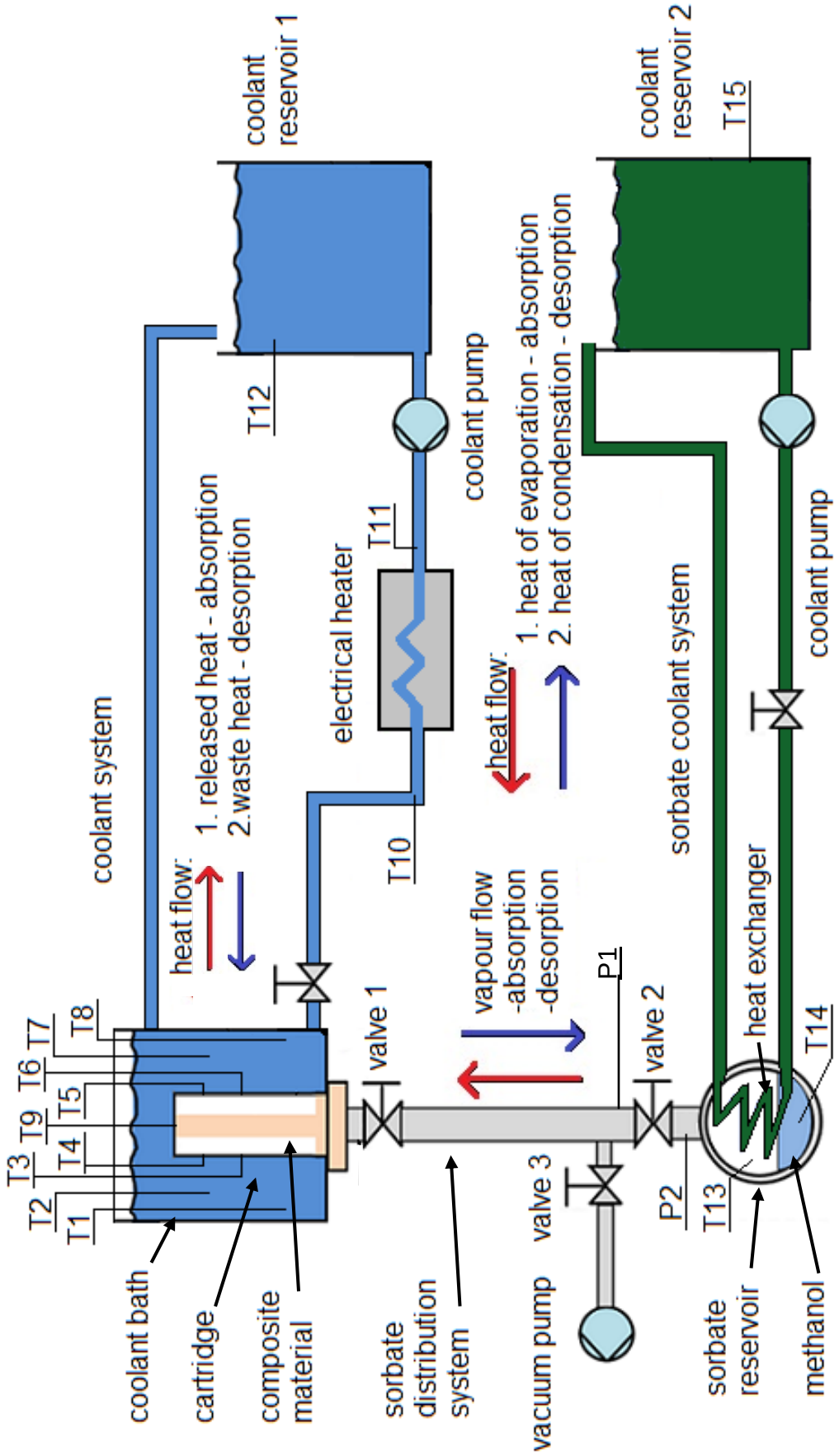

Figure 3.1: Scheme of test facility with instrumentation

During the absorption phase, methanol evaporates in the sorbate reservoir and the vapour flows through the sorbate distribution system to the cartridge due to a pressure difference between the sorbate reservoir and the cartridge. The heat for methanol evaporation is taken from environment. Due to the pressure difference and hygroscopic character of the reactive salt, the methanol vapour flows into the reactive bed, [17], and is absorbed by the thermochemical storage material. The released heat is than exchanged with the coolant in the coolant bath during absorption experiments, which represents an engine coolant system i.e. heat sink at that moment. Additionally, to improve the temperature distribution and to prevent a presence of temperature layers in the cartridge surrounding glycol during the absorption phase, an electric beater is added to the experimental facility in order to stir the glycol, [5], [6].

During the desorption phase, the coolant system is heated at the engine operating temperature by the electric heater. The heat of the coolant, which represents the waste heat of the engine at the moment i.e. heat source, is exchanged with the cartridge in the coolant bath. The appropriate temperatures boot desorption process. From the reactive salt decomposed methanol vapour flows from the cartridge through the sorbate distribution system to the sorbate reservoir due to the pressure difference between the cartridge and the sorbate reservoir. The vapour condenses in the sorbate reservoir and the heat of condensation is taken away with the sorbate coolant system.

In addition, the residual air, which remains in the thermochemical heat storage system after assemblage, is evacuated from the system with the vacuum pump before the experiments were conducted.

Besides the described systems, an electric convection oven is integrated on the facility in order to conduct desorption phases under atmospheric pressure. The oven is manually maintained in temperature range from 0°C to 230°C. Desorption phases were conducted in the electric oven during some experiments.

Table 3.1: List of sensors

symbol	sensor type	position
T1	temperature	coolant bath
T2	temperature	coolant bath
T3	temperature	cartridge wall
T4	temperature	cartridge wall
T5	temperature	cartridge wall
T6	temperature	cartridge wall
T7	temperature	coolant bath
T8	temperature	coolant bath
T9	temperature	cartridge wall
T10	temperature	electric heater inlet
T11	temperature	electric heater outlet
T12	temperature	coolant reservoir 1
T13	temperature	sorbate reservoir - vapour phase
T14	temperature	sorbate reservoir - liquid phase
T15	temperature	coolant reservoir 2
P1	pressure	sorbate distribution system
P2	pressure	sorbate reservoir

LabVIEW is used for a data acquisition, a visualisation and the operation of the facility. The control for coolant pumps and temperature control algorithms are provided by *LabVIEW* [6]. The pressure sensors were calibrated by using linearization. The deviations in pressure measurements are discussed in chapter 5.

A unique feature of this facility is its ability of simple adaption to different variants of sorbate distribution systems and prototypes of cartridges, whereby the real conditions, which occur in an engine, can be simulated.

3.1 Thermochemical Cartridge Design and Development

The cartridge jacket is made out of copper due to its high thermal conductivity (371 W/mK), and high corrosion resistance. Fins were soldered on the inner side of the jacket to increase a heat exchange surface between a reactive composite material and the jacket. The jacket was bended and soldered on the casing in an oven and fixed on a flange of messing, as described in [5].

Furthermore, a prototype of the cartridge was 3D printed of Al-Si alloy. Due to the advanced 3D printing technology and compact design, whereby the jacket and flange are printed together of the same material, less material is needed for production and the cartridge mass was reduced. Lower mass of the cartridge, i.e. passive mass, contributes to higher dynamic of heat exchange between the composite material and the coolant. A disadvantage of the 3D printed prototype cartridge is the lower thermal heat conductivity of Al-Si alloy compared to copper. That causes a time delay in power release during the absorption phase with Al-Si - cartridge. Figure 3.2 shows soldered and 3D printed cartridges.

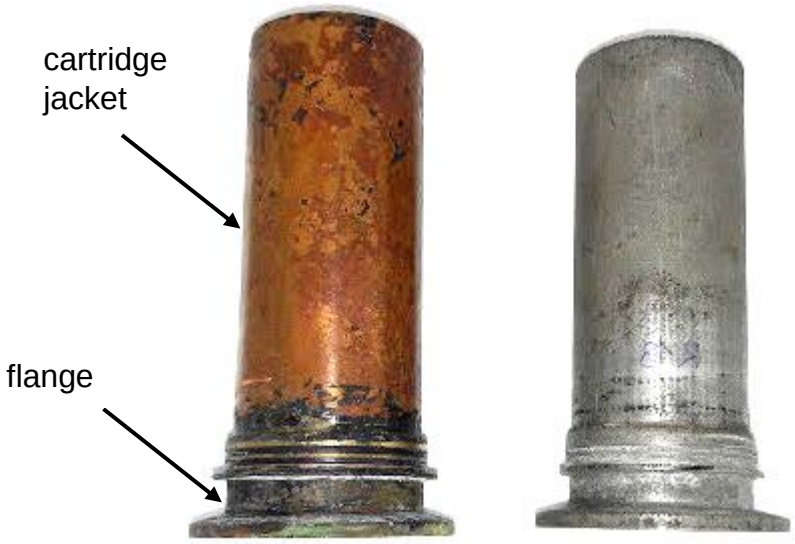

Figure 3.2: Soldered, left and 3D printed cartridge, right

The cartridges were filled with composite material consisting of LiBr and glass wool as discussed in chapter 2.5. Components LiBr and glass wool were chosen due to the best performance showed in research study [43]. The filing method, developed in previous research studies [6] and [43], was modified to keep a high porosity of the material, since the mass transfer through the reactive bed is dependent of the porosity as discussed in chapter 2.3.

Considering the reactive bed construction, the carrier glass wool was cut in small, non-directional (amorphous) pieces (1-2 cm) in order to obtain an optimal density of reactive bed. The cut carrier material was manually impregnated in cartridge between the fins on the cartridge jacket. In the next step, the impregnated carrier material was soaked with oversaturated LiBr - methanol solution and the surplus solution was extracted from the cartridge via the vacuum pump and the side-arm flask.

Thereafter, the filled cartridge was inserted in the electric oven in order to carry out the first desorption process. Thereby, the reactive salt (LiBr) remains impregnated into the carrier material and they form together the composite material. This first desorption process was conducted for more than 24 hours, as long as the overall mass of the filled cartridge remained constant.

The developed cartridges differ from one another in the mass of cartridge as well as in the mass of carrier material and in the mass of reactive salt impregnated into the reactive bed. These differences occur due to manual manufacturing procedure.

Table 3.2 gives an overview of the developed cartridges, its manufacturing method as well as the cartridge mass, the mass of carrier material and the mass of impregnated reactive salt. The cartridge number was given during tests in the laboratory and is not relevant for following results.

Table 3.2: Developed cartridges used for experiments

cartridge number	type	empty cartridge mass [g]	mass of glass wool [g]	mass of LiBr [g]	initial mass of reactive bed [g]
R8	Soldered copper	457,3	34,1	78,8	112,9
R9	Soldered copper	461,7	37,5	84,4	121,9
R11	Soldered copper	462,2	21,1	111,1	132,2
R13	3D print Al-Si	103,2	39,5	89,3	128,8

The maximum theoretical cartridge capacity depends on the amount of dry salt in the composite material. In theory, the more of the dry salt is in the reactive bed, the more energy can be released when thermodynamic equilibrium between the sorbate and the salt is reached. In reality, the reactive bed density and the porosity play important role in reaction kinetics and are limiting factors for the mass transfer in the reactive bed and the power release during the absorption phase (300 s). In order to reach high energy and high power release during the absorption phase, an optimal porosity of the reactive bed is needed.

3.2 Sorbate Distribution System

On one hand, main advantages of the modular concept of the thermochemical heat storage system are compact system size and design, a possibility to integration on feasible heat locations and a drop of the additional coolant distribution system with heat exchangers which contributes to a low overall system mass.

On the other hand, space constraints of an engine compartment, as well as high ambient temperatures near the engine, which might have an adverse effect on the operation of the thermochemical heat storage system, represent possible problems for an implementation of the modular thermochemical heat storage system in automotive applications. These problems might be overcome by an implementation of an optimal sorbate distribution system between the cartridge and the sorbate reservoir.

The sorbate distribution system connects the cartridge and the sorbate reservoir and aims to sorbate transport between them, (see figure 1.3). Besides that, it makes possible for the cartridge and the sorbate reservoir to be positioned separated, on different locations within the passenger car.

Arguments against the sorbate distribution system are an increase of thermochemical heat storage system mass, an occupation of space in engine compartment and a possible adverse impact on the cartridge performance due to sorbate flow losses.

Consequently, the various sorbate distribution systems set ups were developed in this master thesis. The sorbate distribution system compartments were manufactured by Pfeiffer Vacuum Austria GmbH. The compartments were made of stainless steel 1.4301/304 in accordance with DIN 28403. The joints were connected by elastomer seals and clamping rings to avoid air leakage in the system. Vertical as well as horizontal orientations of assembled sorbate distribution systems are shown in figure 3.3 and figure 3.4 respectively.

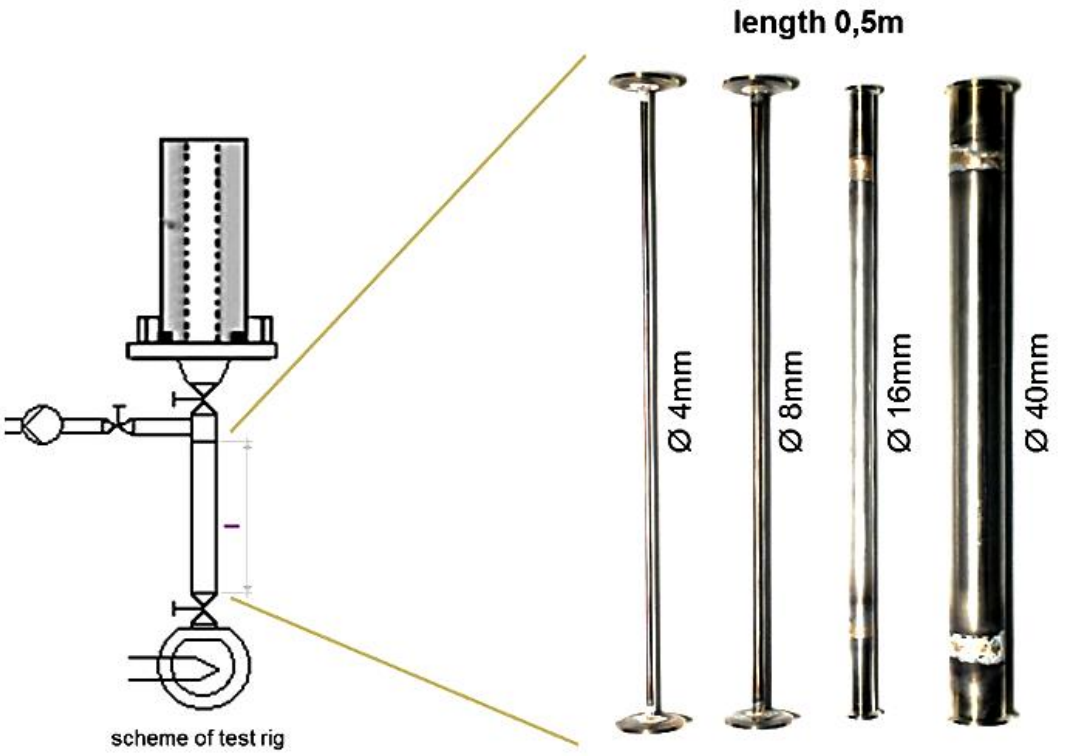

Figure 3.3: Vertical orientation [5]

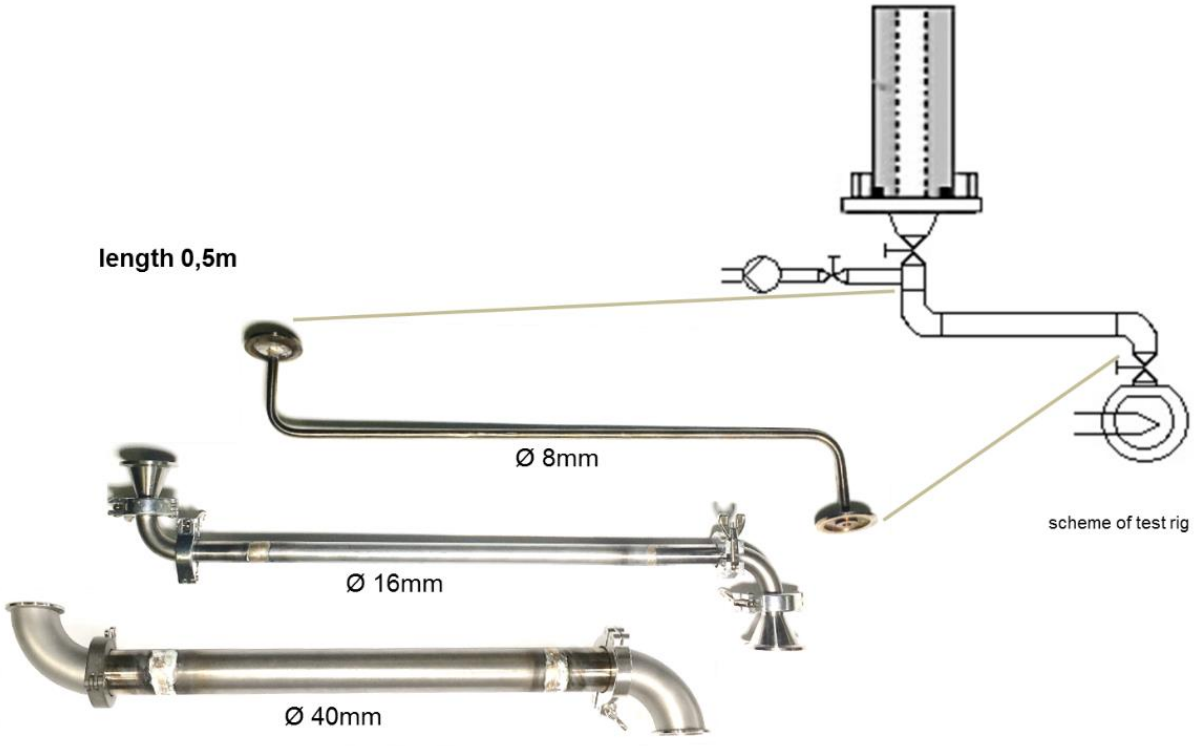

Figure 3.4: Horizontal orientation [5]

The developed sorbate distribution systems set ups with parameters are listed in table 3.3. Tube length of 0,5 m represents a possible offset between the cartridge and the sorbate reservoir in engine compartment. Pipe diameters were chosen in accordance with DIN 28403. Additionally, different orientations were chosen to investigate any possible impact of orientation on the sorbate flow.

Table 3.3: System set ups with parameters

system symbol	set up orientation	tube length [m]	inner tube diameter [mm]	set up orientation
S0	reference system	0	-	reference system
S1	vertical	0,5	16	vertical
S2	vertical	0,5	40	vertical
S3	vertical	0,5	4	vertical
S4	vertical	0,5	8	vertical
S6	horizontal	0,5	8	horizontal
S7	horizontal	0,5	16	horizontal
S8	horizontal	0,5	40	horizontal

3.3 Test Procedure

In order to carry out investigations, the facility was assembled. Due to the fact that the facility has to be reassembled often, a simple design of it, shows imperfections in the component joints. Vacuum tightness was proven through observing the rate of the pressure rise within the system. A continuous rise of absolute pressure would mean that an air leakage occurs. When the pressure measured in the sorbate reservoir at the equilibrium condition was higher than the saturation vapour pressure, equivalent to the temperature in the sorbate reservoir, the presence of non-condensable gases in the system was observed.

Beside an optimal design of the cartridge (optimal reactive bed density, efficient heat conduction in the reactive bed and optimal sorbate flow through the reactive bed), the cartridge performance depends on the conditions listed below:

- **sorbate temperature** is not constant during the absorption phase due to sorbate evaporation, it is depended on the ambient temperature
- **ambient temperature** is maintained to be constant to simulate different conditions at which the phases of thermal conversion might occur in automotive applications
- **sorbate pressure in the system** is equivalent to the sorbate temperature
- **duration of phases of thermal conversions** was chosen to simulate a real cycle, which might occur in automotive applications
- **desorption temperature** (coolant temperature) was chosen to simulate real temperatures occurring in an engine. The desorption temperature must be high enough to boot the decomposition reaction of salt hydrates.

The typical real heat storage cycle conducted on the test facility is represented in figure 3.5. The cycle consists of an absorption and desorption phase.

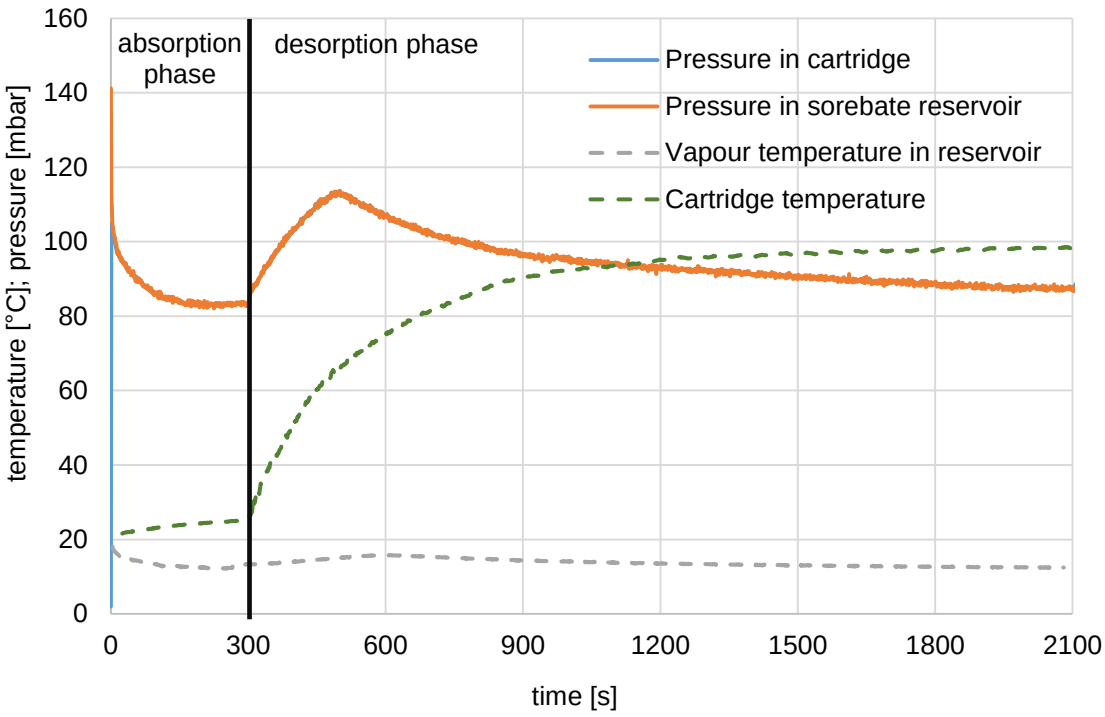

Figure 3.5: Real heat storage cycle

- **Absorption** phase was conducted for 300 seconds. After the cartridge was assembled to the facility, it was evacuated and cooled to an ambient temperature. The cartridge was then immersed into the coolant bath, whereby both were at an ambient temperature. The sorbate pressure in the reservoir at the thermodynamic equilibrium is equivalent to sorbate, i.e. ambient temperature. The pressure in the cartridge is 2 – 3 mbar, equivalent to the ambient temperature.

Figure 3.5 shows that at the start of the absorption phase, the pressures between the sorbate reservoir and the cartridge were balanced immediately. As the sorbate evaporates, the sorbate temperature and therefore, the pressure in the system decreases. Simultaneously with evaporation, vapour is absorbed in the reactive bed and the reactions heat is released. The cartridge temperature increases. The amount of absorbed methanol and the released heat are proportional, while the power release of the cartridge depends on the heat and mass transfer through the reactive bed and the cartridge jacket.

- **Desorption** phase was conducted for 1800 seconds. It follows the absorption phase as represented in figure 3.5. The electric heater (see figure 3.1) heats the coolant to the desorption temperature. The coolant heating phase was included in the desorption phase as well, in order to simulate the possible working conditions that a thermochemical heat storage system would experience during the cold start phase by implementation into an automotive application. The pressure in the system is equivalent to the sorbate temperature. The pressure peak in second 500 (see figure 3.5) is believed to take place due to the beginning of decomposition of the sorbent and sorbate [27]. Thereby, the decomposed vapour flows to the sorbate reservoir and condenses. Due to the released heat of the condensation, the sorbate temperature slightly increases. The heat of condensation is then removed with the sorbate coolant system (see figure 3.1), whereby the sorbate temperature as well as the pressure in the system decrease.

The cartridge masses were measured before and after the cycle. The difference in those masses represents the amount of residual sorbate in the cartridge. During the tests evaluation, the amount of absorbed methanol was predicted, as described in chapter 3.4.2. The ratio of desorbed and absorbed methanol represents the reversibility of the heat storage process.

- **Desorption phase in the electric oven** was carried out under atmospheric pressure. According to figure 2.4, this would be another operating point than in a closed system with lower pressure. However, a temperature of 100°C was chosen for the desorption in order to simulate the temperature occurring in an engine and to assure, desorption will take place. Lower pressure in the system even favours desorption more. The desorption phase was over when the cartridge showed no change in weight during the heating in the oven. The mass of cartridge was measured before and after the desorption process, to evaluate the reversibility of the desorption process.

During the conduction of the absorption and desorption phases, initial conditions in the thermochemical heat storage system must be taken into consideration. Due to the evacuating of the residual air from the sorbate reservoir, the methanol evaporates. Thereby, heat is consumed from the environment and a discontinuity in temperature distribution through vapour and liquid methanol comes into existence. Due to a limited amount of temperature elements, this exact temperature distribution cannot be measured and real conditions in the reservoir cannot be calculated. It was necessary to wait until a uniform temperature distribution was set in the sorbate reservoir. The equilibrium condition in the sorbate reservoir was defined as the methanol vapour temperature only differs 1°C from the methanol liquid temperature. The temperature and the pressure at the equilibrium state in the sorbate reservoir are crucial parameters for the investigation of presence of non-condensable gases in the thermochemical heat storage system, as discussed in chapter 3.4.1.

During this master thesis, following investigations of the thermochemical heat storage system were conducted:

1. **Investigation of the sorbate distribution system** was carried out in order to determine how the cartridge performance is affected by the sorbate distribution system. Different pipe diameters of the sorbate distribution system in different orientations were assembled on the test facility between the cartridge and the sorbate reservoir, (see figures 3.3 and 3.4). Absorption phases were conducted on the test facility with assembled sorbate distribution systems at the ambient temperatures which were in the same range (20°C). The conducted tests were evaluated as described in chapter 3.4.1 and the cartridge performances were compared to each other. In the next step, a flow analysis was conducted in order to obtain flow losses during the absorption phases as described in chapter 3.4.2. Predicted pressure drops for each set up were compared to each other.
2. **Effect of ambient temperature on the cartridge performance** was investigated at ambient temperatures of -10°C, 0°C, 10°C, 20°C and 30°C, maintained in climate chamber. The focus of this investigation was placed on the power release at different ambient temperatures. Under these temperatures the thermochemical heat storage system is to be used in automotive applications. Absorption phases (300 s) were conducted, whereby the initial state of cartridge was the same before the tests. Difficulties with vacuum tightness at low temperatures were overcome with an additional valve connected with the vacuum pump and extra lubrication of butterfly valves, (see figure 3.1). Obtained power releases at different ambient temperatures were compared to each other and discussed.

3. **Durability tests** were conducted with the cartridge connected directly to the sorbate reservoir. The purpose of those experiments was to investigate the behaviour of the cartridge performance in 15 successively conducted tests. Crucial for this investigation was to carry out the desorption phases under the same conditions, at a temperature of 100°C and under atmospheric pressure in the electric oven, until the mass of the cartridge did not change (6 hours). The cartridge mass was measured before the absorption and the mass of the reactive bed was determined. The absorption phases were carried out at an ambient temperature of 20°C. A trend of total released energy after absorption (300 s) with regard to the number of conducted tests was analysed and the occurring phenomena were discussed. Furthermore, a trend of average power release in representative tests was analysed. In order to discuss a decay of performance from the energy trend, the amount of residual air in the thermochemical heat storage system was determined. In addition to the durability tests, relevant conducted tests, which showed low performance, were analysed to investigate **the effect of non-condensable gases on cartridge performance**. Due to imperfections of the test facility, a contamination of dry air might occur and cause fluctuations in the cartridge performance. Therefore, the purpose of those experiments was to investigate how the cartridge performance changes in presence of different amounts of dry air within the thermochemical heat storage system. Moreover, tests conducted at different ambient temperatures were considered as well. Crucial for this investigation was that the initial state of the cartridge was the same before every test, to avoid a possible adverse influence on the cartridge performance due to the reduced theoretical heat capacity and the permeability in the reactive bed (see chapter 3.1). Amounts of dry air within the thermochemical heat storage system were determined in the conducted tests at ambient temperatures of 20°C and -10°C. Total released energies (300 s) were compared to each other and a coherence between the amount of dry air and the total released energy was observed.
4. **Reversibility analysis** was carried out to investigate if a reversible heat storage cycle would be possible under simulated possible engine conditions. The cycle tests consisted of absorption (300 s) followed by desorption (1800 s). Crucial for this investigation was that the states of cartridge (mass of reactive bed) were equal before the compared tests. The absorption phase was conducted at ambient temperature of 20°C and desorption phase was conducted on the test facility, whereby different conditions were maintained. The mass of the reactive bed was measured before and after the cycle. The facility was not reassembled after the absorption phase in order to avoid the contamination of the system with air. Therefore, the mass of absorbed methanol during the absorption phase was not measured. The difference between measured masses of reactive bed

before and after conducted cycle test represents the mass of residual methanol which is not desorbed from the reactive bed. The reversibility of the cycle is defined as the ratio of desorbed and absorbed methanol. If no residual methanol remains within the reactive bed, the heat storage cycle is considered as completely reversible.

3.4 Test Evaluation

The measured temperatures, pressures and cartridge masses were used as the input data for the evaluation of the conducted tests. The logged data were imported in an excel template, to visualize the temperature profiles and to calculate the power release and the released heat during absorption. Additionally, the template was adapted to calculate the amount of the residual air in the sorbate reservoir as well as to predict the evaporation rates and the flow losses in the sorbate distribution system.

3.4.1 Released Energy, Power Release and Dry Air Calculation

The terms power release and the released heat relate to the sensible power and sensible heat developed during the absorption phase. They were calculated using the mass of heated coolant in coolant bath, the heat capacity of the coolant and the temperature rise per second measured in the coolant bath, as suggested in [43] and shown in equation (7). See figure 3.1.

$$P = \frac{dQ}{dt} = \frac{m_{coolant} \cdot c_{p\ coolant} \cdot (\vartheta_{t+1} - \vartheta_t)}{dt} \quad (7)$$

Whereby

P	power release [W]
dQ	released heat [J]
dt	time step [s]
$m_{coolant}$	mass of the coolant in the coolant bath [kg]
$c_{p\ coolant}$	heat storage capacity of the coolant [$Jkg^{-1}K^{-1}$]
$\vartheta_{t+1} - \vartheta_t$	temperature increase of the coolant in coolant bath per second [K].

Since the thermochemical heat storage system helps to reach the operating temperature of an engine faster after the cold start, crucial property is fast heat release. The power release is calculated for each time step and significant power peaks and bottoms might occur between the time steps, due to non-uniform reaction rates and errors in the temperature measurements. Therefore, the average power release is calculated over 30 s, 60 s and 90 s from the beginning of the absorption phase to determine the effective power release of the thermochemical heat storage system. In

addition, the total released energy after 300 s was calculated for every test. Those data were compared to other tests.

As discussed in chapter 2.4, the non-condensable gas within the thermochemical heat storage system accumulates as a gas-rich layer at the solid surface and hinders the absorption process. As the surface of the solid-gas interface is nearly the same by every cartridge and the non-condensable gas always accumulates at the surface where the reaction takes place, an absolute amount of dry air in the thermochemical heat storage system was calculated as suggested in [7].

Although a small air leakage might occurred due to the imperfections in the assembly of the facility as discussed before, an increase of dry air in the thermochemical heat storage system during the test runs could not be calculated due to strongly non-equilibrium conditions. However, it is assumed that the amount of dry air in the thermochemical heat storage system remains constant during the tests. Thus, the cartridge and the sorbate distribution system are evacuated and the amount of dry air in the sorbate reservoir is calculated at the equilibrium condition. This amount is the total amount of dry air in the thermochemical heat storage system.

The logged temperatures of the liquid methanol and vapour - air mixture, as well as the absolute pressure in the reservoir were disposed. The methanol vapour and the humid air from the ambient form the vapour - air mixture in the thermochemical heat storage system. For the simple reason that water contained in the humid air is absorbable, i.e. condensable, and its calculated amount did not exceed $10^{-7}\ \frac{mol_{water}}{mol_{mixture}}$, it is assumed that the mixture consists of methanol vapour and dry air. The saturation pressures of the methanol vapour for measured mixture temperature was calculated with *Antoine equation* (8) and *Antoine parameters* for methanol given in [44] and [45]. The obtained saturation pressures correspond to the values referred in [46].

$$\log(\mathrm{p}) = A - \frac{B}{(T+C)} \tag{8}$$

Whereby

p	partial pressure of component [mbar]
A, B, C	Antoine parameter [K or °C]
T	Temperature [K or °C]

The saturation pressure of the methanol vapour is the partial pressure of the methanol vapour in the mixture. The partial pressure of dry air in the thermochemical heat storage system is obtained from equation (9):

$$p_{dry\ air_TCHS} = p - p_{m_TCHS} \tag{9}$$

Whereby is

$p_{dry\ air_TCHS}$ partial pressure of dry air in the TCHS system [mbar]
p_{m_TCHS} partial pressure of methanol in TCHS system [mbar]
p total pressure measured in TCHS system [bar]

As referred in [7], all gases or vapours exhibit ideal-gas behaviour at very low pressures and therefore, by employing the ideal gas law, the amount of dry air and methanol vapour in the mixture within the sorbate reservoir were calculated in (10):

$$p_{component} \cdot \left(V_{reservoir} - V_{liquid}\right) = n_{component} \cdot R \cdot T_{mixture} \quad (10)$$

Whereby

$p_{component}$ partial pressure of component in vapour-air mixture [mbar]
$V_{reservoir}$ volume of sorbate reservoir [m³]
V_{liquid} volume of liquid phase within reservoir [m³]
$n_{component}$ amount of component in vapour-air mixture [mol]
R universal gas constant [J kg^{-1} K^{-1}]
$T_{mixture}$ temperature of vapour-air mixture [K]

3.4.2 Sorbate Flow Analysis

Considering the thermochemical heat storage system for automotive applications, the focus is placed on a high power density, which ensures a fast heat release to the engine coolant and the increase of the engine temperature during the cold start and the warm up phase. In order to achieve a high power density and a fast heat release, beside the design of the reactive bed, it is necessary to ensure an optimal sorbate transport from the sorbate reservoir through the distribution system to the reactive salt. During the sorbate transport through the sorbate distribution system, viscous actions lead to friction between the fluid and the pipe, causing a loss of energy. The loss of energy is reflected as a fall in pressure along the pipe and depends on the flow rate, [47]. As reported in [27], a reduced valve diameter affected the sorbate flow in an investigated chemical heat storage prototype, resulting in the reduced power release compared to a bigger valve diameter. Considering different sorbate distribution systems set ups, the pressure drop might have an effect on the cartridge performance in our thermochemical heat storage system. Therefore, the flow losses through the sorbate distribution system were investigated.

If changes in the fluid pressure and the temperature do not appreciably affect the fluid density, the flow is considered as incompressible. Thereby, a part of mechanical energy in the flow is converted to thermal energy. This part of mechanical energy is designated as the head[8] loss. The sources of this conversion of mechanical energy to heat energy are surface friction and induced turbulences due to fittings, valves and other changes in the flow path as discussed in more detail in [48]

Flow of methanol vapour in the sorbate distribution system is depended upon *Reynolds* number, friction factor, pipe roughness, pipe diameter, pipe length, temperature, pressure, pressure drop and methanol vapour properties. To analyse the pipe flow, *Bernoulli's* equation (11), which can include basic physics, was applied.

$$\frac{v^2}{2} + gz + \frac{p}{\rho} = constant \tag{11}$$

where:

v velocity at the point of streamline [m/s]
g acceleration due to gravity [ms^{-2}]
z elevation difference [m]
p pressure at the point [bar]
ρ density of the fluid [kgm^{-3}]

The v, z, p depend on the chosen point in the flow and the constant always remains the same. Regarding equation (11), one can assume that the flow is steady, incompressible and inviscid. Since the pressure losses, due to the friction and other physics in the pipe are the most important in the practical analysis of the piping system, equation (11) can be modified to account viscous effects, turbulence, changes in pipe geometry and introduction of valves, as discussed in more detail in [49].

The total difference in vapour pressure is the sum of the pressure drops in three regions of the system:

1. Methanol evaporating region
2. Methanol flow region
3. Methanol condensing/absorption region

The pressure drops in the evaporation and condensation region are not taken into account, because only the flow region, i.e. the sorbate distribution system has been investigated and changed per test setup.

[8] By dividing the equation (11) by g, the obtained terms represent the kinetic energy per unit mass (velocity head), the pressure energy per unit mass (pressure head), the potential energy per unit mass (potential head) and total energy per unit mass (total head) in meters, [7].

First, it is important to classify the flow as a steady or an unsteady flow. A flow is steady if all properties are independent of time. Contrary, if the time dependence of flow properties exists, the flow is unsteady. Generally, real physical flows always have some degree of unsteadiness, but the time dependence may be sufficiently slow to justify a steady state analysis, which is termed as a quasi-steady state analysis [49].

Considering the flow occurring in the thermochemical heat storage system, the average velocity is not constant. The average flow velocity generally depends on space x and time t: $v = v(x, t)$ [50]. The average flow velocity in the sorbate distribution system changes not only with space but also with time and therefore, the flow is considered as unsteady. To obtain the results, a quasi-steady analysis is to perform. Steady state formulas are developed hereafter and it is assumed that these are applied only for a sufficiently short time so that the main characteristics of the flow do not change appreciably, as suggested in [49].

Furthermore, the flow occurred in the system is considered to be incompressible because changes in fluid pressure and temperature do not appreciably affect the fluid density. Since *Mach* number is $M \leq 0{,}3$, the compressible effects are neglected, as discussed in [49].

After the assumptions were set, the flow losses can be calculated. Figure 3.6 shows schematic view of sorbate distribution system geometry divided in sections of components. The sorbate distribution system includes straight pipe, elbows, reduction parts and valves. Flow losses take place as friction losses (major losses) and local losses (minor losses). Friction losses are produced by shear stress along the straight pipe walls (section 3-4). Local losses occur due to internal shear stresses in entry and exit areas, elbows (sections 2-3 and 4-5), reduction parts (sections 1-2 and section 4-5) and valves (sections 0-1 and 6-7), [51]. The total loss at pipe outlet is defined as the sum of friction losses and local losses. Additionally, part of the flow losses due to elevation change Z is added to the total losses.

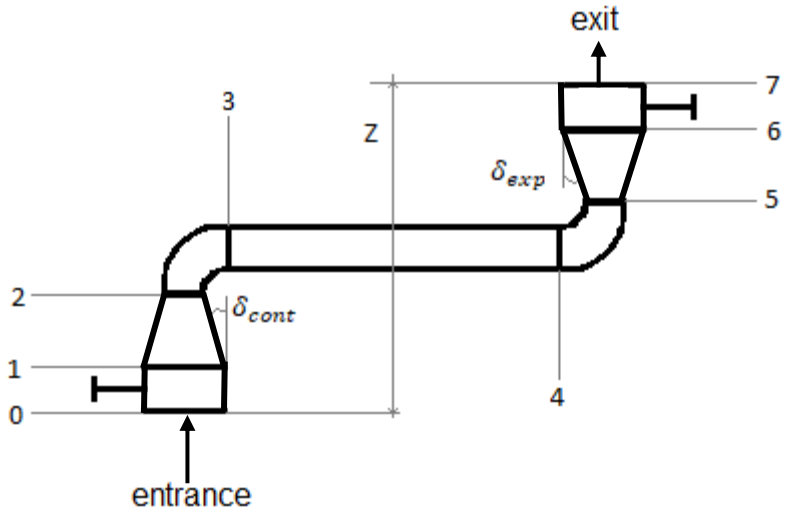

Figure 3.6: Schematic view of sorbate distribution system geometry divided in sections of components. Valves: 0-1 and 6-7, reduction parts: 1-2 and 5-6, elbows: 2-3 and 4-5, straight pipe: 3-4, contraction δ_{cont} and expansion δ_{cont} angles, Z – elevation difference.

Both losses depend on the flow rate, pipe diameter and friction factor. The friction factor depends of the pipes roughness and flow regime. There are laminar, turbulent and transient flow regimes. The flow regime occurring in the pipe is determined by dimensionless *Reynolds* number, whereby, when the *Reynolds* number is less than 2300, the flow is considered to be laminar and when the Reynolds number is higher than 4000, the flow is turbulent. Between these two values, the flow in the pipe can be both, laminar and turbulent.

By entering the pipe, the flow is not fully developed. Figure 3.7 shows the entrance region in the pipe and the variation of wall shear stress in flow direction.

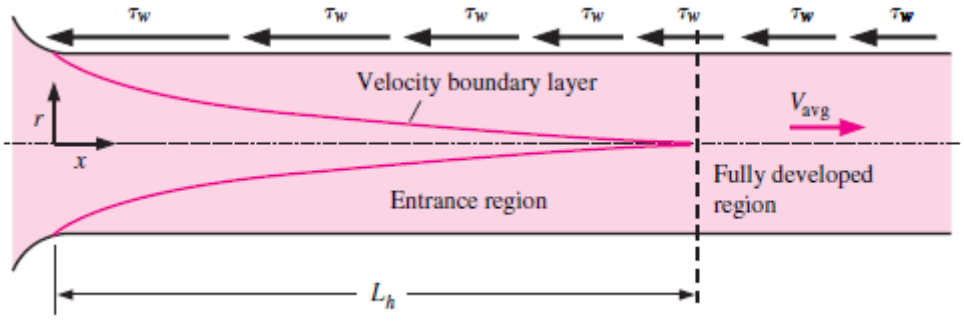

Figure 3.7: The entrance region with variation of wall shear stress in flow direction in a pipe [52]

The entrance region is a region from the pipe inlet to the point at which the velocity boundary layer merges at the centreline. The velocity boundary layer is the region of the flow in which the effects of the viscous shearing forces caused by fluid viscosity are felt. The flow in this region is called developing flow because the velocity profile develops. Beyond the entrance region, the fully developed region occurs, in which the velocity profile is fully developed.

In the entrance region, the pressure drop is always the highest, due to the highest wall shear stress. Therefore, the effect of the entrance region increases the average friction factor for the entire pipe, and significantly for shorter pipes. The entrance length for the laminar flow is approximate to be about the size of the diameter for very low *Reynolds* number, but increases to 115 diameters in case of *Reynolds* number 2300. The entrance length for turbulent flow is estimated as 10 diameters because the entrance effects become insignificant beyond a pipe length of 10 diameters. The flow through the pipes is often assumed to be fully developed for the entire pipe length by longer pipes used in practice. The result obtained for short pipes with this simplification are less accurate, since it underestimates the walls shear stress and thus the friction factor [52]. Considering the sorbate distribution system with pipe lengths of 0,5 m, it is possible that the fully developed flow sometimes does not even occur in the pipe.

In order to simplify the calculations in the quasi-steady state analysis, the flow is presumed to be fully developed for an entire pipe length and the head loss, which indicate the quantities that may be directly converted to produce mechanical energy [7], for fully developed flow was calculated. Additionally, the frictional head loss in entrance region was calculated as referred in literature [53] and has been added to the total head loss.

This simplistic approach gives poor results for some time steps in quasi steady state analysis, especially when laminar flow and turbulent flow with high *Reynolds* numbers occur. Formulas for local losses in the region with developing flow and additional local losses due to elbows, valves and reduction parts are introduced later in this chapter.

3.4.2.1 Evaporation Rate

To examine the impact of the sorbate flow losses on the thermochemical heat storage system, at first, sorbate evaporation rate was defined by the *Hertz relation* as described in literature review [54]. In order to calculate the evaporation rate, the vapour is approximated as an ideal gas in equilibrium with the vapour-liquid interface and with the liquid phase. The equilibrium pressure is the saturation vapour pressure and depends on temperature ($p_{eq}(T_{eq})$).

The *Maxwell-Boltzman* (M-B) velocity distribution function is used to approximate the velocity distribution of vapour molecules. It describes the collision frequency of vapour molecules with the interface per unit of area per second and is given in (12).

$$j_e = p_{eq}(T_{eq})\sqrt{\frac{m}{2\pi k T_{eq}}} \tag{12}$$

j_e molecular flux [kgm^{-2}s^{-1}]

p_{eq} equilibrium pressure [Nm^{-2}]

m molecular mass [kg]
k Boltzmann constant [JK^{-1}]
T_{eq} equilibrium temperature on the interface, equivalent to p_{eq} [K]

The molecular flux from the liquid phase across the interface j_e^L (i.e. evaporation flux) must be equal to the molecular flux from the vapour phase across the interface j_e^V (i.e. condensation flux) under equilibrium conditions. Thereby, the molecular flux from the vapour phase represents the maximum theoretical collision frequency of vapour molecules with the interface. Since the M-B velocity distribution is correct under equilibrium conditions, it is assumed that the M-B velocity distribution is still applicable under near equilibrium conditions as referred in [54]. By introducing the interfacial liquid T_I^L and vapour T_I^V temperatures and vapour pressure p^V in equation (12), the *Hertz relation* is formed (13).

$$j_e^{LV} = p_s(T_I^L)\sqrt{\frac{m}{2\pi k T_I^L}} - p^V\sqrt{\frac{m}{2\pi k T_I^V}} \tag{13}$$

Whereby:
j_e^{LV} net evaporation flux [kgm^{-2}s^{-1}]
p_s saturation vapour pressure [Nm^{-2}]
p^V vapour pressure [Nm^{-2}]
m molecular mass [kg]
k Boltzmann constant [JK^{-1}]
T_I^L interfacial liquid temperature [K]
T_I^V interfacial vapour temperature [K]

The net evaporation flux is difference between the evaporation flux and condensation flux. j_e^L and j_e^V only depend on the properties of their respective phases.

By introducing the empirical coefficients of evaporation and condensation as referred in literature review [54], equation (13) can be further modeled into the *Hertz-Knudsen relation*. The coefficients represent the ratio of molecule flux compared to the maximum flux predicted from classical kinetic theory. The determination of the coefficients have produced inconsistencies, especially due to the existence of an interfacial temperature discontinuity across the liquid−vapor interface. Numerous assumptions about the coefficient which have been exanimated were referred in literature review [54]. However, a disagreement with experimental studies was observed with the *Hertz-Knudsen relation* as well. Therefore, the actual values of the coefficients remain unresolved at present.

Since the determination of the coefficients in the *Hertz Knudsen relation* produces inconsistencies and does not give accurate results, the *Hertz relation* (13) was used to determine evaporation rate due to its simplicity and reasonable results.

Due to the constraints of data acquisition system, the interfacial temperatures were not measured. It was assumed that the interfacial temperatures T_I^L and T_I^V were equal as referred in [54] and the assumption was introduced in (13). Measured hydrostatic pressure of the methanol in the gas phase p^V, temperature of the liquid phase near the interface T_I and saturation vapour pressure $p_s(T_I)$ equivalent to the T_I were introduced in the expression (14) as suggested in [55]

$$\frac{j_e^{LV}}{A} = (p_s(T_I) - p^V)\sqrt{\frac{m}{2\pi k T_I}} \tag{14}$$

Whereby

j_e^{LV} net evaporation flux [kgm^{-2}s^{-1}]
p_s equilibrium pressure [Nm^{-2}]
p^V hydrostatic pressure of the evaporant in the gas phase [Nm^{-2}]
m molecular mass [kg]
k Boltzmann constant [JK^{-1}]
T_I temperature on the liquid phase near the interface [K]
A methanol surface in sorbate reservoir [m^2]

The equilibrium pressure of the liquid methanol p_s was calculated with equation (8). The *Antoine* parameters for methanol and the temperature of liquid methanol near the interface T_I in the sorbate reservoir were introduced in the equation.

The determined net evaporation flux $\frac{j_e^{LV}}{A}$ is the rate of mass flow of the sorbate through methanol surface in the sorbate reservoir. Under assumption that the total amount of evaporated methanol is transferred from the sorbate reservoir through the sorbate distribution system into the cartridge and no condensation occurs on the tube walls, $t_{wall} > t_{vapour}$, the mass flow rate represents the absorption rate.

The volumetric flow rate is calculated in (15)

$$q = \frac{\frac{j_e^{LV}}{A}}{\rho_g} \tag{15}$$

whereby

q volumetric flow rate [m^{3}s^{-1}]
ρ_g saturated vapour density [gm^{-3}]
$\frac{j_e^{LV}}{A}$ mass flow rate [kgs^{-1}]

Saturated methanol vapour densities have been introduced from the *IUPAC* tables referred in [46]. The thermodynamic properties of methanol given in the tables were calculated using the analytic equation of state based on a dimensionless *Helmholtz energy function* (16).

$$\frac{A(\omega,\tau)}{RT} = \frac{A^{id}(\omega,\tau)}{RT} + \frac{A^{r}(\omega,\tau)}{RT} \tag{16}$$

The equation is divided into ideal gas part (*id*) and real fluid part (*r*). Independent variable ω represents reduced density ρ_g/ρ_c and variable τ represents reduced temperature T_g/T_c. ρ_c and T_c represent vapour density and temperature in critical point (see equations (17) and (18)). This equation enables all equilibrium properties to be calculated by differentiation and it is easily adapted in computer programme for process design. The genesis of equation (16) is described in [46].

Since only saturated vapour density is required in following calculations, separate equation given in [46], which is function of temperature alone, was used. The auxiliary equation for density of saturated methanol vapour (17) with the numerical values of the coefficients n_i was introduced in *MS Excel* template.

$$\frac{\rho_g}{\rho_c} = n_1\theta^{\frac{1}{6}} + n_2\theta^{\frac{1}{3}} + n_3\theta^{\frac{2}{3}} + n_4\theta^{\frac{7}{6}} + n_5\theta^{\frac{3}{2}} + n_6\theta^{\frac{5}{2}} + n_7\theta^{\frac{8}{3}} + n_8\theta^{\frac{7}{2}} + n_9\theta^{5} +$$

$$n_{10}\theta^{6} + n_{11}\theta^{15} + n_{12}\theta^{21} + n_{13}\ln\frac{T_g}{T_c} \tag{17}$$

where

$$\theta = 1 - \frac{T}{T_c} \tag{18}$$

and

ρ_g saturated vapour density [gm^{-3}]
ρ_c vapour density in critical point is equal 279068 [gm^{-3}]
T_g temperature of vapour [K]
T_c temperature of vapour in critical point is equal 512,6 [K]
n_i coefficients, represent properties along the saturation curve

Equation (17) is not thermodynamically consistent with equation of state. It was fitted to values calculated from the equation of state and it was constrained to the critical temperature and to the reducing parameter for the density. The calculated densities from equation of state and (17) agree over most of the temperature range.

3.4.2.2 Major Losses

Average velocity of the fluid in section 3-4 (see figure 3.6) is calculated in equation (19):

$$v = \frac{4q}{d^2 \cdot \pi} \tag{19}$$

Whereby

v velocity [ms^{-1}]

q volumetric flow rate [m^{3}s^{-1}]

d internal pipe diameter [m]

Thereafter, the dimensionless *Reynolds* number is calculated in equation (20).

$$Re = \frac{\rho v d}{\mu} \tag{20}$$

Whereby

Re Reynolds number

ρ density [kgm^{-3}]

v velocity [ms^{-1}]

d internal pipe diameter [m]

μ dynamic viscosity [kgm^{-1}s^{-1}]

Dynamic gas viscosity for methanol was calculated as a function of a temperature by the equation (21), as suggested in [56]

$$\mu_{gas} = A + B \cdot T + C \cdot T^2 \tag{21}$$

where

μ_{gas} dynamic viscosity [10^{-7} kgm^{-1} s^{-1}]

$A, B \; and \; C$ regression coefficients for methanol, (valid in temperature range 240K – 1000K)

T temperature of vapour [K]

Regression coefficients for methanol are referred in [56]. They were determined from both experimental data and estimated values, whereby a comparison of correlation (21) and experimental data showed good agreement.

After the *Reynolds* numbers and the flow regimes are determined, the friction can be calculated. For laminar flow regime, the friction losses occur due to viscous effects. The resistance to flow is independent of the pipe wall roughness and the friction factor is a function of the *Reynolds* number, as given in equation (22), [57]. For laminar flow in circular pipe follows:

$$f = \frac{64}{Re} \tag{22}$$

Whereby is

f friction factor

Re Reynolds number

The friction factor depends on the *Reynolds* number and the relative wall roughness in the turbulent flow. The relative wall roughness is a ratio of the internal wall roughness to pipe diameter, as given in equation (23).

$$\varepsilon = \frac{k_s}{d} \tag{23}$$

Whereby

ε relative roughness

k_s internal wall roughness [m]

d diameter [m]

It is evident from the equation (23) that pipes with a smaller diameter will have higher relative roughness than pipes with a bigger diameter. Therefore, pipes with smaller diameters will have higher friction factors than pipes with bigger diameters of the same material. The internal roughness for a stainless-steel pipe is given in [48] and [53]. A universal law for the friction factor, as a function of relative wall roughness and the *Reynolds* number, has been developed by *Colebrook* and *White* and is given in equation (24). The equation is graphically represented in *Moody* chart, which is an empirical fit of the pipe flow pressure drop. The equation is valid for the entire non-laminar range of *Moody* chart.

$$\frac{1}{\sqrt{f}} = -2log\left[\frac{\varepsilon}{3.7} + \frac{2.51}{Re \cdot \sqrt{f}}\right] \tag{24}$$

whereby

f friction factor

Re Reynolds number

ε relative roughness

Since equation (24) cannot be solved explicitly, a *Colebrook* equation solver has been developed in *MS Excel* template, to determine the friction factors.

The energy losses due to the friction are expressed as a static pressure drop given in equation (25).

$$\Delta p_{major} = \frac{\rho f L v^2}{2d} \tag{25}$$

whereby is

Δp_{major} pressure drop [Pa]

f friction factor

L pipe length [m]

v velocity [ms^{-1}]

d diameter [m]

ρ density [kgm^{-3}]

Since the diameter and the average velocity in the pipe section 3-4 (see figure 3.6) are constant, the head loss between sections is calculated with *Darcy-Weisbach* equation (26)

$$h_{major} = \frac{f L v^2}{2dg} \tag{26}$$

h_{major} head loss [m]

f friction factor

L pipe length [m]

v velocity [ms^{-1}]

d diameter [m]

g gravitational acceleration [ms^{-2}]

It is evident from equation (26), that the pipe length has influence on the pressure drop due to friction losses. The longer the pipe, the higher the pressure loss.

3.4.2.3 Minor Losses

Local flow losses occur, wherever flow streamlines are directed away from the axial direction, as in case of an enlargement of cross-section, bends, elbows or valves. Separated flow appear on the two sides of the main stream. The energy is extracted from the main stream and the local losses occurs as described in more detail in [51]. To determine these losses, the loss coefficient K_L has to be specified. Typical values for the loss coefficients are given in literature [49] and [53].

In addition, the reference flow velocity v_r has to be defined. As suggested in [51], v_r is equal to the average velocity of the incoming or the outgoing flow velocities in the investigated elements. Therefore, it was assumed that the reference velocity v_r is equal to the average velocity v in section 3-4 (see figure 3.6).

For a given value of the loss coefficient, the head loss is proportional to the square of the velocity as show in equation (27)

$$h_{local\ loss} = K_L \frac{v^2}{2g} \tag{27}$$

Whereby

$h_{local\ loss}$	head loss due to local losses [m]
K_L	loss coefficient
v	velocity [ms^{-1}]
g	acceleration due to gravity [ms^{-2}]

Furthermore, the pressure drop is given in equation (28)

$$\Delta p_{minor} = K_L \rho\, v^2 \frac{1}{2} \tag{28}$$

Whereby

ρ	fluid density [kgm^{-3}]
K_L	loss coefficient
v	velocity [ms^{-1}]
Δp_{minor}	pressure drop [Pa]

The extreme cases where local losses occur, involve flow into a pipe from the reservoir (flow losses in entrance region) and out of the pipe into the cartridge. A shape entrance has an associated loss coefficient. The entrance loss coefficient for sharp edged geometry, as on the facility, is taken as $K_{L\text{-entry}}$ =0,5. When the fluid flows from the pipe into the cartridge, the entire kinetic energy of fluid at the exit is dissipated through the viscous effect because the stream of fluid mixes with the fluid in the cartridge. Thereby, $K_{L\text{-exit}}$ is 1. The value of $K_{L\text{-elbow}}$ for elbows, section 2-3 and section 4-5 (see figure 3.6) adapted on the facility at horizontal orientation depends on the shape of the component and only very weakly on the *Reynolds* number for the sorbate flow. The value of $K_{L\text{-elbow}}$ =0,2 for a long radius flanged elbow 90° used in the facility is suggested in [53]. The loss coefficient of reducers on the entrance and exit of the pipe, section 1-2 and section 5-6 (see figure 3.6), were determined as suggested in [51]. An expansion occurs on the exit of the tube and a contraction occurs on the entrance of the tube. The expansion loss coefficient is calculated with the *Borda Carnot* equation (29) considering the effect of expansion angle δ_{exp}.

Thereby, the loss coefficient is split in a part depending only on the angle δ_{exp} and a part depending only on the area ratio $d_{entrance}/d_{exit} > 1{,}4$. Equation (29) is generally applied in practise and has been experimentally confirmed for incompressible flow [48].

$$K_{L-expansion} = \left[\frac{\delta_{exp}}{90°} + \sin(2\delta_{exp})\right]\left[1 - \frac{d_{entrance}}{d_{exit}}\right]^2, 0 \leq \delta_{exp} \leq 30° \quad (29)$$

Whereby

$K_{L-expansion}$	local loss coefficient for diffusor
δ_{exp}	expansion angle
$d_{entrance}$	diameter on flow entrance in diffusor [mm]
d_{exit}	diameter on exit of diffusor [mm]

By the contraction, the geometry is equal to a reversal of flow direction by expansion. The flows in these two elements are fundamentally different due to differences in their separation structures. Therefore, $K_{L\text{-contraction}}$ is calculated in equation (30) as suggested in [51]. The flow is influenced by the angle of contraction δ_{cont} and the area ratio $d_{entrance}/d_{exit} < 1$.

$$K_L = \frac{1}{2}\left[1 - \frac{d_{entrance}}{d_{exit}}\right]\left[\frac{\delta_{cont}}{90°}\right]^{1{,}83\cdot\left[1-\frac{d_{entrance}}{d_{exit}}\right]^{0{,}4}}, 0 \leq \delta_{cont} \leq 30° \quad (30)$$

Whereby is

$K_{L-contraction}$	local loss coefficient for diffusor
δ_{cont}	contraction angle
$d_{entrance}$	diameter on flow entrance in diffusor [mm]
d_{exit}	diameter on exit of diffusor [mm]

The contraction loss coefficient is always smaller than the corresponding expansion loss coefficient because the contracted flow is nearly free of energy loss and it is attributed to the expansion of flow downstream of the contracted flow. δ_{cont} and δ_{exp} angles (see figure 3.6) are given by the manufacturer and they have a value of 17° for used components. Furthermore, the value of $K_{L\text{-valve}}$ =0,4 for butterfly valve, section 0-1 and section 6-7 (see figure 3.6), is also given by the manufacturer. The $K_{L\text{-valve}}$ for closed valve is infinite and by opening the valve, the $K_{L\text{-valve}}$ is reduced, producing the desired flow rate. Since the valves were always full opened, the pressure drop was calculated for both valves and added to total pressure drop.

The following local losses were considered by evaluating the tests:

- local losses at entrance in the pipe $K_{L\text{-}entry}$ =0,5
- local losses at exit from the pipe $K_{L\text{-}exit}$ =1
- local losses of expansion and contraction
- local losses of elbows $K_{L\text{-}elbow}$ =0,2
- local losses due to fully opened valve $K_{L\text{-}valve}$ =0,4

In addition, pressure drop due to elevation difference is calculated in (31).

$$\Delta p_{gravitation} = \rho \cdot g \cdot Z \tag{31}$$

Whereby

ρ fluid density [kgm^{-3}]

Z elevation difference [m]

g acceleration due to gravity [ms^{-2}]

$\Delta p_{gravitation}$ pressure drop [Pa]

Combining the losses for the sorbate distribution system, the total pressure drop at outlet of the sorbate distribution system is the sum of all pressure losses along the sorbate distribution system (32).

$$\Delta p_{total} = \Delta p_{major} + \Delta p_{minor} + \Delta p_{gravitation} \tag{32}$$

Since the friction loss coefficients and local loss coefficients, as well as the vapour density and viscosity are based on the empirical data and estimated values, the results obtained in this analysis deviate from the real conditions that occur in the thermochemical heat storage system. Moreover, the assumption of fully developed flow in the entire pipe, made during the calculation of pressure drops, as well as the constraints in the estimation of the evaporation rates contribute to poor results. However, the obtained results represent a reasonable interrelation between the different set ups of the sorbate distribution system. Therefore, it can be investigated, how the cartridge performance is changed with regard to the different sorbate distribution systems.

3.5 Conclusion of Materials and Methods

This chapter reviews about the materials and methods of investigation in this master thesis. Firstly, the thermochemical heat storage test facility as well as the operation and conditions occurring during the phases of thermal conversion were described. As possible issues during the experimental work, the shortcomings in the data acquisition system and a possible air leakage into the test facility are listed. Design of the cartridge and the sorbate distribution system were discussed as well. Manufacturing procedure of the reactive bed was described as well as the different sorbate distribution systems set ups were represented. Later, the test procedures for the investigations of the sorbate distribution system, the effect of ambient temperature on the cartridge performance, the durability test and the reversibility analysis were defined. The evaluation methods for conducted tests were described. The average power release, the total energy release, the presence of non-condensable gases within the system as well as the flow analysis were determined in order to evaluate the conducted tests. The obtained results are represented and discussed in the next chapter.

4 Results and Discussion

Referring to defined investigations and test procedures introduced in the previous chapter, the results of conducted experiments are represented and discussed in the following.

4.1 Sorbate Distribution System Investigation

The effect of different sorbate distribution systems on the cartridge performance is discussed in this chapter.

4.1.1 Performance Analysis

In order to examine the cartridge performance on the facility assembled with different set ups of the sorbate distribution system, the conducted tests were evaluated and the obtained results were compared to each other. Average power releases over 30 s, 60 s and 90 s, according to different pipe diameters of the sorbate distribution system assembled to the test facility, are represented in figure 4.1 for vertical and in figure 4.2 for horizontal orientation. In addition, the power peak, the reactive bed mass before and after absorption phase as well as the total released energy during the absorption phase are listed in table 4.1 for vertical and in table 4.2 for horizontal set up.

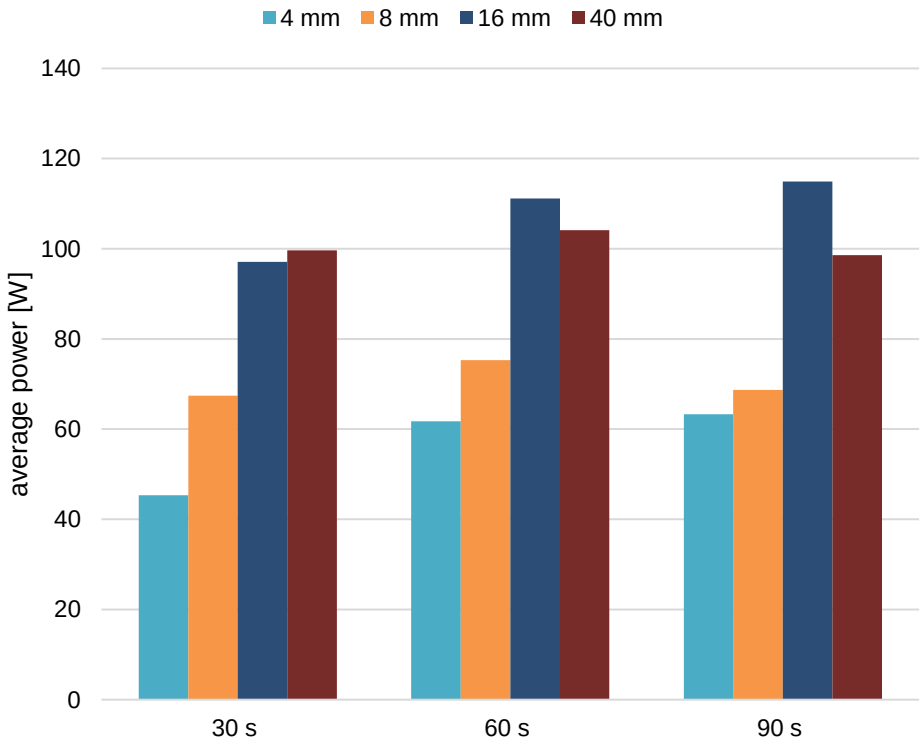

Figure 4.1: Average power release in vertical orientation (R8)

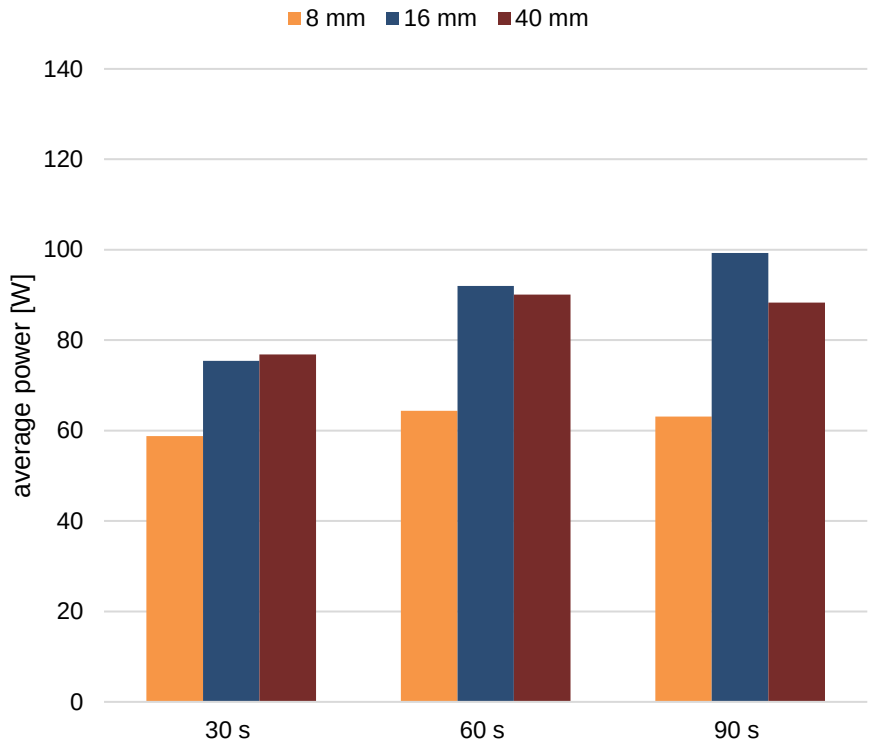

Figure 4.2: Average power release in horizontal orientation (R9)

Table 4.1: Obtained results with cartridge R8 in vertical orientation

R8 - Ø vertical	average power release [W]			power peak [W]	reactive bed mass before absorption [g]	reactive bed mass after absorption [g]	total released energy [kJ]
	30 s	60 s	90 s				
4 mm	45	61	63	89	125,1	136,2	11,9
8 mm	67	75	69	96	125,8	136,8	11,7
16 mm	97	111	115	127	114,1	133,3	19,6
40 mm	99	104	98	121	120,7	137,1	16,7

Table 4.2: Obtained results with cartridge R9 in horizontal orientation

R9 - Ø horizontal	average power release [W]			power peak [W]	reactive bed mass before absorption [g]	reactive bed mass after absorption [g]	total released energy [kJ]
	30 s	60 s	90 s				
8 mm	59	64	63	78	127,6	140,1	12,7
16 mm	75	92	99	115	122,3	143,3	21,0
40 mm	77	90	88	110	124,3	139,9	15,4

The obtained average power release increases with an increase of the sorbate distribution system pipe diameter, both for vertical and horizontal orientations. Besides that, the differences in the reactive bed masses before absorption are observed as well.

For the vertical orientation (see figure 4.1 and table 4.1), average power release over 30 s increases from 45 W to 67 W and to 97 W, as the pipe diameter increases from 4 mm to 8 mm and to 16 mm. Average power release over 30 s at 16 mm is in the same range as at 40 mm pipe diameter. The trend of average power release according to the increase of the pipe diameter shows similar behaviour over 30 s, 60 s and 90 s. A slightly lower average power release at 40 mm than at 16 mm pipe diameter is observed over 60 s and 90 s. The mass of the reactive bed before test at 16 mm (114,1 g) is lower than at 40 mm (120,7 g) and significantly lower than at 4 mm and 8. The mass of the reactive bed before absorption is nearly the same before tests conducted at 4 mm and 8 mm pipe diameter (125,1 g and 125, 8 g, respectively).

For the horizontal orientation (see figure 4.2 and table 4.2), average power release over 30 s increases from 59 W to 75 W, as the pipe diameter increases from 8 mm to 16 mm. Average power releases at a 16 mm and 40 mm pipe diameter are in the same range. The trend of average power release according to the increase of the pipe diameter shows similar behaviour over 30 s, 60 s and 90 s. A slightly lower average power release at 40 mm than at 16 mm pipe diameter is observed over 90 s. The mass of the reactive bed before absorption at 16 mm, (122,3 g), is lower than at 40 mm pipe diameter (124,3 g), whereas the mass at 8 mm pipe diameter is obviously higher (127,6 g).

Further, the average power release over 30 s is slightly lower than average power release over 60 s and 90 s in every case. In both orientations, the power peak occurs between a time interval of 30 s and 60 s. The power peak increases with the increase of pipe diameter, whereby the power peaks at 16 mm and 40 mm pipe diameter are in the same range for both orientations as listed in table 4.1 and table 4.2.

Considering the represented results, there might be two reasons for behaviour of cartridge performance observed during this investigation.

On the one hand, the observed difference in the reactive bed masses before absorptions might contribute to the different cartridge performance in the conducted tests. The mass growth is believed to occur due to insufficient desorption temperature (100°C) at atmospheric pressure and it negatively affects the cartridge performance as discussed later in chapter 4.3. However, the cartridges R8 and R9 used in this investigation could not be desorbed at higher temperature due to their construction.

On the other hand, a difference in the cartridge performance is observed in tests at 4 mm and 8 mm pipe diameter in vertical orientation, although the reactive bed masses before absorption are in the same range. Therefore, it might be possible that some other phenomenon has an effect of the cartridge performance as well.

As the two power releases differ between each other according to differences in the sorbate distribution systems geometry, it might be possible that flow losses, which occur in the sorbate distribution system, affect the cartridge performance. Considering the differences between the sorbate distribution systems dimensions, different flow losses occur in different sorbate distribution systems. Therefore, the sorbate flow analysis was performed to investigate the pressure drops along the sorbate distribution system for these tests.

In addition, since the adverse effect of non-condensable gases is observed and discussed in chapter 4.3.4, note that the presence of any non-condensable gases within the system before the tests is not observed during this investigation.

4.1.2 Sorbate Flow Analysis

Firstly, the mass flow rates, i.e. the absorption rates are predicted for every time step during the conducted absorption phases as described in chapter 3.4.2.1. An integration of predicted mass flow rates over the time duration of the absorption phases (300 s) gives the predicted total sorbate uptake (total mass of absorbed methanol) in the absorption phases. To check the plausibility of the obtained results, the predicted sorbate uptakes are compared with the measured sorbate uptakes during the absorption phases. The measured sorbate uptake represents the difference between the measured reactive bed masses after and before absorption phase. The predicted

sorbate uptake as well as the measured sorbate uptake are listed in table 4.3 and table 4.4 for experiments conducted on the facility with vertical and horizontal orientation of the sorbate distribution system, respectively. The differences between predicted and measured sorbate uptakes occur due to the evaluation errors and the simplifications introduced in the calculation model as referred in chapter 5. However, the comparison of predicted sorbate uptakes and measured sorbate uptakes shows good agreement.

Table 4.3: Predicted and measured sorbate uptake of R8 in vertical orientation

R8 - Ø vertical	predicted sorbate uptake (300 s) [g]	measured sorbate uptake (300 s) [g]
4 mm	12,7	11,1
8 mm	12,5	11,0
16 mm	20,7	19,2
40 mm	17,1	16,4

Table 4.4: Predicted and measured sorbate uptake of R9 in horizontal orientation

R9 - Ø horizontal	predicted sorbate uptake (300 s) [g]	measured sorbate uptake (300 s) [g]
8 mm	13,6	12,5
16 mm	21,4	21
40 mm	16,1	15,6

Considering the progress of an absorption phase, the highest flow rates occur at the beginning of the absorption phase, immediately after the valve opening, due to pressure balancing between the sorbate reservoir and the cartridge, (see figure 3.5). Since the highest flow rates occur at the beginning of the absorption and therefore the highest vapour propagation velocities, the mass flow rates in the time interval of the first 20 seconds are presented both for vertical, (see figure 4.3), and horizontal (see figure 4.4) orientations.

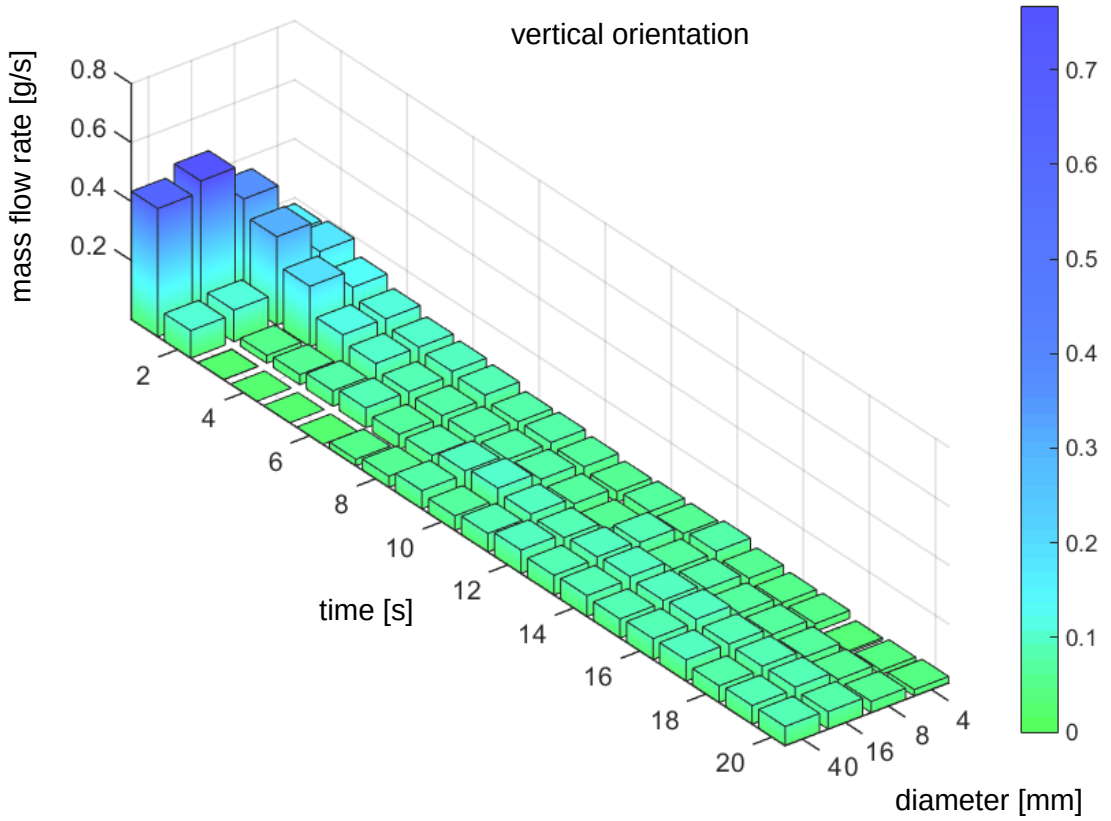

Figure 4.3: Mass flow rates in sorbate distribution systems with different pipe diameters - vertical orientation

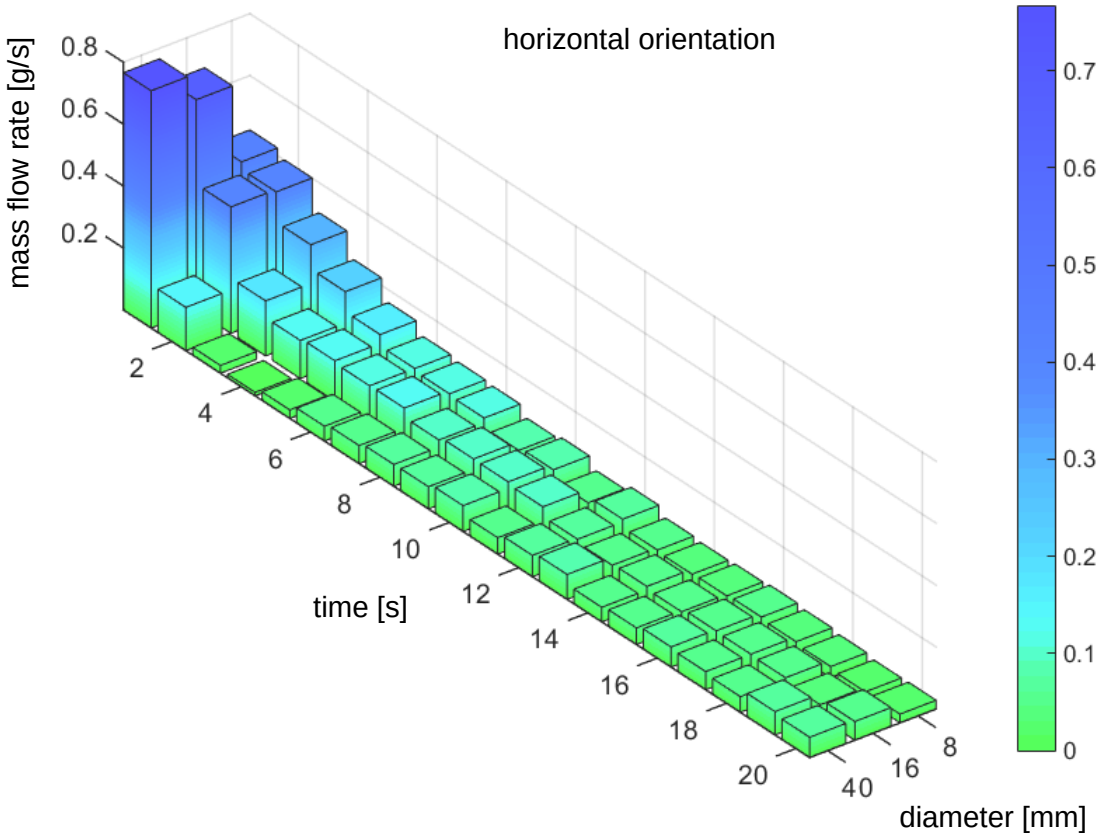

Figure 4.4: Mass flow rates in sorbate distribution systems with different pipe diameters - horizontal orientation

The sorbate flow rates are the highest immediately after the valve is opened, for all pipe diameters and orientations, because the sorbate evaporates and fulfils the sorbate distribution systems volume. The sorbate flow rates exponentially decrease in the first few seconds and reach a constant value for every pipe diameter in both orientations.

Considering the pipe diameters of the sorbate distribution systems, the sorbate flow rates slightly decrease with a decrease of pipe diameter in both orientations. A significant decrease of sorbate flow rates with the decrease of pipe diameter is observed in the first second, due to differences in volume of the sorbate distribution system. More methanol flows into the sorbate distribution system with a bigger pipe diameter, in order to fulfil a bigger pipe volume. This is reflected in high flow rates in the first second for 16 mm and 40 mm pipe diameters in both orientations.

Further, the flow rates in 40 mm and 16 mm pipe diameters (see figure 4.3) and flow rates in 40 mm pipe diameter (see figure 4.4) are reduced from second 2 to 6, after the sorbate distribution systems volume is fulfilled with the sorbate. It is believed that, due to bigger sorbate distribution systems volume, a big amount of sorbate evaporates at 40 mm and 16 mm pipe diameter in the first second. It might be possible that all evaporated sorbate cannot be immediately absorbed and that the sorbate evaporation in the sorbate reservoir is reduced for a short time. The phenomenon is discussed in more detail in chapter 4.2.

Since the vapour propagation velocity through the sorbate distribution system is defined with the mass flow rate and pipe geometry, different flow regimes occur in different sorbate distribution system set ups. The flow regimes that occurred in the sorbate distribution systems are determined and *Reynolds* numbers are represented in figure 4.5 for vertical orientation and in figure 4.6 for horizontal orientation.

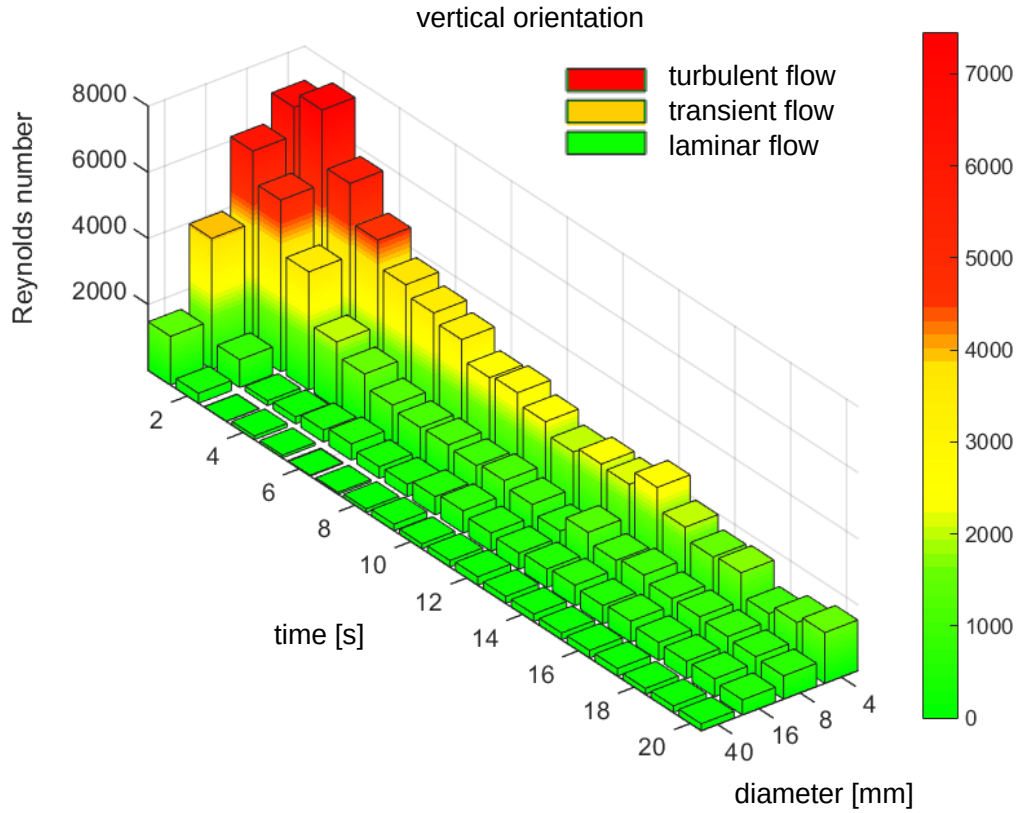

Figure 4.5: *Reynolds* numbers in sorbate distribution systems with different pipe diameters, in vertical orientation: green-laminar, yellow-transient and red-turbulent flow

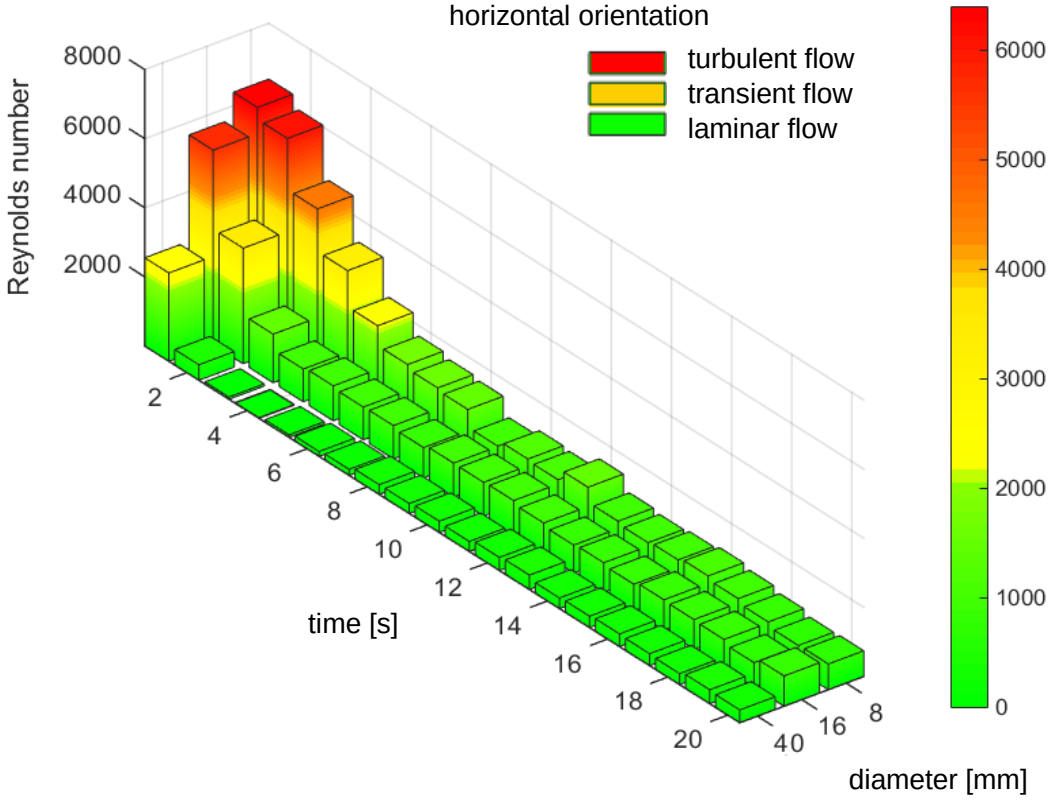

Figure 4.6: *Reynolds* numbers in sorbate distribution systems with different pipe diameters, in horizontal orientation: green-laminar, yellow-transient and red-turbulent flow

Reynolds numbers increase with a decrease of pipe diameter. The decrease of *Reynolds* numbers with time from the absorption start is proportional to the decrease of mass flow rates with time from the absorption start in every case, (see figure 4.3 and figure 4.4 for mas flow rates).

As represented in figure 4.5, for vertical orientation, the turbulent flow occurs from second 1 to 4 and from second 1 to 2 at a 4 mm and 8 mm pipe diameter, respectively. The turbulent flow becomes transient from second 5 to second 14 at 4 mm, and in second 3 at 8 mm. The laminar flow occurs immediately after the transient flow at 4 mm and 8 mm pipe diameters. At a pipe diameter of 16 mm, the transient flow occurs in second 2 and immediately becomes laminar, whereby the laminar flow occurs immediately after the valve opening at a pipe diameter of 40 mm.

Further, at the horizontal orientation (figure 4.6) the turbulent flow occurs from second 1 to second 3 and in second 1 only at a 8 mm and 16 mm pipe diameter, respectively. The turbulent flow then crosses to the laminar flow. At 40 mm, the laminar flow occurs immediately after the valve is opened.

Since *Reynolds* numbers indirectly provide information about the flow losses due to friction, it is obvious that the flow losses increase as the pipe diameter decreases. The frictional losses and the local losses due to the pipe geometry are reflected in a total pressure drop. Pressure drops at the outlet of the sorbate distribution systems were predicted and represented in figure 4.7 for vertical and in figure 4.8 for horizontal orientations.

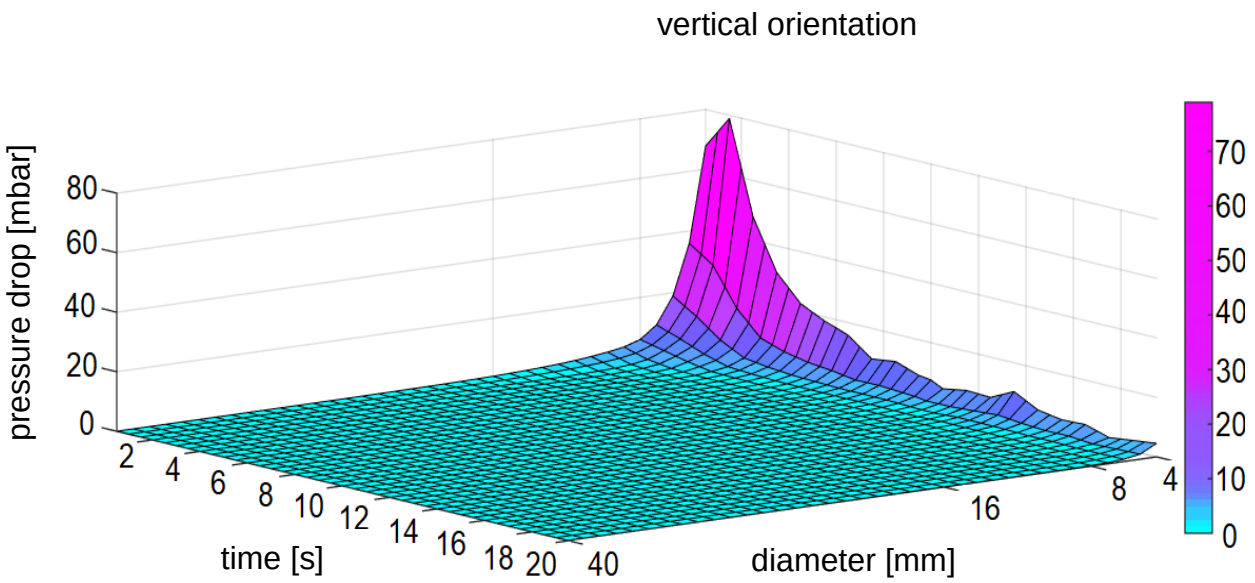

Figure 4.7: Pressure drop in sorbate distribution systems with different pipe diameters - vertical orientation

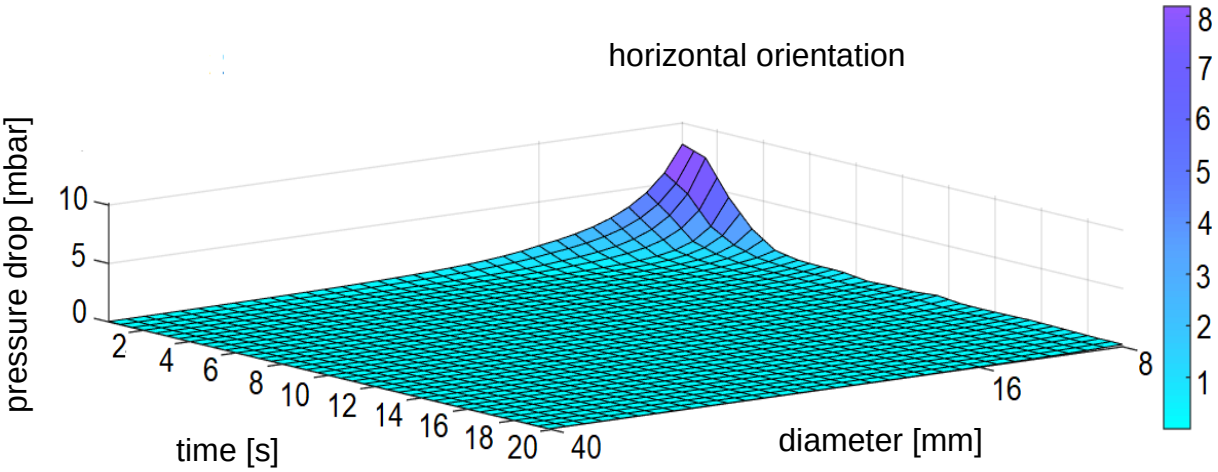

Figure 4.8: Pressure drop in sorbate distribution systems with different pipe diameters - horizontal orientation

The predicted pressure drop significantly decreases with an increase of the pipe diameter of the sorbate distribution system, especially in the beginning of the absorption phase. In addition to that, pressure drop exponentially decreases with time in the first few seconds in every case, and reaches a constant value.

Figure 4.7 shows that the highest pressure drop, of approximately 80 mbar, occurs in second 2, at a 4 mm pipe diameter, in vertical orientation, during the turbulent flow (see figure 4.5 for flow regimes). By crossing to the transient (second 4) and later to the laminar flow regimes (second 16), the pressure drop decreases and varies between 22 and 10 mbar, and between 6 and 2 mbar respectively, at a 4 mm pipe diameter. Looking at a pipe diameter of 8 mm, the pressure drop varies between 8 and 5 mbar in turbulent flow (second 1-2) and under 1 mbar in a laminar flow regime (from second 3). The pressure drop of 0,7 mbar in the transient flow (second 1) at 16 mm pipe diameter decreases under 0,3 mbar later on. At a 40 mm pipe diameter, the pressure drop was under 1 mbar during the absorption phase.

Figure 4.8 shows that the highest pressure drops of 8 - 4 mbar occur at a 8 mm pipe diameter in horizontal orientation, during turbulent flow (second 2-4), (see figure 4.6 for flow regimes). Subsequently, pressure drop decreases and varies from 0,7 mbar to 0,01 mbar later. The pressure drop is under 0,01 mbar at a 16 mm and 40 mm pipe diameter during the whole absorption phase.

No additional effects due to different orientations are observed during the conducted absorption phases.

It might be possible that pressure drop, due to the flow losses in the sorbate distribution system, reduces the pressure difference between the sorbate and the reactive bed. Since it is believed that the sorbate flow through the reactive bed is mostly driven by pressure gradient along the reactive bed, the reduced pressure difference might

reduce sorbate flow through the reactive bed. The reduced sorbate flow, i.e. mass transfer through the reactive bed results with a reduced power release.

Pressure drops under 1 mbar, which occurred at a 16 mm and 40 mm pipe diameter in both orientations are insignificantly small compared to the pressure within the system under which the reaction occurs (e.g. 126 mbar at 20°C). The pressure drops under 1 mbar insignificantly affect the pressure difference between the sorbate and the reactive bed. Therefore, it can be stated that the sorbate distribution systems with 16 mm and 40 mm pipe diameters have an insignificantly small effect on the cartridge performance, (see chapter 4.1.1 for the cartridge performance).

The pressure drops, which occurred from second 1 to 4 at 8 mm pipe diameter in both vertical and horizontal orientations might slightly reduce the pressure difference between the sorbate and the reactive bed in the beginning of absorption phase. However, the pressure drops under 1 mbar, which occurred from second 3, insignificantly affect the pressure difference between the sorbate and the reactive bed. Therefore, it can be stated that the sorbate distribution system with 8 mm pipe diameter has an insignificantly small effect on the cartridge performance.

On the contrary, significant pressure drops, which occurred at 4 mm pipe diameter in vertical orientation, reduce the pressure difference between the sorbate and the reactive bed. As the pressure difference between the sorbate and the reactive bed is reduced, the sorbate flow through the reactive bed might be hindered. Consequently, the reduction in power release with a decrease of pipe diameter (see figure 4.1 power release at 4 mm and 8 mm) might have occurred due to the reduced pressure difference between the sorbate and the reactive bed. Note that the reactive bed mass before absorption are the same in these tests, (see table 4.1, 4 mm and 8 mm).

Generally higher pressure drops in the beginning of the absorption phase might partially contribute to the delay of the power peak, which occurred in average over 60 s, (see chapter 4.1.1 for the cartridge performance). It might be possible that the power peak occurs in average over 60 s due to the increase of reactive bed masses before absorption. The phenomena is observed and discussed in more detail in chapter 4.3.

Further, though lower power release at 4 mm than at 8 mm pipe diameter, the sorbate uptake and consequently the total released energy are the same at both pipe diameters, (see table 4.1). Therefore, it can be stated that, the pressure drop in the sorbate distribution system does not reduce the maximum total heat release.

Moreover, it can be stated that the difference in the cartridge performance between 8 mm, 16 mm and 40 mm pipe diameter in both orientations occurs due to differences in the state of the reactive bed before absorption. The state of the reactive bed before

absorption is crucial for the cartridge performances as discussed in chapter 4.3. The higher the mass of the reactive bed, the lower the theoretical heat capacity.

In conclusion, 40 mm and 16 mm pipe diameters in both orientations show potential for integration in the thermochemical heat storage system, due to insignificantly small predicted pressure drops which occurred during the absorption phase. Among the two, 16 mm pipe diameter would be preferable due to less space occupation. Small pressure drops (max. 8 mbar) are predicted at 8 mm in the beginning of the absorption phase. Therefore, the 8 mm pipe diameter is not to be considered for integration in the thermochemical heat storage system.

4.1.3 Summary of Sorbate Distribution System Investigation

The cartridge performance was examined on the test facility assembled with the different sorbate distribution system set ups. A decreasing trend of cartridge performance with a decrease of the sorbate distribution systems pipe diameter was observed. In order to examine the possible influence of the sorbate flow losses to the cartridge performance, the sorbate flow analysis was carried out.

Generally, the highest flow rates occurred immediately after the valve was opened. The flow rates further rapidly decreased until a constant value was reached. The flow rates slightly increased with an increase of pipe diameter, whereas *Reynolds* numbers exponentially increased with a decrease of pipe diameter. Finally, the pressure drop at the outlet of the sorbate distribution system increased with a decrease of pipe diameter. The pressure drop was the highest in the beginning of the absorption phase and it decreased rapidly in the first few seconds until the constant value was reached.

It is believed that the sorbate flow through the reactive bed is mainly driven by pressure gradient along the reactive bed. Therefore, it was stated that reduction of the pressure difference between the sorbate and the reactive bed, which is caused by the pressure drop at the pipe outlet, reduces the sorbate flow, i.e. mass transfer along the reactive bed. That results in a reduction of the cartridge performance. The pressure drops at a 16 mm and 40 mm pipe diameter were insignificantly small compared to the pressure at which the reaction occurs. Therefore, it was stated that 16 mm pipes are favoured by the possible integration of the sorbate distribution system in automotive applications due to an insignificant effect on the cartridge performance and a less space requirements than 40 mm pipe diameter.

Pressure drops could not be measured, since the pressure sensors were not sensible enough to measure small pressure differences in an appropriate time span. Therefore a comparison to measured values was not done.

4.2 Effect of Ambient Temperature on Cartridge Performance

The absorption phases were conducted at different ambient temperatures. The average power releases over 30 seconds, 60 seconds and 90 seconds for each temperature are represented in figure 4.9.

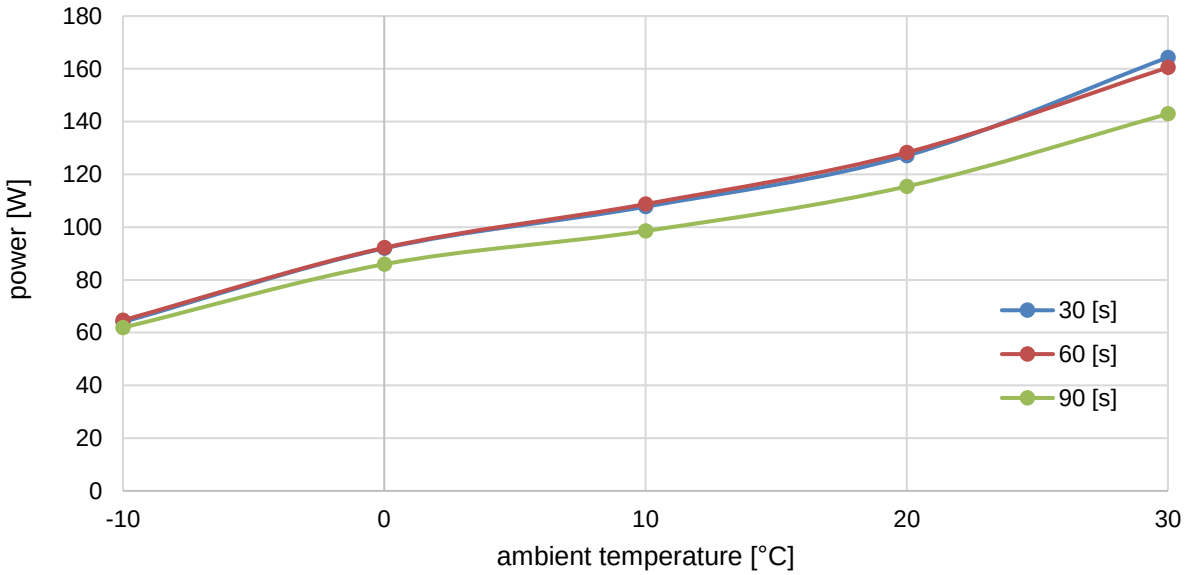

Figure 4.9: Average power release at different ambient temperatures

Two phenomena of performance behaviour at different ambient temperatures were observed. The average power release linearly increases with a linear increase of the ambient temperature. At the same time, average power over 90 s increases less intensively than average power over 30 s and 60 s, as the ambient temperature increases. Average power releases over 30 s and 60 s increase with the same intensity. Increase of average power releases over 30 s and 90 s according to an increase of temperature as well as masses of reactive bed before absorption are listed in table 4.5**.** The mass of reactive bed before absorption is in the same range in all conducted test in this investigation. The small differences in the reactive bed mass do not drastically change the results obtained in this investigation.

Table 4.5: Characteristic average power behaviour according to ambient temperature

	30 [s]		90 [s]		mass of reactive bed before absorption - (R13) [g]
$T_{ambient}$ [°C]	average power [W]	increase	average power [W]	increase	
-10	64		62		126,9
0	92	44%	86	39%	129,5
10	108	68%	97	56%	130,8
20	127	99%	119	93%	129,9
30	164	157%	143	131%	127,6

During the storage phase, there is a constant difference between the saturation pressure; the equivalent to the temperature in the sorbate reservoir, and the desorbed cartridge pressure; the equivalent to the cartridge temperature. Considering the equilibrium state in both the reservoir and the cartridge before absorption, the pressure difference between the sorbate reservoir and the evacuated cartridge depends on the ambient temperature. The pressure in the cartridge insignificantly increases with an increase of ambient temperature and it is assumed to 1 – 3 mbar. The pressure in the sorbate reservoir, and therefore the difference between this pressure and the pressure in the cartridge, exponentially increases with the linear increase of ambient temperature, as represented in figure 4.10.

At low ambient temperatures, the pressure difference between the sorbate reservoir and the cartridge is small (20 mbar at -10°C). During the absorption phase, the temperature in the cartridge increases. Consequently with the increase of temperature in the cartridge, the equilibrium pressure increases as well (see figure 2.4 left) reducing thereby the pressure difference between the sorbate reservoir and the cartridge.

As the ambient temperature increases, and therefore the pressure difference between the sorbate reservoir and the cartridge (40 mbar at 0°C, 72 mbar at 10°C, 126 mbar at 20°C and 211 mbar at 30°C) increases, it might be possible that the mass transfer, i.e. the sorbate flow through the reactive bed and the reaction kinetics are improved. That is apparent from the fact that the sorbate flow along the reactive bed is believed to be driven mainly by the pressure gradient, (see chapter 2.3). Since the power release is governed by the mass transfer of the sorbate to the reactive salt, an improvement of cartridge performance with an increase of ambient temperature is apparent.

In addition to reduced mass transfer through the reactive bed, the quality of sorbate evaporation might be affected due to low ambient temperature as well, as shown in [27]. Insufficient sorbate evaporation with regard to sorbate demand in the reactive bed might hinder the absorption process and results in a lower power release.

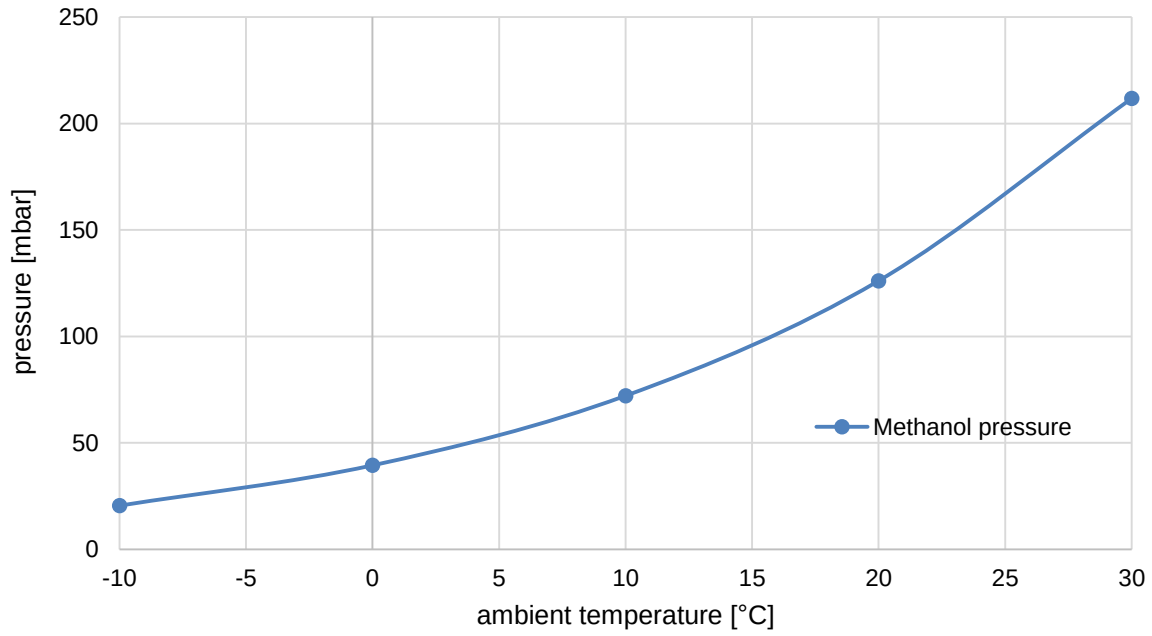

Figure 4.10: Methanol pressure at different ambient temperatures – pressure difference between sorbate reservoir and cartridge

Generally, during the absorption phase, temperature and pressure in the system decrease due to the sorbate evaporation in the sorbate reservoir. As the pressure in the system decreases, the pressure difference between the sorbate and the reactive bed decreases, reducing thereby the sorbate flow through the reactive bed. At the same time, the reactive bed becomes more saturated during absorption. The porosity as well as the permeability of the reactive bed decrease, causing higher mass transfer resistance. Due to the higher mass transfer resistance, the sorbate flow is reduced. Thus, as the pressure difference decreases and as the mass transfer resistance increases during the absorption phase, the sorbate flow through the reactive bed decreases, causing reduction in power release.

Considering the different ambient temperatures, the absorption phases occur at different pressure levels. Figure 4.11 shows the pressure progress during absorption phases at different ambient temperatures. The pressure progress during the absorption phase is on the highest level at the highest ambient temperature (200 – 79 mbar at 30°C) and decreases as the ambient temperature decreases. Temperature and pressure drops (difference between initial and final sorbate temperature and pressure), which occurred during the absorption phases, are listed in table 4.6.

It is clear that sorbate temperature $\Delta T_{sorbate\ 300s}$ and pressure drops Δp_{300s} increase with an increase of ambient temperature. The pressure drop is the decrease of the pressure difference between the sorbate and the reactive bed.

Table 4.6: Sorbate temperature and pressure drops during absorption phase at different ambient temperatures

$T_{ambient}$ [°C]	$\Delta T_{sorbate\ 300s}$ [°C]	$\Delta p_{sorbate\ 300s}$ [mbar]
-10	9,3	11,2
0	10,0	22,5
10	11,5	38,9
20	14,0	71,8
30	18,0	119,2

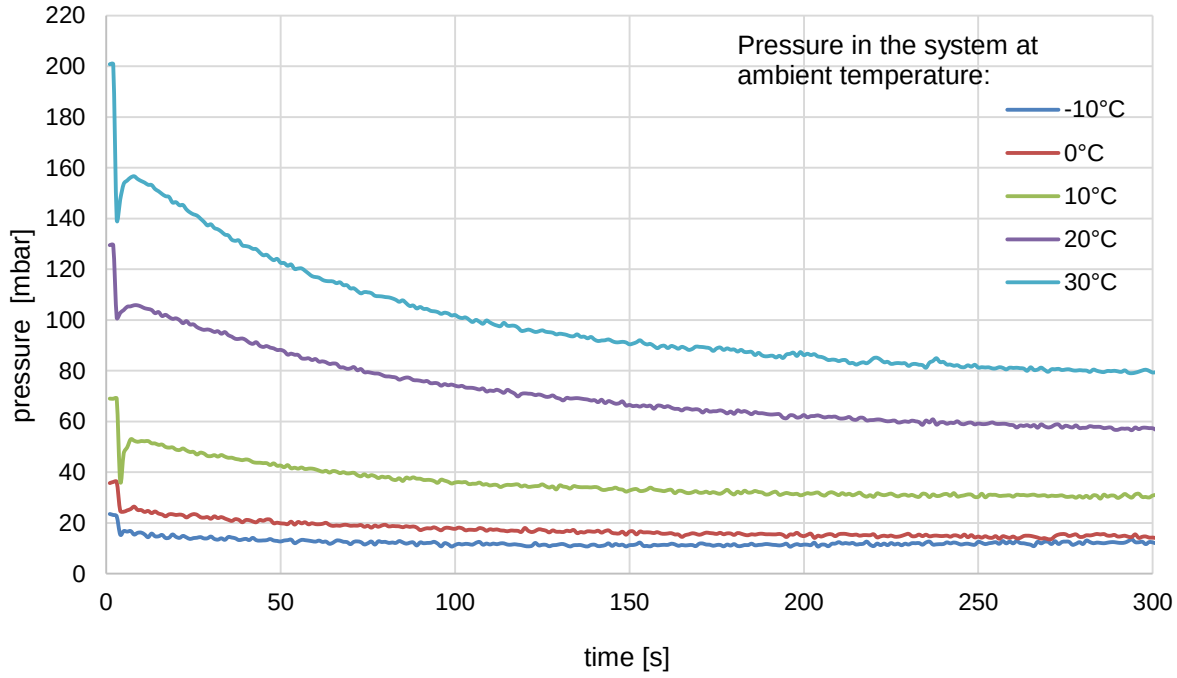

Figure 4.11: Pressure progress during absorption at different ambient temperatures

It might be possible that the sorbate flow through the reactive bed decreases more intensively, as the pressure difference between the sorbate and reactive bed decreases, resulting in a less intensive increase of average power release over 90 s than over 30 s.

In addition to that, it might be possible that reduced permeability and porosity of the reactive bed contribute to the decrease of power release with time as well. The more sorbate is absorbed in the reactive bed, the lower the permeability and the higher the mass transfer resistance through the reactive bed.

Further, an additional phenomenon is represented in figure 4.11. After the valve was opened, a rapid pressure drop occurred due to balancing of sorbate pressure and cartridge pressure. Simultaneously, intensive evaporation of methanol occurs, which fills the sorbate distribution system. It follows a pressure surge reflected in the pressure peak, which is believed to happen due to a lower absorption rate than evaporation rate in the first second. The pressure surge occurs by a sudden increase in pressure which is produced by the change in velocity of the moving fluid in the pipe [58]. After the valve is opened, the sorbate flows towards the cartridge with high propagation velocity. It might be possible that, once the sorbate reaches the cartridge, the flow velocity suddenly decreases, whereas the energy of the fluid moving forward leads to a rise of pressure.

The pressure peak was not observed at ambient temperatures of -10°C and 0°C. It might be possible that, due to low evaporation rates and therefore low sorbate velocities, the apparent pressure surge does not occur. However, the absorption is not delayed due to the pressure surge, since a power release occurs immediately.

4.2.1 Summary of the Chapter

The cartridge performance was examined at different ambient temperatures. It was showed that the cartridge performance decreases as the ambient temperature decreases. A reduction is believed to be caused by lower pressure difference between the sorbate and the reactive bed. Since the sorbate flow through the reactive bed is believed to be driven mainly by pressure gradient along the reactive bed, the sorbate flow might be reduced with a reduction of the pressure difference between the sorbate and the reactive bed. It resulted in a low power release. With an intensive absorption at high ambient temperature, the pressure difference between the sorbate and the reactive bed decreases more intensively than at low ambient temperatures, resulting in a less intensive increase of average power release over 90 s than over 30 s. In addition, the pressure surge phenomenon was observed in the beginning of absorption phase. It is believed, that a big amount of evaporated methanol could not be immediately absorbed, causing a pressure increase.

4.3 Durability Tests

Figure 4.12 shows trend of total released energy during absorption phases in 15 successively conducted tests. Additionally, the difference between the dehydrated reactive bed mass before absorption and the initial reactive bed mass before the first absorption (test 1); is defined as the change of reactive bed mass and it is represented for every test.

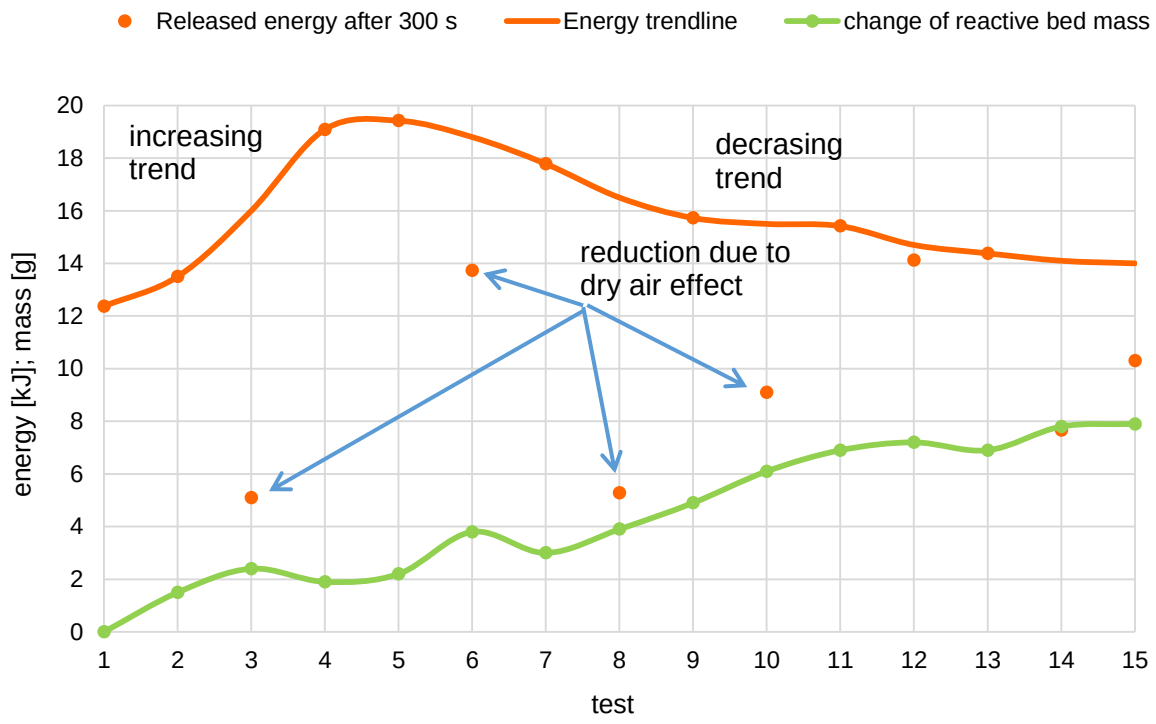

Figure 4.12: Durability tests – energy trend and change of reactive bed mass

The total released energies show an increasing trend from test 1 to test 4. After the peak is reached in tests 4 and 5, the total released energies show a tendency to decrease with the number of conducted tests. Simultaneously, the mass difference of the dehydrated reactive bed before absorption linearly increases with the number of conducted tests. In addition, a deviation from the energy trend is observed in tests 3, 6, 8, 10, 14 and 15, which is believed to be caused by the presence of non-condensable gases in the thermochemical heat storage system.

4.3.1 Released Energy Trend and Reactive Bed Mass Growth

Considering the kinetics of thermal dehydration of crystalline hydrates reviewed in [59], chemical changes on particle level occur within the reaction interface due to strain at the plane of contact between the crystalline reactant and the product phases. During the dehydration of hydrates, the interface advances into the unchanged reactant, for example LiBr in our case, whereby the amount of product, methanol in our case, increases.

The reaction is accompanied by a contraction because the dehydrated particle occupies a smaller volume than the hydrated one. The dehydrated particle is then penetrated by the system and provides the escape routes for the product.

Considering the cartridge manufacturing procedure reported in [60], methanol is decomposed from lithium bromide - methanol solution during the first decomposition phase. It is believed that, during the first decomposition process, the particles are fixed to host material on different places by forming the porous structure of the reactive bed. It might be possible that the particles change the position during the first few desorption phases, thereby forming interconnected pores in the reactive bed, especially in areas[9] with a high reactive bed density. In that way, the porosity and the permeability of the reactive bed increase, improving the sorbate flow through the reactive bed during desorption and absorption phases. Due to an increased porosity and permeability of the reactive bed, a bigger amount of reactive salt is being dehydrated and is available for absorption. Since the amount of released energy is proportional to the absorbed methanol, an increase of porosity and permeability results in an increase of the performance from test 1 to test 4 represented in figure 4.12.

It might be possible that an optimal porosity and permeability of the reactive bed are reached in tests 4 and 5, whereby a peak of released energy occurs. The peak of released energy is followed by a decrease of the cartridge performance from test 5 to test 15, which is believed to be caused by an increase of reactive bed mass and reduction of the porosity and the permeability of the reactive bed.

There might be two reasons which can cause growth of reactive bed masses with ongoing tests (see figure 4.12), such as insufficient desorption temperature at atmospheric pressure and contamination of the reactive bed.

As reviewed in [6] and [43], $LiBr{\cdot}2H_2O$ (dihydrate) exists at a temperature range from 4°C to 49,1°C and $LiBr{\cdot}H_2O$ (monohydrate) from 49,1°C to 156 °C, at atmospheric pressure. Since no literature about $LiBr{\cdot}nCH_3OH$ (LiBr hydrates with methanol) was found, it is believed that the temperatures at which the transition from $LiBr{\cdot}nCH_3OH$ to a different hydrate occurs, are lower than in the case of $LiBr{\cdot}nH_2O$ (LiBr hydrates with water). That is apparent from the fact that methanol has a lower dipole moment than water. A lower dipole moment of methanol leads to weaker van der Waals binding forces between absorbed methanol and LiBr in the reactive bed. Therefore, the transition from a higher to a lower hydrate step might occur at lower temperatures as referred in [6]. It might be possible that the transition from $LiBr{\cdot}CH_3OH$ (monohydrate)

[9] The area with high reactive bed density exists due to imperfections in the reactive bed design, where the impregnated salt solution was concentrated on one side of the cartridge as reported in [43].

to pure LiBr (anhydrate) already begins during the desorption phase at a temperature of 100°C, under atmospheric pressure.

Due to the fact that cartridge mass increases with the number of conducted tests, it is assumed, that the desorption temperature of 100°C is not sufficient to obtain pure anhydrate under atmospheric pressure. Thereby, anhydrate and monohydrate might co-exist in the reactive bed. Due to a bigger volume of monohydrate, some pores are narrowed or completely blocked. A part of decomposed gas is not able to flow through narrowed or completely blocked pores, especially in reactive bed areas with high density. It might be possible, that the amount of decomposed methanol blocked in the reactive bed increases with the number of conducted tests, causing a constant growth of reactive bed mass. Thereby, the theoretical heat release decreases, as the amount of dehydrated salt as well as the porosity decreases with ongoing tests, resulting in a reduction of performance.

Further, the reactive bed mass growth is observed from test 1 to 4, (see figure 4.12), although the cartridge performance increases. It is believed that the performance improvement occurs due to a formation of reactive bed, while the mass growth occurs due to an insufficient desorption temperature. On one hand, new interconnected pores are being formed in the high-density part of reactive bed, improving the mass transfer and the heat release. On the other hand, pores are being blocked in the optimal-density part of the reactive bed, reducing the mass transfer during desorption and resulting in a mass increase.

Considering the contamination of the reactive bed, corrosion of copper (Cu) with LiBr in composite material and amplification of shades of green colour of the reactive bed were reported in [6] and [43] respectively. The second phenomenon was observed during this investigation and it is presented in figure 4.13. The green colour of the reactive bed might be an indicator of the corrosion product in the reactive bed. Since the corrosion of LiBr and methanol with copper was not found in literature, the corrosion of copper in aqueous lithium bromide solution analysed in [61], is reviewed. The corrosion products are believed to be associated with a mixture of copper bromide (CuBr) and $CuO\text{-}Cu(OH)_2$, and a mixture of CuBr and $CuBr_2 \cdot 3Cu(OH)_2$. However, the formation of corrosion products might partially contribute to the increase of the reactive bed masses in this investigation.

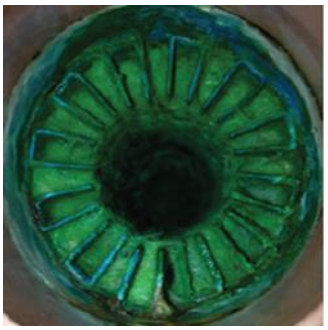

Figure 4.13: Amplification of shades of green colour of the reactive bed

4.3.2 Average Power Release Trend

The power release is defined as the amount of released energy in a unit of time. It depends on the amount of LiBr in the reactive bed, which can absorb an exact amount of methanol. In theory, the highest power release would occur, if all LiBr would absorb methanol immediately after the initiation of the absorption phase. In reality, the power release is governed by the sorbate flow through the reactive bed and is dependent on the amount of dehydrated LiBr. Not only the theoretical heat release but also the porosity and the permeability of the reactive bed are reduced due to incomplete dehydration. Therefore, the average power release is expected to show the same behavior as the released energy trend (see figure 4.12).

Figure 4.14 shows the average power release over 30 s, 60 s and 90 s in the conducted tests. The tests, which deviate from the energy trend represented in figure 4.12, were not taken into account in the following analysis.

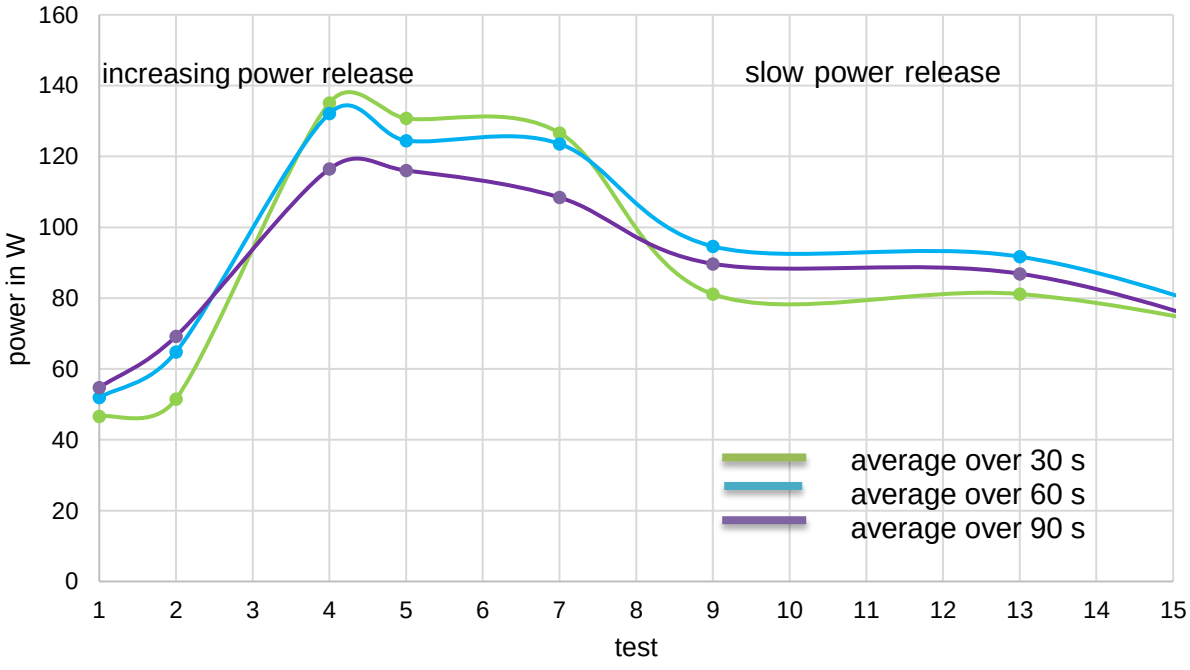

Figure 4.14: Durability tests - average power release

Figure 4.14 shows that average power release increases from test 1 to 4. The average power release increases with time as well. A peak is reached in average over 90 s, which is believed to be caused by the formation of interconnected pores. Due to the formation of interconnected pores, the porosity and the permeability of the reactive bed increase and the mass transfer is improved, resulting in an increase in power release.

Correspondingly to the energy trend, the highest power release occurs in tests 4 and 5 with a peak in average over 30 s. It is believed that optimal porosity and permeability of the reactive bed are reached in test 4 and 5. Thereby, the highest amount of salt reacts with the sorbate in the beginning of absorption phase. The average power release decreases over 60 s and 90 s, as the reactive bed becomes saturated and approaches to the theoretical heat release with time of absorption.

From test 5 to 15, the power release decreases as the mass of the reactive bed increases, reducing the maximum of theoretical heat capacity, the porosity and the permeability of the reactive bed. The phenomenon of mass increase is believed to be caused due to an insufficient desorption temperature under atmospheric pressure. The decomposition process is hindered and residual methanol remains within the reactive bed.

4.3.3 Deviation from the Energy Trend Due to the Presence of Dry Air

The effect of non-condensable gases on the sorption processes has been reviewed for liquid-gas systems in [25] and for solid-gas systems in [35] and [60]. Significant reduction of the sorption process was reported in those research reviews.

Since the deviation, i.e. the reduction in the cartridge performance was observed in tests 3, 6, 8, 10, 14 and 15 (see figure 4.12) it is believed to be caused by the presence of dry air within the thermochemical heat storage system. The amount of dry air in conducted tests was determined as described in chapter 3.4.1. The measured equilibrium vapour-air temperatures in the sorbate reservoir, the determined partial air pressures in vapour-air mixture, the determined amounts of dry air in the sorbate reservoir and the total released energies during the absorption phases are listed in table 4.7. Additionally, the deviation from the energy trend, i.e. the reduction of cartridge performance according to the energy trend was calculated for every test affected by the phenomenon. The obtained results are represented in figure 4.15.

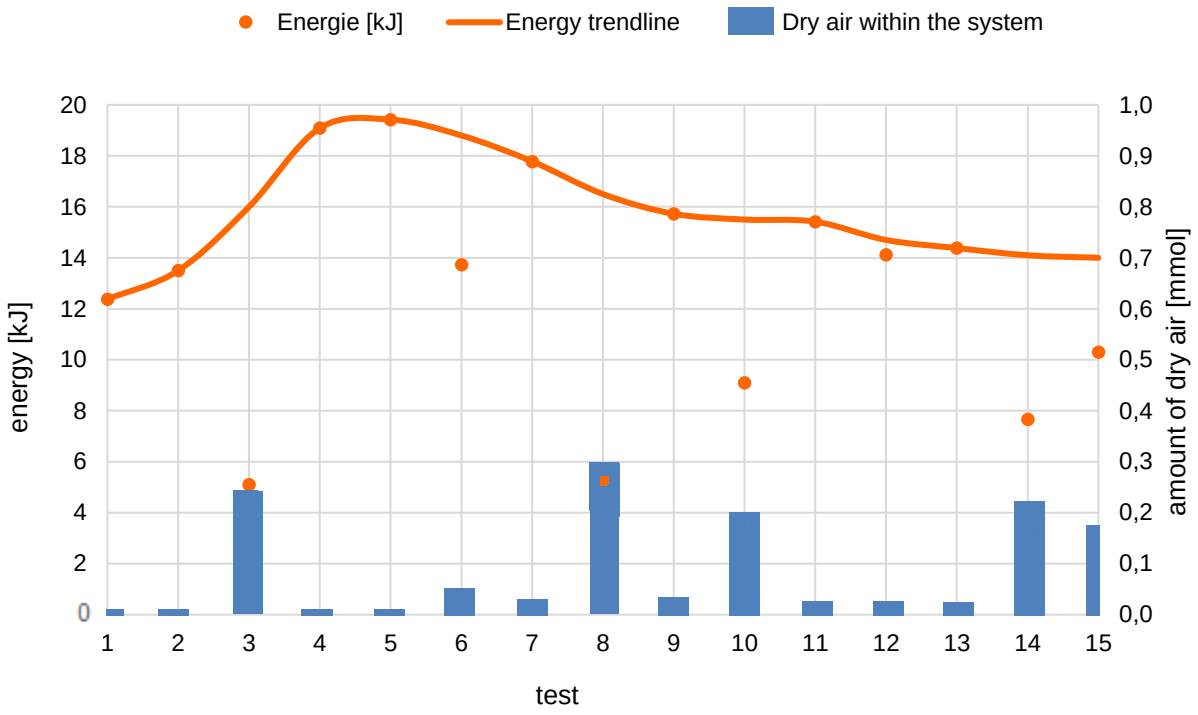

Figure 4.15: Durability tests, non-condensable gasses and deviation of energy trend

Table 4.7: Initial conditions and cartridge performance of durability tests

R11 - test no.	$T_{mixture\ (eq)}$ [°C]	$p_{air(eq)}$ [mbar]	$n_{dry\ air}$ [mmol]	total released energy [kJ]	the energy trend [kJ]	reduction according to energy trend
1	19,5	0,4	0,01	12,37		
2	19,3	0,2	0,01	13,50		
3	18,8	7,5	0,24	5,10	16	68%
4	17,2	0,4	0,01	19,09		
5	17,8	0,2	0,01	19,42		
6	18,4	1,6	0,05	13,73	18,8	27%
7	16,9	0,9	0,03	17,78		
8	20,5	9,4	0,30	5,29	16,5	65%
9	16,9	0,9	0,03	15,73		
10	21,0	6,2	0,20	9,10	15,5	41%
11	17,1	0,9	0,03	15,42		
12	16,7	0,8	0,03	14,12		
13	20,0	1,0	0,03	14,38		
14	18,9	7,1	0,22	7,67	14,1	48%
15	13,6	5,3	0,17	10,30	14	26%

Figure 4.15 shows that the reduction of total released energy according to the energy trend is mainly induced due to the presence 0,24 mmol, 0,05 mmol, 0,3 mmol, 0,2 mmol, 0,22 mmol and 0,17 mmol dry air in the facility during tests 3, 6, 8, 10, 14 and 15. A reduction of total energy release according to energy trend of 68%, 27%, 65%, 41%, 48% and 26% was observed in the tests respectively. Additionally, the fluctuations of reactive bed masses might partially contribute to the observed reductions, (see figure 4.12 and table 4.7).

In addition, the ambient temperatures, i.e. the temperatures in the sorbate reservoir before absorption are in the same range (20°C). Small differences in the temperatures do not drastically changes the obtained results in this investigation.

As the cartridge performances were significantly reduced due to the presence of dry air in the absorption phases conducted for 300 s, an effect of non-condensable gases on sorption process was investigated and discussed in more detail in the following chapter.

4.3.4 Effect of Non-Condensable Gases on Cartridge Performance

In order to investigate how the cartridge performance changes in presence of non-condensable gases, the relevant tests conducted under different conditions were analysed. The dry air is considered as the non-condensable gas in this investigation.

Figure 4.16 shows a correlation between total released energy during the absorption phase and the amount of dry air within the thermochemical heat storage system at ambient temperatures of 20°C and -10°C. The total released energies during the absorption phases, the reduction of the of the total released energies, the measured vapour-air equilibrium temperatures in sorbate reservoir, the partial air pressures, the calculated amount of dry air in the sorbate reservoir and the masses of the reactive bed before absorption are listed in table 4.8.

The masses of the reactive bed before absorptions are in the same range in this investigation. The ambient temperatures, i.e. the temperatures in the sorbate reservoir before absorptions are in the same range (20°C). Small differences in the mass of the reactive bed before absorption and in the temperatures do not drastically changes the obtained results in this investigation, (see table 4.8).

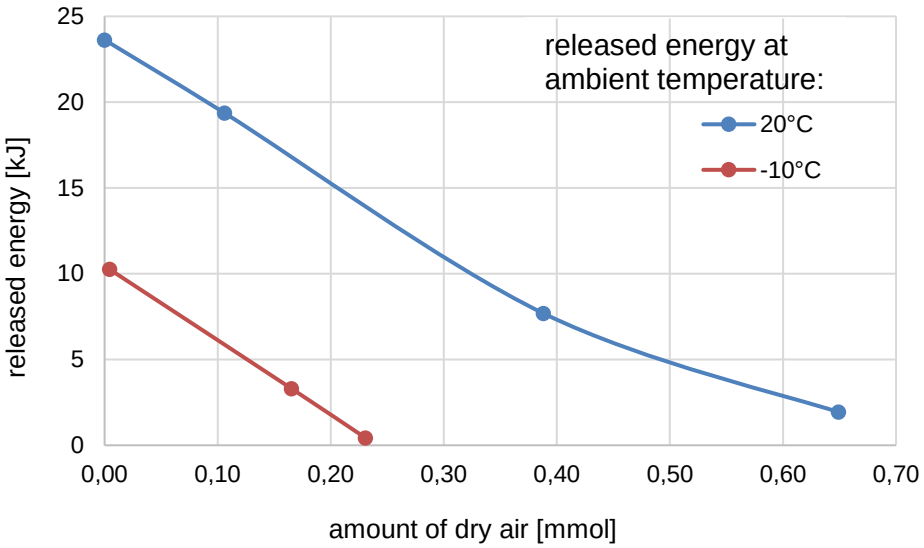

Figure 4.16: Released energy in presence of dry air at 20°C and at -10°C ambient temperature

Table 4.8: Cartridge performance and initial conditions of conducted tests

$T_{ambient}$ [°C]	total released energy [kJ]	reduction	$T_{mixture\ (eq)}$ [°C]	$p_{air(eq)}$ [mbar]	$n_{dry\ air}$ [mmol]	mass of reactive bed before absorption – R13 [g]
20	23,6		19,9	0,1	0,00	132,9
	19,4	18%	23,6	3,4	0,11	133,7
	7,7	67%	22,9	12,4	0,39	132,6
	1,9	92%	19,5	20,5	0,65	132,8
-10	10,3		-9,4	0,1	0,00	130,8
	3,3	68%	-8,2	4,7	0,17	131,3
	0,4	96%	-9,7	6,5	0,23	130

Figure 4.16 shows that the total released energy linearly decreases with the linear increase of the amount of dry air in the system, in both cases.

Considering the ambient temperature of 20°C, total released energy of 23,6 kJ was observed in absence of dry air. Released energy was reduced for 18% in presence of 0,11 mmol dry air, for 67% in presence of 0,39 mmol and for 92% in presence of 0,65 mmol of dry air within the thermochemical heat storage system.

At ambient temperature of -10°C, total released energy of 10,3 kJ was observed in presence of no dry air within the thermochemical heat storage system. The released energy was reduced for 68% in presence of 0,17 mmol dry air and for 96% in presence of 0,23 mmol dry air within the thermochemical heat storage system.

The absorption process (300 s) conducted at an ambient temperature of -10°C was almost completely reduced in presence of 0,23 mmol dry air, whereas the absorption conducted at 20°C was almost completely reduced in presence of 0,65 mmol of dry air. Comparing these both cases, it is clear that the lower ambient temperature yielded a higher reduction of the absorption process with regard to the amount of non-condensable gases within the thermochemical heat storage system.

Generally, in the presence of non-condensable gases, absorption rates are significantly reduced, as reviewed in more detail in chapter 2.4. During absorption phase, non-condensable gases from the vapour-air mixture create a layer on the absorption interface. The mass and heat transfers through this layer are hindered and therefore, the absorption is significantly reduced. The higher the amount of non-condensable gas in the system, the slower the absorption process and the lower the total released energy during the absorption phase (300 s).

In theory, the presence of non-condensable gases within the system would only retard the absorption process, and should not affect the theoretical amount of heat. However, some pores in the reactive bed might be blocked with non-condensable gas and therefore, unavailable for the absorption process as reported in [35].

Further, a reason for higher reduction of the absorption process in presence of non-condensable gases at -10°C than at 20°C, might be a lower mass diffusivity. As reported in [35], higher temperatures of vapour and air result in a higher mass diffusivity, and therefore, the vapour might diffuse through the accumulated layer of dry air and reach the salt grain more efficiently. Considering the pressures within the thermochemical heat storage system, the ratio of partial air pressure to total pressure varies with temperature. As the temperature decreases, the saturation vapour pressure decreases and the ratio of partial air pressure to saturation vapour pressure increases. Therefore, the reduction of the absorption process is higher at lower temperatures since the ratio of air pressure is higher, although the amount of dry air in system remains constant.

Since the non-condensable gases significantly reduce cartridge performance, only the tests conducted in absence of non-condensable gases within the thermochemical heat storage system were taken into consideration for a further evaluation of the thermochemical heat storage system performance.

4.3.5 Summary of Durability Tests

The behaviour of the cartridge performance was tested in 15 successively conducted tests. An increasing trend and a decreasing trend of the total released energy (300 s) were observed. It is believed that, the porous structure of the reactive bed is being formed in absorption and desorption phases in tests 1 to 4. Thereby, the sorbate flow, i.e. the mass transfer through the reactive bed is being improved and the cartridge performance increased. A peak of performance was reached when the reactive bed was completely formed and possessed an optimal porosity in tests 4 and 5. Thereafter, the cartridge performance decreased with the number of conducted tests, as the mass of the reactive bed increased. The mass increase is believed to be due to an insufficient desorption temperature. Both the anhydrate and the monohydrate might co-exist in the reactive bed, reducing the maximum theoretical heat capacity and the reactive bed porosity. That is reflected in the reduced performance. The corrosion of LiBr with Cu might contribute to the mass increase. Further, it has been confirmed that the decays from the energy trend occurred due to the presence of non-condensable gasses within the system. In addition, the effect of non-condensable gases on the cartridge performance was analysed at different ambient temperatures. The performance decreased as the amount of non-condensable gas increased. The non-condensable gasses accumulate in a gas rich layer, reducing the sorbate transfer to the reactive salt. The sorbate must diffuse through the gas rich layer, whereby low diffusion rates reduce the absorption rate. The reduction is higher at low temperatures due to lower diffusivity.

4.4 Reversibility Analysis

The main characteristic of the thermochemical heat storage system for automotive applications is a fast heat release. Beside construction properties of the reactive bed, the heat release depends on the state of the reactive bed. As discussed in chapter 4.3, the cartridge performance decreases as the theoretical heat capacity decreases. Therefore, the reversibility of heat storage cycle under simulated possible engine conditions is crucial for the implementation of the thermochemical heat storage system in automotive applications. The focus of the reversibility analysis is placed on the desorption phase, since the sorbate must be completely removed from the reactive bed, in order to reach a high cartridge performance in the next absorption phase. During the desorption phase, by heating the salt hydrate, the produced gas in the decomposition reaction is supposed to diffuse from the salt grain into the pores of the reactive bed. It is believed that, on the way out of the reactive bed, the mass transfer occurs mostly from advection, since the pressure gradient along the reactive bed is much bigger than diffusion coefficient, as referred in chapter 2.3.

The completeness of the desorption phase is dependent on the desorption temperature, the sorbate temperature and the duration of the desorption phase. During this investigation, the duration of desorption phase was constant, whereas the desorption and sorbate temperatures were varied. The cycle tests were conducted with cartridge R9 as described in chapter 3.3. The cycle test consists of an absorption and a desorption phase which are conducted without interruption in between. The cycle test is not interrupted between absorption and desorption phases and the test facility was not reassembled to avoid the contamination of the system with the air from environment. The mass of the reactive bed is measured before and after the cycle tests. The difference in measured masses before and after the conducted cycle represents the mass of residual sorbate, which remains within the reactive bed. The heat storage cycle is considered as completely reversible if no residual methanol remains within reactive bed.

4.4.1 Variation of Desorption Temperature

The desorption temperatures were maintained at two temperature ranges, whereas the sorbate temperature was maintained constant at 18°C:

1. regular temperature range corresponds to possible temperature in an engine (90°C - 95°C)
2. high temperature range (95°C - 105°C)

The progresses of desorption phases in test 1 and test 2, with maximum temperatures, are represented in figure 4.17. The total released energy, the mass of reactive bed before the cycle test as well as the residual methanol within the reactive bed (R9), the maximum temperature difference between desorption and sorbate temperature $\Delta T_{max.des\text{-}sorbate}$ and the reversibility of the heat storage cycle are listed in table 4.9.

At a higher desorption temperature, the absorbed methanol was completely removed from the reactive bed during the desorption phase. Therefore, it can be stated that the heat storage process was reversible during maintained conditions. On the other hand, at a lower desorption temperature, the 2,8 g of residual sorbate remained in the reactive bed after the desorption phase (1800 s).

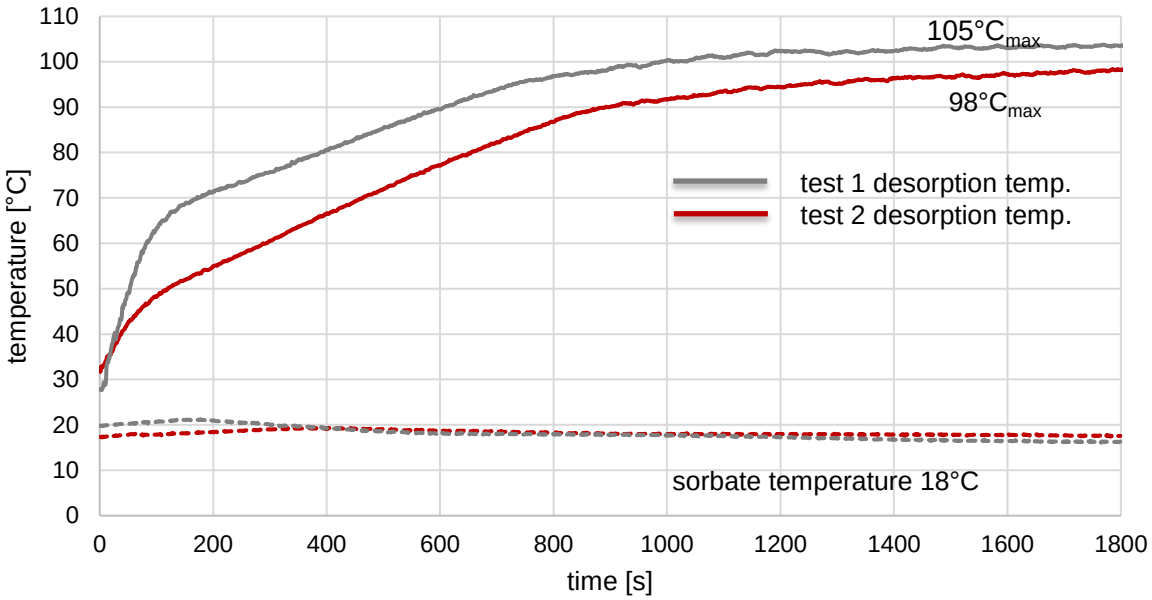

Figure 4.17: Desorption phase at different desorption temperatures

Table 4.9: Desorption phase at different desorption temperatures

	released energy [kJ]	mass of reactive bed before test [g]	residual sorbate [g]	$\Delta T_{max.des-sorbate}$ [°C]	reversibility
test 1	14,1	124,6	0	87	100%
test 2	13,9	124,6	2,8	80	

4.4.2 Variation of Sorbate Temperature

The sorbate temperatures were maintained in two temperature ranges, which corresponded to possible ambient temperatures during the operation of engine:

3. lower temperature range (16°C - 14°C)
4. high temperature range (16°C - 22°C)

The desorption temperature was maintained constant at a temperature range 95°C - 100°C. The progresses of the desorption phases in tests 3 and 4 with maximum temperatures are represented in figure 4.18. The total released energy, the mass of reactive bed before the cycle test (R9) as well as the residual methanol in the reactive bed, the maximum temperature difference between desorption and sorbate temperature $\Delta T_{max.des-sorbate}$ and the obtained reversibility of the heat storage cycle are listed in table 4.10.

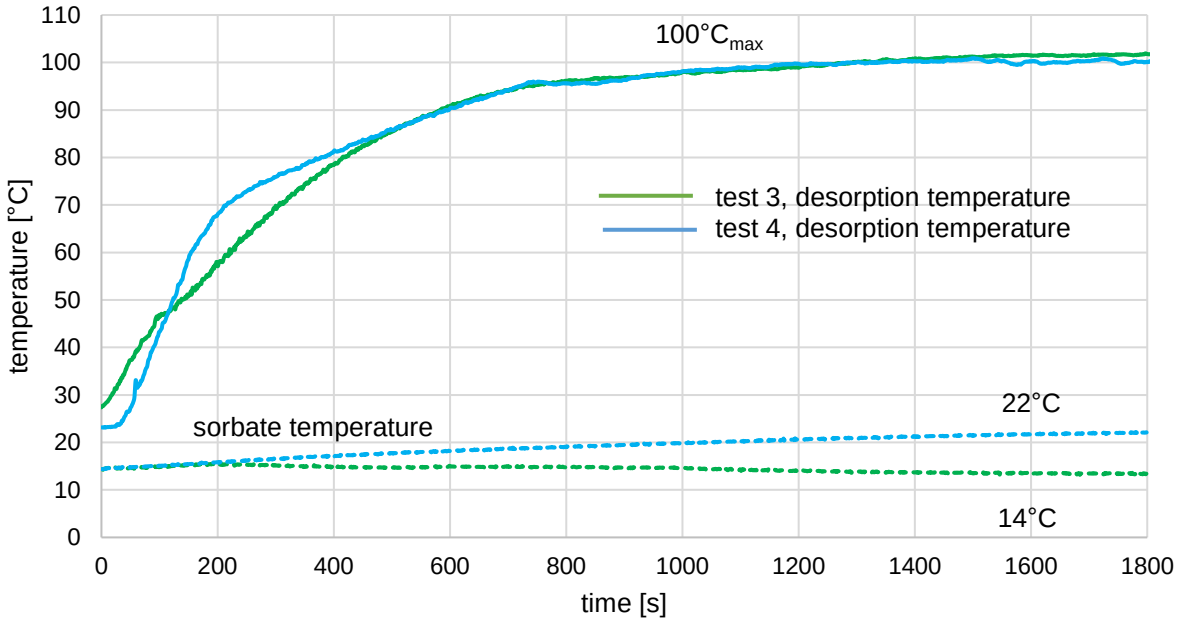

Figure 4.18: Desorption phase at different sorbate temperatures

Table 4.10: Desorption phase at different sorbate temperatures

	released energy [kJ]	mass of reactive bed before test [g]	residual sorbate [g]	$\Delta T_{max.des-sorbate}$ [°C]	reversibility
test 3	10,6	125,8	0	86	100%
test 4	10,6	126	4,1	78	

At the maintained lower sorbate temperature range, the absorbed methanol was completely removed from the reactive bed during the desorption phase. The reactive bed was in the same stage as before the conducted cycle test. Therefore, it can be stated that the heat storage cycle was completely reversible under the lower maintained temperature range. On the other hand, 4,1 g of absorbed methanol was not removed from the reactive bed during the desorption phase at the higher sorbate temperature range.

Considering the conditions during desorption phases, a completely reversible process, between sorbate and reactive bed (see table 4.9 and table 4.10), occurred at higher temperature, (i.e. pressure) difference.

The complete desorption of the reactive bed occurred in test 3 at a desorption temperature of 100°C$_{max}$ and in test 1 at a desorption temperature of 105°C$_{max}$, The difference between the desorption and the sorbate temperature in test 1 and test 3 was in the same range (86°C and 87°C respectively). Therefore, it might be possible that,

once the decomposition temperature is reached and the sorbate is decomposed from the reactive salt, the reversibility of the heat storage cycle is mostly dependent on the sorbate flow through the reactive bed. It might be possible that due to the higher temperature difference $\Delta T_{max.des\text{-}sorbate}$, the pressure gradient along the reactive bed is higher, resulting in an improved sorbate flow, i.e. mass transfer through the reactive bed. However, it is believed that the duration of the desorption was too short for a complete removal of methanol from the reactive bed in tests 2 and 4, since the methanol condensation was visually observed in the sorbate reservoir at the end of the desorption phase.

Considering the cartridge performance during absorption phases, the lower total released energies in test 3 (10,6 kJ) and test 4 (10,6 kJ) than in test 1 (14,1 kJ) and test 2 (13,9 kJ) are believed to be due to presence of 0,1 mmol of dry air within the thermochemical storage system during the test 3 and test 4. In addition to that, slightly higher mass of the reactive bed before absorption phases in test 3 (125,8 g) and test 4 (126 g) than in test 1 (124,6) and test 2 (124,6 g) might partially contribute to lower total released energies in test 3 and test 4. However, the complete desorption occurred in test 3 in presence of air within the system. As referred in [43], the desorption phase was less affected by non-condensable gases than absorption phase because the gas-rich layer was not formed in that case. None the less, the desorption rates might be reduced if the gas-rich layer is formed at the liquid-gas interface in the condenser as discussed in chapter 2.4. Therefore, the presence of air within the system during test 4 might be the reason for higher amount of the residual sorbate in test 4 (4,1 g) than in test 2 (2,8 g), although the temperature difference $\Delta T_{max.des\text{-}sorbate}$ is in the same range, (78°C and 80°C, respectively). Besides that, it might be possible that the desorption rates in test 3 and test 4 are lower than in test 1 and test 2 due to the presence of dry air within the system.

4.4.3 Summary of Reversibility Analysis

The reversibility analysis was conducted in cycle tests. The desorption and the sorbate temperatures were varied. The reversibility is defined as a ratio of the desorbed methanol and the absorbed methanol in the previous absorption phase, whereby the thermochemical heat storage cycle is considered as completely reversible, if no residual methanol remained in the reactive bed after the conducted test. The thermochemical process was completely reversible at a higher temperature difference between the desorption and the sorbate temperature (86°C and 87°C). At a lower temperature difference in test 2 (80°C) and in test 4 (78°C), 2,8 g and 4,1 g of residual methanol remained in the reactive bed after the cycle tests, respectively. It is believed that the pressure gradient along the reactive bed was higher at a higher temperature difference between the sorbate and the reactive bed. It has been shown that

the completely reversible cycle is possible under an optimal difference between the desorption and the sorbate temperature. At an insufficient difference between the desorption and the sorbate temperature, the desorption duration was too short. Further, it was stated that the desorption rates might be reduced due to the presence of 0,1 mmol of dry air within the system during test 3 and test 4. Lower desorption rates might be the reason for more residual methanol in the reactive bed after test 4 (4,1 g) than test 2 (2,8 g) since the temperature difference was in the same range (78°C and 80°C, respectively).

5 Error Analysis

5.1 Systematic Errors

The data acquisition system was developed in [6]. The thermocouples “Type K” were combined with on-board input settings for “Type K” provided by LabVIEW software. The inaccuracy range of “Type K” thermocouple is ±2,2°C or ±0,75% [62]. MKS Type 122A Absolute Pressure Gauge was used to measure the pressure in the thermochemical heat storage system. Lower readings are possible for stable operating temperature and flow. The lowest suggested pressure reading is 0,0399 mbar for a stable operating environment [63]. In order to calibrate the pressure sensor, linearization was used, as suggested in [6].

5.2 Operating and Evaluation Errors

The cartridges were developed using methods from previous research work [6]. The cartridge development is an error source, since every cartridge has a different amount of salt and glass wool and a different mass of cartridge jacket. Therefore, the performance of different cartridges can vary. The small differences in the reactive bed densities occurred due to the difficult implementation process of glass wool and reactive salt into the cartridge.

Since it was showed that the cartridge performance depends on the state of the reactive bed before desorption, the obtained performance might not be representative for comparison due to slight differences between the reactive bed states before absorption. However, difference of ±2,5 g of residual sorbate in reactive bed between compared tests is taken as criteria for the relevant test.

The vacuum in the system was controlled by monitoring the pressure over time. Due to imperfections in the compartment joints, the pressure in the sorbate distribution system might increase due to air leakage over time. During the absorption phase,

strong non-equilibrium conditions occur and it is not possible to indicate air leakage in the system.

Discontinuities in the temperature profile of the coolant bath and sorbate reservoir represent an error source in measurement of temperatures which are introduced in calculations for the cartridge performance, the calculations of the amount of air in the system, the evaporation rates and the flow analysis. In order to calculate the cartridge performance, average measured temperature with sensors on different positions was obtained. For determining the exact amount of air within the thermochemical heat storage system, the thermodynamic equilibrium in the sorbate reservoir was stated. To predict evaporation rates, the temperature of the liquid phase near the interface in the sorbate reservoir was introduced.

Thereby, sensor distance from the interface as well as surface of the interface might vary in the conducted test and thus, the sensor position represents an error source in the prediction of evaporation rates and flow analysis.

5.3 Simplifications

Simplifications of the mathematical model, developed for prediction of presence of non-condensable gases in the system, prediction of evaporation rates and flow analysis were conducted.

Firstly, dry air is considered as the non-condensable gas, present in the system. The contamination of the system occurred with ambient humid air which is assumed as dry air, since water is condensable and it is present in an insignificantly small amount. For the dry air presence calculation, it is assumed that the facility was leak tight during the test. Only the residual air in sorbate reservoir was assumed as total amount of air in the thermochemical heat storage system. The sorbate vapour is assumed as an ideal gas.

Secondly, a simplified relation for the prediction of evaporation rates was used, whereby the temperatures on both sides of the liquid gas interface in the sorbate reservoir are assumed to be equal to the measured temperature of the liquid phase near the interface. The used relation does not take into account the presence of dry air during evaporation prediction. Therefore, the evaluated tests are assumed to be conducted with an absence of dry air in the system. However, in presence of even small amount of air within the system (0,01 mmol), obtained results deviate from real state, which is obvious especially after the integration over the whole time interval of absorption steps. Therefore, a sorbate vapour temperature correction ($\mp 1°C$) is introduced in the model in order to reduce the errors and simplifications referred in this

chapter. Note that the calculation is done under strongly non-equilibrium conditions, where the measured data might strongly deviate from the real conditions.

Thirdly, the flow that occurred in the system, is considered to be incompressible and fully developed for the entire sorbate distribution system region. Vapour properties are based on empirical data and estimated values referred to in literature. The flow is analysed for a quasi-steady state, since it is assumed that the time dependence of real flow is sufficiently slow to justify a steady state analysis.

5.4 Relevant Errors

Effects of systematic errors were reduced by numerous sensors for temperature. In order to reach the thermodynamic equilibrium in the sorbate reservoir before the test, a time gap of at least one hour between the two tests, at constant ambient conditions had to be taken into account.

Relevant errors are differences in initial states of the reactive bed during the performance analysis, discontinuities in the temperature distribution for the prediction of evaporation rates and the presence of dry air in the system, as well as simplifications of the developed model for flow analysis.

The results obtained in the flow analysis deviate from real conditions occurring in the thermochemical heat storage system due to introduction of assumptions (incompressible fully developed flow), empirical values (friction loss coefficients, local loss coefficients, vapour density, viscosity) and constraints in estimation of flow rates. However, obtained results reflect a real behaviour of investigated phenomena which are described in literature.

6 Summary and Outlook

6.1 Summary

The presented master thesis was performed with the main goal to optimise an existing thermochemical storage system. A distribution system for methanol (reaction partner) was developed and tested, as well as performance behaviour under different ambient temperatures, durability of developed cartridge and reversibility of the storage cycle were examined.

The sorbate distribution system connects the cartridge and the sorbate reservoir. The effect of the sorbate distribution system on the cartridge performance was investigated. It was shown that the cartridge performance decreased with a decrease of the sorbate distribution systems pipe diameter.

Flow analysis predicted a pressure drop along the sorbate distribution system. The predicted pressure drops on the outlet of the sorbate distribution system significantly increase with a decrease of pipe diameter. Considering the sorbate flow through the reactive bed, it is believed to be driven mainly by pressure gradient. Therefore, it was stated that a reduced pressure difference between the sorbate and the reactive bed, which is caused by a pressure drop at the outlet of the sorbate distribution system, reduces the sorbate flow through the reactive bed. The result is a reduction in the cartridge performance. The predicted pressure drops to 16 mm and 40 mm pipe diameters were insignificantly small in both orientations (less than 1 mbar). Therefore, it was stated that 16 mm pipes are favoured by a possible integration of the sorbate distribution system, due to the insignificant effect on the cartridge performance and space requirements.

The investigation of the effect of ambient temperatures on the cartridge performance was carried out in a climate chamber, whereby the ambient temperatures were maintained at -10°C, 0°C, 10°C, 20°C and 30°C. It was shown that the cartridge performance decreases as the ambient temperature decreases. The power release was 157% higher at an ambient temperature of 30°C than at –10°C. The reduction of the performance is caused by a lower pressure difference between the sorbate and the reactive bed at a lower ambient temperatures. As the sorbate flow through the reactive bed is believed to be driven mainly by a pressure gradient along the reactive bed, a reduction of the pressure difference hinders the sorbate flow. That resulted in low power release at low ambient temperatures.

During durability tests, the cartridge performance showed both, an increasing trend and a decreasing trend of the total released energy (300 s) in 15 successively conducted tests. It was stated that the reactive bed structure is built during the desorption and absorption phases from test 1 to 4, thereby improving the mass transfer through the reactive bed. The improved mass transfer resulted in an increased power release. After the performance peak was reached in tests 4 and 5, the performance decreased as the mass of the reactive bed increased. It is believed that the porosity and the permeability of the reactive bed were reduced due to residual methanol in the reactive bed which cannot be desorbed at an insufficient desorption temperature of 100°C under atmospheric pressure.

Further, a performance deviation from the energy trend occurred due to the presence of non-condensable gasses within the thermochemical heat storage system. Therefore, the effect of non-condensable gases on the cartridge performance was analysed at ambient temperatures of 20°C and -10°C. The performance decreased as the amount of non-condensable gas increased, whereby the absorption (300 s) was

almost completely blocked in the presence of 0,65 mmol and 0,23 mmol of dry air within the thermochemical heat storage system at 20°C and -10°C respectively.

The reversibility analysis showed that a completely reversible heat storage process occurred at a difference between the sorbate and the desorption temperature of 86°C and 87°C, during the desorption phase of 1800 s. At lower temperature differences, 80°C and 78°C, 2,8 g and 4,1 g of residual methanol remained in the reactive bed after test 2 and test 4 respectively. It is believed that the pressure gradient along the reactive bed was higher at a higher difference between the sorbate and the desorption temperature. It was showed that a completely reversible cycle is possible under maintaining optimal conditions. It was stated that the lower desorption rates due to the presence of 0,1 mm dry air within the system in test 4 might be the reason that more residual methanol remained in the reactive bed than in test 3, since the temperature difference was in the same range.

6.2 Improvements and Outlook

The main excellence of the thermochemical heat storage systems is a high energy density. In order to benefit from the thermochemical heat storage in automotive applications, optimal heat and mass transfers within the reactive bed are crucial. Optimal density and porosity of the reactive bed enable a high power release during the absorption phase.

In the next step, the thermochemical heat storage system can be integrated into an engine test bench. Thereby, the effect of the heat storage on the gas emissions and the fuel consumption during an engine cold start and warm up phase as well as the performance of the system under real conditions can be investigated.

For integration of the thermochemical heat storage system into the engine test bench, feasible heat locations should be defined. The cartridge can be immersed into the engine coolant, which represents optimal heat sink and heat source. An optimal cartridge case needs to be constructed to ensure the heat transfer between the engine coolant and the cartridge.

Further, development of a compact sorbate reservoir is necessary for an integration of the thermochemical heat storage system on the engine test bench. In addition, automatically controlled valves can be integrated to ensure the start and the end of the absorption phases at appropriate times.

In order to investigate the effect of the thermochemical heat storage system on the reduction of gas emissions and fuel consumption during the engine cold start and the warm up phase, a scaling of the thermochemical heat storage system in terms of number of integrated facilities is necessary. An optimal scaling of the thermochemical

heat storage system will ensure a sufficient heat release to the engine coolant in order to realize the reduction in the gas emissions and the fuel consumptions.

Since the thermochemical heat storage system aims to reduce gas emissions and fuel consumption during the engine cold start and the warm up phase, the maximum potential of the thermochemical heat storage system would be achieved by an implementation into a motor vehicle in which more cold starts and warm up phases occur. A hybrid car can be considered as well.

Since it was shown that the reactive bed was completely desorbed during 30 min of the desorption phases, the thermochemical heat storage system might be implemented into a motor vehicle in which the operating engine temperature is kept for at least 30 min before the next cold start. The difference between the sorbate temperature and the desorption temperature must be considered.

7 Bibliography

[1] Eurostat Pocketbook: Energy, transport and environment indicators. Luxembourg: Publications Office of the European Union, ISBN 978-92-79-33105-3, 2013.

[2] Şenzeybek, M.; Tietge, U.; Mock, P.: CO_2 emissions from new passenger cars in the EU: Car manufacturers' performance in 2016. The International Council on Clean Transportation. Retrieved from http://www.theicct.org/sites/default/files/publications/PV-EU-OEM_ICCT-Briefing_03072017_vF.pdf , 2017, Zugriff am 29.10.2017.

[3] Osborne, S.; Kopinsky, J.; Norton, S.; Sutherland, A.; Lancaster, D.; Nielsen, E.; Isenstadt, A.; German, J.: Automotive Thermal Management Technology. The International Council on Clean Transportation. 2016.

[4] Dvorak, S.: Untersuchungen zur Wirkungsgradsteigerung in Kraftfahrzeuganwendungen durch thermochemische Energiespeicher. Diplomarbeit am IFA der TU Wien, 2014.

[5] Havlik, Fabian: Präsentation FVV-Projekt: Restwärmenutzung im Fahrzeug durch thermochemische Energiespeicher. TU Wien: Institut für Fahrzeugantriebe & Automobiltechnik, 2016.

[6] Ulrich, M.: Chemische Wärmespeicherung für Kraftfahrzeuge – Praktische Analyse von Wärmespeichermaterialien für den Einsatz im KFZ. Diplomarbeit am IFA der TU Wien, 2016.

[7] Dincer, I.; Rosen, M. A.: Thermal Energy Storage Systems and Applications, Second Edition. Ontario: John Wiley & Sons Ltd. ISBN: 978-0-470-97073-7, 2011.

[8] Fisch, Norbert, et al. : Wärmespeicher. Berlin: Solarpraxis AG, ISBN-13: 978-3-934595-54-5, 2005.

[9] Liu, C.; Rao, Z.: Challenges in various thermal energy storage technologies. Science Bulletin, 62/2017, Pages: 231–233.

[10] Ning-Wei Chiu, J.: Latent Heat Thermal Energy Storage for Indoor Comfort Control. Doctoral Thesis at KTH School of Industrial Engineering and Management, 2013.

[11] Garg, H. P.: Solar Thermal Energy Storage. Holland: D. Reidel Publishing Company. Dordrecht, 1985.

[12] Gil, A.; Medrano, M.; Martorell, I.; La´zaro, A.; Dolado, P.; Zalba, B.; Cabeza, L. F.: State of the art on high temperature thermal energy storage for power generation. Part 1—Concepts, materials and modellization. Renewable and Sustainable Energy Reviews, 14/2010, Pages: 31–55.

[13] Haider, M.; Werner, A.: An overview of state of the art and research in the fields of sensible, latent and thermo-chemical thermal energy storage. Elektrotechnik & Informationstechnik, 2013, 130/6, Pages: 153–160.

[14] Steinmann, W. D.; Eck, M.: Buffer storage for direct steam generation. Solar Energy, 80/2006. Pages: 1277–1282.

[15] Sharma, A. A.; Tyagi, V. V.; Chen, C.R,; Buddhi, D.: Review on thermal energy storage with phase change materials and applications. Renewable and Sustainable Energy Reviews, 13/2009, Pages: 318–345.

[16] Yan T.; Wang, R.Z.; Li, T.X.; Wang, L.W.; Fred Ishugah, T.: A review of promising candidate reactions for chemical heat storage. Renewable and Sustainable Energy Reviews, 43. 2015, Pages: 13–3.

[17] Fopah Lele, a.: A Thermochemical Heat Storage System for Households: Thermal Transfers Coupled to Chemical Reaction Investigations. Dissertation am Faculty of Sustainability (Fakultät Nachhaltigkeit), Lüneburg, 2015.

[18] Michel, B.; Mazet, N.; Mauran, S.; Stitou, D.; Xu, J.: Thermochemical process for seasonal storage of solar energy: Characterization and modeling of a high density reactive bed. Energy 47/2012, Pages: 553-563.

[19] Fopah Lele, A.: A Thermochemical Heat Storage System for Households. Switzerland: Springer Theses, DOI 10.1007/978-3-319-41228-3_2, 2016.

[20] N'Tsoukpoe, K. E.; Liu, H.; Le Pierre` s, N.; Luo, L.: A review on long-term sorption solar energy storage. Renewable and Sustainable Energy Reviews, 13/2009, Pages: 2385–2396.

[21] Lele, F. A.; Kuznik, F.; Rammelberg, H. U.; Schmidt, T.; Ruck, W. K. L.: Thermal decomposition kinetic of salt hydrates for heat storage systems. Applied Energy, 154/2015, Pages: 447–458.

[22] Posern, K.; Kaps, Ch.: Calorimetric studies of thermochemical heat storage materials based on mixtures of $MgSO_4$ and $MgCl_2$. Thermochimica Acta, 502/2010, Pages: 73–76.

[23] Gordeeva, L. G.; Restuccia, G.; Freni, A.; Aristov, Yu. I.: Water sorption on composites ''LiBr in a porous carbon''. Fuel Processing Technology 79/2002, Pages: 225– 231.

[24] Wang, L. W.; Wang, R. Z.; Oliveira, R. G.: A review on adsorption working pairs for refrigeration. Renewable and Sustainable Energy Reviews, 13/2009, Pages: 518–534.

[25] Miller, W. A.: The Experimental Analysis of Aqueous Lithium Bromide Vertical Film Absorption. Dissertation at University of Tennessee – Knoxville, 1998.

[26] Lefebvre, E.; Fana, L.; Gagnière, E.; Bennici, S.; Auroux, A.; Mangin, D.: Lithium bromide crystallization in water applied to an inter-seasonal heat storage process. Chemical Engineering Science, 133/2015, pages: 2–8.

[27] Jakobi, M.: Entwicklung eines thermochemischen Wärmespeichers auf Basis von Salzhydraten zur Verwendung in Kraftfahrzeugen. Dissertation am IFA der TU Wien, 2015.

[28] Gordeeva, L. G.; Restucciab, G.; Cacciolab, G.; Aristova, Yu. I.: Selective Water Sorbents For Multiple Applications, 5. Libr Confined In Mesopores Of Silica Gel: Sorption Properties. Reaction Kinetics and Catalysis Letters, 63/1998, Pages: 81-88.

[29] Moreno-Pirajan, J. C.: Thermodynamics of Metal Hydrides: Tailoring Reaction Enthalpies of Hydrogen Storage Materials. INTECHOPEN, ISBN 978-953-307-563-1, 2011.

[30] Goodwin, R. D.: Methanol Thermodynamic Properties From 176 to 673 K at Pressures to 700 Bar, Journal of Physical and Chemical Reference Data, 16/1987.

[31] Lu, H. B.; Mazet, N.: Mass-Transfer Parameters in Gas-Solid Reactive Media to Identify Permeability of IMPEX. AIChE Journal, 45/1999.

[32] Delgado, J. M. P. Q.: Heat and Mass Transfer in Porous Media. Berlin: Springer-Verlag, e-ISBN 978-3-642-21966-5, 2012.

[33] N'Tsoukpoe, K. E.; Restuccia, G.; Schmidt, T.; Py, X.: The size of sorbents in low pressure sorption or thermochemical energy storage processes. Energy, 77/2014, Pages: 983-998.

[34] Glaznev, I.S.; Aristov, Yu.I.: Kinetics of water adsorption on loose grains of SWS-1L under isobaric stages of adsorption heat pumps: The effect of residual air. International Journal of Heat and Mass Transfer, 51/2008, Pages: 5823–5827.

[35] Bayman, O. A.: Effect Of Non-Condensable Gases On The Adsorption Properties Of Adsorbent Porous Media, Mater Thesis at Middle East Technical University, 2014.

[36] Rahimi, P.; Ward, C. A.: Kinetics of Evaporation: Statistical Rate Theory Approach. lnt. J. of Thermodynamics, 8/2005, Pages:1-14.

[37] Rose, J. W.: Condensation heat transfer. Springer-Verlag: Heat and Mass Transfer 35, 1999, Pages: 479-485.

[38] Theodore, L.: Heat Transfer Applications for the Practicing Engineer. John Wiley & Sons, Inc. ISBN: 978-0-470-64372-3, 2011.

[39] Tang, G.H.; Hu, H.W.; Zhuang, Z.N.; Tao, W.Q.: Film condensation heat transfer on a horizontal tube in presence of a noncondensable gas. Applied Thermal Engineering, 36/2012, Pages: 414-425.

[40] Belkassmi, Y.; Gueraoui, K.; Hassanain, N.: Numerical Study in Condensing of Methanol Vapor in a Vertical Tube by Mixed Convection in the Presence of Non-condensable Gas. Adv. Studies Theor. Phys., 6/2012, Pages: 1065 – 1076.

[41] Collier, J. G.; Thome J. R.: Convective Boiling and Condensation, 3th edition. Clarendon press, Oxford. ISBN: 0-19-856282-9, 1994.

[42] Kameneckij, F.; David A.: Diffusion and heat transfer in chemical kinetics. New York: Plenum Press, 1969.

[43] Reifeltshammer, J.: Chemische Wärmespeicherung für Kraftfahrzeuge – Auslegung und Optimierung von Modularen Wärmespeicherpatronen. Diplomarbeit am IFA der TU Wien, 2017.

[44] DDBST Dortmund Data Bank Software & Separation Technology GmbH, www.ddbst.com/, [Online], Saturated Vapor Pressure, http://ddbonline.ddbst.com/AntoineCalculation/AntoineCalculationCGI.exe Zugriff am 4.2.2018.

[45] Beuth Hochschule für Technik Berlin, http://www.beuth-hochschule.de , [Online], http://public.beuth-hochschule.de/~wseifert/lmr/thermo/BilderThermo/Theorie/Antoine_Parameter.pdf , Zugriff am 24.10.2017.

[46] De Reuck, K. M.; Craven, R. J. B.: Methanol International Thermodynamic Tables of the fluid state – 12, IUPAC, Thermodynamic Tables Project Centre, Imperial College, London. ISBN: 0-632-03455-6, 1993.

[47] Wilkes, J.O.: Fluid Mechanics for Chemical Engineers, 2ndedition, Prentice Hall, 2006.

[48] Rennels, D. C.; Hudsom, H. M.: Pipe Flow: A Practical and Comprehensive Guide. John Wiley & Sons. New York, 2012. ISBN 978-0-470-90102-1

[49] McDonough, J. M.: Lectures In Elementary Fluid Dynamics: Physics, Mathematics and Applications. Lexington: University of Kentucky, 2009.

[50] Dane, H. J.: Ultrasonic measurement of unsteady gas flow. Flow Meas. Instrum, Elsevier Science, 1998.

[51] Hager, W.H.: Wastewater Hydraulics. Berlin: Springer-Verlag, DOI 10.1007/978-3-642-11383-3_2, 2010.

[52] Çengel, Y. A.; Boles, M. A.: Thermodynamics: An Engineering Aproach. 6th edition, McGraw-Hill Higher Education, Boston, 2009, ISBN 0071257713

[53] Young, D. F.; Munson, B. R.; Okiishi, T. H.; Huebsch, W. W.: Introduction to Fluid Mechanics. Singapore: John Wiley & Sons, ISBN: 978-0-470-90215-8, 2012.

[54] Persad, A.H.; Ward, C.A.: Expressions for the Evaporation and Condensation Coefficients in the Hertz-Knudsen Relation. Chemical Reviews. University of Toronto. Chem. Rev. 116. 2016, Pages: 7727−7767.

[55] Herman, M.A., Richter, W., Sitter, H.: Physical Principles and Technical Implementation. Springer Verlag Berlin. ISBN: 3-540-67821-2. 2004.

[56] Yaws, C. L.: Chemical Properties Handbook: Physical, Thermodynamic Environmental, Transport, Safety, and Health Related Properties for Organic and Inorganic Chemicals. Beaumont Texas: McGraw-Hill, ISBN: 0-07-073401-1, 1999.

[57] Hacişevki, H.: Internal Flow, Lecture slides. The McGraw-Hill Companies, 2010. Retrieved from: http://opencourses.emu.edu.tr/pluginfile.php/4503/mod_resource/content/1/Chapter8.pdf, Zugriff am 24.10.2017.

[58] Mylapilli, L.K.; Reddy Gogula, P. V.; Arya, A.K.: Hydraulic and Surge Analysis in a Pipeline Network using Pipeline Studio. International Journal of Engineering Research & Technology, Vol. 4, 2015

[59] Tanaka, H.; Koga, N.; Galwey, A. K.: Microscopic Studies and Introductory Experiments to the Kinetics of Solid-state Reactions. Thermal Dehydration of Crystalline Hydrates, 72/1995.

[60] Hofmann, P.; Jakobi, M.: Wärmespeicherung Vorhaben Nr 1007 - Restwärmenutzung durch intelligente Speicher- und Verteilungssysteme - Abschlussbericht. IFA der TU Wien, im Rahmen des CO2-Sonderforschungsprogramms der Forschungsvereinigung für Verbrennungskraftmaschinen e.V. (FVV), 2015.

[61] Muñoz-Portero, M.J.; García-Antón, J.; Guiñón, J. L.; Pérez-Herranz, V.: Analysis of Cu corrosion product in aqueous lithium bromide concentrated solutions. 9th International Symposium, Paris: Passivation of Metals and Semiconductors, and Properties of Thin Oxide Layers, 2006, Pages 131–136.

[62] Powell, R.L.; Hall, J.L.; Hynk, C.H.; Sparks, L.L.; Burns, G.W.; Scroger, M.G. and Plumb, H.H.: Thermocouple Reference Tables Based on the IPTS-68. National Bureau of Standards, Monograph 125. Washington, D.C. 1974

[63] MKS Instruments: MKS Baratron Type 122A Absolute Pressure Gauge, General Information. Website: https://www.mksinst.com , [Online], Zugriff am 24.10.2017.

[64] Schaschke, C: A Dictionary of Chemical Engineering. Oxford: Oxford University Press, ISBN 978-8211-0-8211, 2014, Page 136.